RL-81-006

Rutherford and Appleton Laboratories
CHILTON, DIDCOT, OXON, OX11 0QX

A Theoretical Study of a Target Reflector and Moderator Assembly for SNS

F Atchison

April 1981

RL-81-006

RL 81 - 006
SNS/TRAM/P5/80 REVISED

A THEORETICAL STUDY OF A TARGET REFLECTOR AND MODERATOR ASSEMBLY FOR SNS

F ATCHISON

Target Group
SNS Division
Rutherford and Appleton Laboratories
Chilton
Didcot
Oxon OX11 0QX

APRIL 1981

CONTENTS

ACKNOWLEDGEMENTS

The design for the target reflector and moderator system modelled is principally the work of Alan Carne, Mike Holding, Ken Roberts, Andrew Taylor and Ron Wimblett.

The preparation of this report has been helped by several people. My thanks to:

Tim Broome, David Perry and Andrew Taylor for their comments on the contents;

Mike Holding and Graham Toplis for production of the diagrams;

Kokila Patel for doing the majority of the typing and to Myra Gilbert and Sheila Evans who were also involved in this task.

I also gratefully acknowledge the role of The Radiation Shielding Information Centre, Oak Ridge National Laboratory, USA in making the basic computer codes used available.

REFERENCES

(1) A D Taylor Paper III in Proc. meeting on targets for neutron beam spallation sources KFH Julich June 11-12 1979 JUL-CONF-34 (1980)

(2) F Atchison Paper II Ibid.

(3) HETC. RSIC Computer code collection No CCC-178

(4) W A Coleman & T W Armstrong ORNL-4606 (1970)

(5) R R Coveyou, J G Sullivan, H P Carter, D C Irving, R M Freestone Jr., & F B Kam ORNL-3622 (1965)

(6) K C Chandler & T W Armstrong ORNL-4744 (1972)

(7) R R Fullwood, J D Cramer, R A Haarman, J F Forrest Jr, & R G Schrandt LA-4789 (1972)

(8) H W Bertini Phys. Rev 188, 1711 (1969)

(9) R Serber Phys. Rev 72, 1114 (1947)

(10) V F Weisskopf Phys. Rev 52, 295 (1937)

(11) L W Dresner ORNL-TM-196 (1962)

(12) D Garber, C Dunford, S Pearlstein BNL-NCS-50496 (1975)

(13) ORIGEN: RSIC Computer Code collection No CCC-217

(14) M J Bell ORNL-4628 (1973)

(15) C M lederer, V S Shirley, E Browne, J M Dairiki, R E Doebler, A A Shihab-Eldin, L J Jardine, J K Tuli A B Buyrn "Table of Isotopes" (7th edn), John Wiley & Sons Inc.(New York) (1978)

(16) F Atchison TRAM/P3/79 (1979)

(17) R W Wimblett Private Communication (1979)

(18) D R Perry SNS/ENV/N3/80 (1980)

(19) M Barbier "Induced Radioactivity" North Holland Pub. Co.(Amsterdam) (1969)

(20) K M Broom Phys. Rev. 126, 627 (1962)

(21) A C Wahl, R L Ferguson, D R Nethaway. D E Troutner & K Wolfsberg Phys. Rev. 126, 1112 (1962)

(22) E F Neuzil & A W Fairhall Phys. Rev. 129, 2705 (1963)

(23) K W Roberts Private Communication (1980)

(24) F Yiou, M Baril, J Dufaure De Citres, P Fontes, E Gradztajn & R Bernas Phys. Rev 166, 968 (1968)

(25) H Kschwendt & H Rief EUR 4519e (1970)

(26) A D Taylor Private Communication (1979)

(27) H Takahashi, H J C Kouts, P Grant, M Steinberg, J R Powell. Invited paper at 2nd International Conference on "Emerging Nuclear Energy Systems" April 8 - 11 1980 Lausanne (1980)

(28) B Hudson & C Steer AERE R8978 (1978)

(29) B Hudson In preparation (1980)

CHAPTER 1

CODES IN BRIEF

1. INTRODUCTION TO REPORT AS A WHOLE

This report presents results from a calculation to examine aspects of the performance of a Target, Reflector And Moderator assembly for use on SNS. The TRAM system modelled is based on a possible design (as of October 1979) for the first assembly to be installed. The majority of previous calculations have been made to examine particular areas of this system and some of these are summarised in References 1 and 2. In the case of this calculation the whole TRAM assembly is treated as a single entity.

The TRAM assembly is complex, and there are still several years before operation; changes in the design will inevitably occur and the relevance of the results of this calculation under such modifications will need careful consideration.

The scale of the calculation is large and there are aspects which have not been included; in particular thermal neutron and gamma transport. The stages of the study are (i) Particle transport, (ii) Analysis of particle transport results to obtain relevant macroscopic quantities, (iii) The collecting together and assessment of the results. This report represents the third stage.

The study examines what happens when $\sim$ 200 litres of inhomogeneous material is bombarded by 800 MeV protons. Using rough numbers, each proton causes a cascade of 30 secondary particles of which 10 succeed in escaping, and the other 20 are lost in some way. In each cascade roughly 1000 particle-nucleus collisions occur. The principal quantities of interest are energy deposition, induced activity†, and damage, with the major emphasis on the estimation of these quantities for the target uranium. Damage estimates are limited to translation of the collision information into terms of primary atomic displacements and no attempt made to further interpret this data, or for example include the contribution from the displacement cascade.

†The SI unit of activity is the 'Becquerel', throughout this report the unit of activity the 'Curie' has been used. The conversion factor is 1 Ci = 3.7×10^{10} Bq.

The following sections of this chapter deal with the codes used - both transport and analysis. Chapter 2 presents the results from the transport calculation in a general way, with chapters 3, 4 and 5 giving results and some further analysis for the target, the rest of the target assembly and for the reflector moderator and decoupler; each of these chapters is designed to be self contained although some cross-reference is unavoidable. The final chapter presents a general discussion.

The numbers quoted in this report do not have a tolerance attached and also in a lot of cases are given with unrealistic precision. Formal error estimation has not been made and although a statistical error from the calculation could be given, this is considered misleading as it would almost certainly be smaller than the real errors. Values quoted might be realistic with two figures; the use of more figures has been done to aid clarity (in following for example, contributions to a particular estimate); rounding for a particular final quantity should be done once at the end of the calculation.

Figures are located at the end of each chapter and have a numbering scheme to link them with a particular section; eg Fig II 7.2 will be the second figure of section 7 in chapter 2. Tables are also located at the end of the appropriate chapter with an arabic numeral for the chapter reference and a Roman numeral for the number within the chapter.

2. TRANSPORT CODES

The calculation uses a locally modified version of the HETC[3] code package from the Radiation Shielding Information Centre operated by Oak Ridge National Laboratory. This code package consists of the union of an extended version of the high energy transport code NMT[4] and the neutron transport code 05R[5], as made by Chandler & Armstrong[6]. The code package contains two large Monte Carlo transport codes - HET for high energy

transport and 05R for neutron transport - these mneumonics will be used to identify them throughout this report.

Both codes employ the Analogue Monte Carlo technique in which individual particles are transported and a 'nuclear physics' history built up, by moving from event to event and each time selecting a single outcome from all possible, (or more correctly, all programmed). The two codes differ in the way possible histories are obtained, which in turn is dictated by the different physics relevant to the transport of high energy particles and of MeV and below neutrons; neutron transport is also able to employ more efficient calculational techniques.

2.1 HET

The physics content of HET may be found in Refs 3, 4 and 6 and also in the target studies of Fullwood et al [7] and only a brief resume will be given here. The particle-nucleus interaction model used, restricts transport to nucleons of energy less than 3.5 GeV and charged pions of energy less than 2.5 GeV; scaling models are included to allow energies above these limits to be used. At the low end of the energy scale, neutron histories are terminated at a user selected energy, normally in the region 15 to 50 MeV, when the intranuclear cascade and evaporation (ICE) model is no longer valid, and for charged particles at an energy (again round 15 MeV for protons, and a factor of .15 and .11 lower for charged pions and muons) at which they may be considered to have slowed to rest. In the case of π^- the user may select either that the pion decays at rest, or will be captured by a nucleus. Neutrons created below, or reaching the lower energy limit are passed to 05R for completion of their transport.

Ionisation loss and decay, as appropriate, is treated by HET and in addition the trajectory of the source particle (only) is subject to coulomb scattering. Particles (either source or collision products) are transported between collisions using a cross section close to the geometric ($\pi r_o^2 A^{2/3}$), with the actual interaction computed with the ICE model. The ICE model is the calculational realisation by Bertini

(eg Ref 8) of the Serber[9] model for high-energy particle-nucleus interaction, linked to the Weisskopf[10] evaporation model as implemented by Dresner[11]. It should be noted that this model allows for a non (pseudo) interaction and hence does not assume that the geometric and total cross sections are the same. Code is also included to allow for scattering of high energy neutrons based on cross-section information.

2.2 05R

05R uses pre-processed cross section data to carry out neutron transport. Interactions are classified as scattering (both isotropic and anisotropic are treated), nuclear collisions (which may be productive and also decouple the input from the output neutron energy), fission and absorption. The probabilities are calculated by the preprocessor code on a $\log_2$ energy basis from cross section data. The first three event types occur on an either/or basis, with nuclear collisions calculated using the Bohr compound nucleus model (using the same evaporation code as HET but with specialised parts to treat ^{9}Be and ^{2}H collisons). Fission and absorption may both occur at every interaction. The treatment of fission has been up-dated in our local version of 05R. For absorption, the process is averaged over all nuclei within a particular medium and results in a loss of neutron weight. This results in more efficient transport but makes analysis more complicated. The code allows use of the techniques of Russian Roulette and Splitting.

2.3 The Geometry Routines

The two codes share a powerful geometry package which allows representation of inhomogenous three dimensional systems. The code allows for boundaries between materials which may be specified by (up to) quadric surfaces, i.e.

$$ax^2 + by^2 + cz^2 + dxy + exz + fyz + gx + hy + iz + j = 0$$

where a to j are constants any of which may be zero. The versatility of the geometry routines carries with it the sometimes formidable task of forming the data deck.

The geometry routines carry out the physical transport of the particle. A distance of travel is picked randomly from the familiar exponential probablity law using a mean free path based on the appropriate cross section for the medium and code (HET or 05R). This distance together with the starting co-ordinates and direction are passed to the geometry routines. The outcomes are: (i) The trajectory passes into a new medium, from which point it is necessary to use a new mean free path. (ii) The trajectory escapes from the system and the history of the particle is to be terminated. (iii) The trajectory is completed and the codes should then proceed to compute an interaction.

Other facilities are available with the geometry routines, these are described in the code references cited.

2.4 HETC at Rutherford and Appleton Laboratories

The modifications to the HETC package to allow our problems to be tackled have been described in Ref 2: These are in brief:-

(i) The treatment of high-energy particle-induced fission in HET.

(ii) The modification of the coulomb scattering to accommodate the use of highly inhomogenous systems.

(iii) The revision of the fission treatment in 05R.

(iv) The extension of the geometry routines to allow larger systems to be modelled.

(v) The provision of a new cross section preprocessor code for 05R, to allow use of ENDF/BIV [12] cross section data.

Reference 2 also presents some results for checks made on the physics of the code.

3. ANALYSIS CODES

The transport calculation provides a magnetic tape of events as output. This is analysed to calculate the quantities of interest. In this section, some of the analysis routines are briefly discussed to show assumptions made which reflect the reliability of the answers presented, and also may help in interpreting some of the results.

3.1 Energy Deposition ENDEN

To estimate energy deposition and its distribution, the most full analysis of the history tape is required. The energy deposition analysis has taken roughly half the computer time of the actual transport.

The following are the major assumptions made:-

(i) Ionisation loss is uniform along the length of a complete trajectory and the distribution is obtained by depositing 20% of the total energy at five uniformly separated points.

(ii) Nuclear recoil energy is deposited at the event point.

(iii) All gamma energy is deposited at the event point. (Including the HE γ's from π^0 decay). This may be considered a temporary expedient until gamma transport is implemented. The contribution of gamma energy is in general small.

The calculation of energy distribution has been made with two separate versions of the code - the first employs an independent co-ordinate system to divide up the total volume and is used for the target and the second uses the geometry routines (Section 2.3) to collect results into

volumes as specified in the model geometry. This latter version is used for calculating the energy distribution in the full system, where it is appropriate to isolate the various components, but these tend to have awkward orientations; it does lead to odd shapes being used.

3.2 Escape Neutron Distributions. MERCAT

The trajectory of an escape neutron is forward projected onto the surface of a circumscribed sphere. The surface of the sphere is divided into equal areas by using uniform angular increments in longitude and a SINE distribution for latitude.

The output is displayed as a 3-D projection histogram or plot on the longitude-latitude plane with orientation chosen to obtain a good view.

3.3 Nuclide Build-up and Decay - ORIHET

The RSIC code ORIGEN[13] due to Bell[14], which solves the Bateman equations for the build-up and decay of activity in reactor cores, has been adapted to use HETC nuclide production rates.

The code solves the system of equations.

$$\frac{dx_i}{dt} = \sum_{j=1}^{N} \ell_{ij}\,\lambda_j\,X_j - \lambda_i\,X_i + \alpha_i \qquad i = 1 \text{ to } N$$

where X_i is the concentration of nuclide i (at some time t) which has a decay constant λ_i and is produced at a rate α_i. The ℓ_{ij} are the branching ratios for production of i from nuclide j which has a concentration X_j and a decay constant λj.

The details of the method of solution may be seen in reference 14.

HETC gives nuclides more widely distributed in charge and mass than for reactors. The data libraries containing the ℓ_{ij} and X_i along with decay energy information have been approximately doubled in size using information from the 7th edition of the Table of Isotopes[15]. Code size limitation has meant that the calculation has had to be split into three mass ranges - from 40 to 119 & from 120 to 170 for fission products and from 207 to 250 for spallation products.

During the modification to allow HETC nuclides to be used, the code was also altered to allow the listing of α activities and to give information concerning neutron emitters. In the case of neutron emitters, the small contribution from mass chain skipping has been neglected.

3.4 Nuclide Analysis

HET provides direct information on nuclide production which may be taken straight from the history tape. In the case of 05R, because of the technical details of the calculation some of the information is not so readily obtained.

The 05R cross section information for full system running contains just under 700,000 data items; within this large amount of data, absorption information is averaged over all nuclei forming a material, so to find the contribution to a particular absorption channel it must be unfolded by analysis. This requires maintaining the separate identity of each absorption cross section (to reduce the amount of data implied by this, the cross sections were averaged over coarser bins) and folding them with the spectrum of neutrons inducing reactions in the medium. This technique may be applied to all cross-sections to give two valuable advantages, firstly good estimates may be made for some of the lower probability channels and secondly a check is made on the code. The checking was made by comparing estimates by the off-line spectral folding technique and direct analysis of the history tape where this gave an unique estimate. A further comparison was made by unfolding the output spectra from interactions via the cross sections in particular

channels to give estimates for other channels. Numerical agreement was found at the percent level in most cases.

Neutron activation channel information quoted in this report has been based on the results of the off-line unfolding technique.

CHAPTER 2

AN OVERVIEW OF THE CALCULATION

1. INTRODUCTION

In this chapter, some technical details of the transport calculation are given along with a general summary of the results. The system being modelled consists of many media distributed in three dimensions. The arrangement is transmitted to the transport codes by the geometry routines. The overall transport calculation has been made in five stages - two using HET and three O5R. At each stage, magnetic tapes of events are produced; these are analysed to provide source particle information for subsequent stages and also contributions to the macroscopic quantities of interest.

The chapter ends with a section on particle generation and fluxes.

2. THE GEOMETRY OF THE MODEL

The major concern is the operating conditions for the target, and most particularly with what is going on in the uranium. The uranium is also the source of all particles for the transport calculation and hence it provides a good sub-division for the system.

Two geometry data decks were used - the first to represent the uranium discs and the second the full TRAM assembly; perspective views of these are shown in Figs. II 2.1 (a) & (b) and II 2.2. In the third diagram, the target assembly is omitted for clarity and fits between the four moderators; the numbers identify moderator faces and neutron beam holes and are for use later in this report.

The coordinate system for the calculation has been chosen with the positive Z axis along the proton beam axis, Y positive as up and X positive as left, as viewed from the proton beam end of the target. The origin is the point on the Z axis vertically below the centre of the front moderator (at the proton beam end of the target).

For the purposes of this calculation the 'target' is defined as the 9 cm diameter cylinder of length 34.7 cm, containing all the uranium and part of the cladding and coolant.

The cylinder is symmetric about the Z axis with its front surface in the Z = -6.0 cm plane. The uranium is divided into plates of varying thickness and each face clad with .025 cm of Zircaloy. Coolant channels of width 0.175 cm separate each clad plate. The geometry deck divides the 'target' cylinder into 55 sections which alternate between two media; the first the uranium, and the second the coolant and cladding which is represented in the codes by an uniform mixture. This gives a systematic variation of material as the cascade procedes down the target,

The choice of target in this form allows comparisons to be made with the results from more general studies (eg Ref 7) where isolated targets are normally modelled; it also separates the contributions from reflections by surrounding materials which will always be present in real systems.

The full system geometry data deck is large and its construction complex. The additional burden of having the full plated structure for the target in this arrangement was avoided on the basis that the effects of reflection would be small; the 'target' is simulated by a 9 cm diameter by 34.7 cm long cylinder of a uniform mixture of uranium, coolant and cladding in their average proportions. The geometry was split into 13 layers so that similarities and symmetries could be exploited during the task of forming the data deck. The arrangement of the layers is described in Fig. II 2.3 with details of the layout referred from this to figures II 2.4, II 2.5 and II 2.6, and describes a four moderator system with dimensions corresponding to the design in October 1979. Some changes have been introduced for modelling purposes; the upper and lower moderators are the same excepting for the X→ -X transform; no containers for the moderators have been included although some dimensional relaxation has been made to allow for their presence in the real system. All four moderators consist of 10 x 12.6 x 5 cm^3 blocks of H_2O. The front moderators have both 10 cm wide x 12.6 cm high faces open and the back only a single face. The moderators are angled to the

proton beam direction and along with their associated beam ports, are lined with boron carbide. For modelling convenience the bevelled corners of the reflector are represented by a cylindrical surface.

The materials, volumes, and masses of the components of the full system so represented are listed in Table 2-I and the nuclear densities used for the calculations in Table 2-II.

3. ORGANISATION OF THE CALCULATION

The transport calculation has been made in five stages:-

1) HET for 'target' - 800 MeV protons, started on the front surface of the target, propogate a high energy particle cascade through the target cylinder.

2) O5R for 'target' - The sub-15 MeV neutrons created in stage 1 are transported to the surface of the target cylinder. The (phase-space) starting coordinates are passed from stage 1.

3) O5R for full system - The neutron 'escapes' in stage 2 are used as source particles for transport through the full system. The neutrons are followed until they escape or reach a lower cut - off energy of 0.1 eV.

4) HET for full system - The high energy 'escapes' in stage 1 are used as the source for a high energy cascade calculation with the full system.

5) 2nd O5R for full system - The sub-15 MeV neutrons created in stage 4 are transported through the full system.

The general layout of the transport calculation is shown in Fig. II 3.1 For stage 1 20000 proton cascades were calculated. These gave 430000 neutrons to be transported in stage 2. The distribution of these neutrons is exponential in the Z direction. To assist in the analysis the neutrons are batched by distance in this direction so that similar statistical weights are available for all depths without using all neutron histories. Five regions were used with boundaries at 3.4, 6.8, 10.4 and 17.1 cm. The distances were chosen so that the boundaries were within a coolant channel.

Again to assist in the analysis, the source neutrons for stage 3 were batched in the Z direction. The five sets of 'target' escape neutrons from stage 2 were merged and then split into five regions to give similar numbers of neutrons in each. Because in the modified neutron-induced fission treatment splitting is employed there are now 1.4 million 'neutrons' available for transport, but these on average have a weight of ~ one-third. Only some of these neutrons were used; the criterion for deciding enough histories had been calculated being to compare analysis results for symmetric positions.

The final two stages consisted of transporting the high energy 'target' escapes (protons, neutrons, pions and muons) through the full system, followed by neutron transport for those created. The number of escape particles at stage 1 was limited and additional statistics were obtained by splitting. A fivefold split was used.

The transport calculation wrote 64 tapes of information (containing roughly 2×10^9 'numbers') for analysis.

4. COLLECTED INFORMATION FROM TRANSPORT CALCULATION

In this section the general results from the transport calculation are given: In chapters 3, 4 and 5 more detailed results are presented. The results from all five stages have been scaled to units of per proton incident at the target. The numbers quoted are, in some cases, given with an unrealistic numerical precision; this has been done to aid clarity in following the information.

4.1 HET for Target

The protons were started with an energy of 800 MeV from a uniform density in 4-D phase space of volume 300 (H) x 250 (V) (π mm rad)^2 with a 35 mm waist in both planes. 20000 histories were calculated.

(a)	High energy particle induced fissions		1.3	
(b)	^{238}U spallations		0.42	
(c)	Non-uranium spallations		0.14	
(d)	Total energy deposited		646	MeV
(e)	Total sub-15 MeV neutrons		21.4	
(f)	Sum kinetic energy for sub-15 MeV neutrons		76.7	MeV
(g)	Total high energy neutron escapes		1.4	
(h)	Sum kinetic energy for high energy neutron escapes		109.6	MeV
(i)	Total proton escapes		0.12	
(j)	Sum kinetic energy for proton escapes		23.4	MeV
(k)	Total meson ($\pi^{\pm}$ + $\mu^{\pm}$) escapes		0.017	
(l)	Sum kinetic energy for meson escapes		1.4	MeV
(m)	Total cascade protons slowed to rest		1.5	
(n)	Charged evaporation fragments	protons	0.48	
		deuterons	0.13	
		tritons	0.06	
		^3He	0.004	
		alphas	0.12	

4.2 O5R for Target

Transport of the 21.4 neutrons of sum energy 76.7 MeV from their production point to the surface of the target.

(a)	Total neutrons at surface of target	24.7	
(b)	Sum kinetic energy for these neutrons	48.3	MeV
(c)	Total energy deposited	337.3	MeV
(d)	Number of fissions	1.8	
(e)	Total neutron-nucleus collisions	82.6	
(f)	Number of neutrons created by fission	3.7	
(g)	Number of neutrons created by (n,xn) reactions	0.7	
(h)	Number of neutrons absorbed	1.1	

4.3 O5R for Full System

Transport of the 24.7 neutrons of sum kinetic energy 48.3 MeV through the full system. A low energy cut-off of 0.1 eV was used; neutrons reaching this energy had their history terminated.

(a)	Total neutrons escaping	8.9	
(b)	Sum kinetic energy for these neutrons	5.7	
(c)	Total energy deposited	129	MeV
(d)	Number of fissions (in target)	0.14	
(e)	Total neutron nucleus collisions	850	
(f)	Neutrons created by fission	0.2	
(g)	Neutrons created in (n,xn) reactions	1.5	
(h)	Neutrons absorbed	12.4	
(i)	Neutrons reaching an energy of $\leq$ 0.1 eV	4.9	

4.4 Transport of High Energy 'Target' Escapes Through the Full System

A total of 1.54 neutrons, protons and mesons of sum energy 134 MeV are transported with HET through the full system.

(a)	Total high energy neutron escapes	0.83	
(b)	Sum kinetic energy for high energy neutron escapes	69.0	MeV
(c)	Total proton escapes	0.022	
(d)	Sum kinetic energy for proton escapes	0.3	MeV
(e)	Total meson escapes ($\pi^{\pm}$ and $\mu^{\pm}$)	0.002	
(f)	Sum kinetic energy for meson escapes	0.09	MeV
(g)	Total sub-15 MeV neutrons produced	1.7	
(h)	Sum kinetic energy for sub-15 MeV neutrons	6.5	MeV
(i)	Total energy deposited	43.9	MeV
(j)	Total nuclear collisions	1.1	
(k)	Total spallation fragments released	0.84	

4.5 Transport of Sub-15 MeV Neutrons Created by the High Energy Cascade through the Full System

1.7 neutrons of sum energy 6.5 MeV distributed throughout the full system are transported using O5R.

(a)	Total neutron escapes	0.98	
(b)	Sum kinetic energy for the neutron escapes	1.2	MeV
(c)	Total energy deposited	13.0	MeV
(d)	Number of fissions (in target)	0.02	
(e)	Number of neutron nucleus collisions	66.0	
(f)	Neutrons created by fission	0.04	
(g)	Neutrons created by (n,xn) reactions	0.32	
(h)	Neutrons absorbed	0.70	
(i)	Neutrons reaching an energy of $\leq$ 0.1eV	0.38	

4.6 Overall Summary

4.6.1 Energy Deposition

The contribution to energy deposition in the components of the system are now tabulated:

Where Deposited \ Transport Calculation	HET For Target	O5R for Target	O5R For Full System	HET for Full System	O5R for Supra-target Neutrons	Totals
TARGET	630	330	32.8	0.8	2.4	996.0
COOLANT	5	4.6	9.33	6.02	0.65	25.6
CLADDING	11	2.7	6.7	11.3	0.2	31.9
CAN	-	-	21.4	3.6	6.8	31.8
MODERATORS	-	-	2.36	0.78	0.21	3.35
REFLECTOR	-	-	15.4	20.11	0.49	36.0
DECOUPLER	-	-	41.01	1.29	2.25	44.55
TOTALS	646	337.3	129.0	43.9	13.0	1169.2

That is a total of 1170 MeV deposited per 800 MeV proton incident. A total energy 'turnover' of ~ 2800 MeV is involved; an approximate account is shown in Table 2-III and is summarised pictorially in Fig. II 4.1.

4.6.2 Particles

9.88 neutrons of energy $\leq$ 15 MeV escape the system with a sum kinetic energy of 6.9 MeV.

14.2 neutrons are absorbed and 5.28 enter the energy region $\leq$ 0.1 eV.

23.1 neutrons are created by high energy nuclear interactions and high energy fission, 3.94 are created by neutron induced fissions and 2.52 created in (n,xn) reactions.

There are a total of 1000 collisions throughout the full system.

For high energy escapes 0.83 n° take 69 MeV kinetic energy, 0.022 protons 3 MeV and 0.002 mesons 0.09 MeV.

5. LOW ENERGY NEUTRONS

In section 4, 5.28 neutrons reached an energy of $\leq$ 0.1eV. When this occurs, transport of the neutron is terminated as the version of 05R used does not contain an adequate treatment for thermal neutrons.

The breakdown of where these events occur is:-

0.11	In the target coolant
4.11	In the reflector
1.06	In the four moderators

These neutrons have not been subject to a formal transport and their effect will be discussed in the appropriate chapters.

6. COMMENTS

The careful reader may have noted some numerical disagreement in the neutron balance - this is not due to a misprint. At each stage of the calculation, there are a few quick checks to indicate that all is well. The analysis of gross particle and energy balance provides just such a check. The values quoted in section 4 come from such analysis. In the case of neutrons, absorption is treated by weight changing and in view of the vagaries of computer round-off problems etc., the agreement is excellent.

7. PARTICLES

In this section, data on particle generation and spectra are presented. Moderator fluxes are dealt with in chapter 5.

7.1 Target Production

The majority of neutrons are created by evaporation from excited nuclei created by fission and spallation in the uranium. The distribution of neutron production in the high energy cascade is shown in Fig. II 7.1, in which the neutron production density is shown for 10 radial x 10 longitudinal bins. The first seven bins have been compared with the original proton beam distribution function

$$\frac{I(r)}{I_o} = 1 - \frac{r^2}{a^2}$$

For uniform radial intervals, $I/(2N+1)$ should be linearly related to $N(N+1)$ where N is the bin number (range 0→9). The results so treated are shown in Fig. II 7.2. From the linear relation the distributions' width 'a' may be deduced and these are displayed in Fig. II 7.2 as an inset. The results do not refute the proposition, and yield a width at the front end of the target close to that for the input beam.

The energy spectrum for these neutrons is shown in Fig. II 7.3 along with the energy spectrum for the neutrons escaping the target cylinder. To try and offset the effect of the logarithmic energy bins, the average energy for each of these sets of neutrons is also shown.

The average neutron energy falls from 3.6 MeV to ~ 2 MeV. This reduction is due to the decoupling effect of neutron induced fission: The mean kinetic energy is both a function of the evaporating mass and its excitation (Fig. II 7.4). The higher energy component (>1→2MeV) of the spectrum of cascade-produced neutrons will cause the fissions, and also will induce lower nuclear excitation energies than in case of high energy fission, hence softening the escape spectrum.

The complete neutron escape spectrum is plotted in Fig. II 7.5 (a) as a double log plot and on a linear energy scale in Fig. II 7.5 (b).

It should be remembered that the calculation is broken at 15 MeV neutron energy, with those below transported by 05R; the two spectra join in a reasonable fashion at 15 MeV, but the spectrum between say 10 and 50 MeV should be viewed with some caution.

The longitudinal variation of neutron escape intensity follows the familiar shaped curve (Fig. II 7.6). The escapes from the end of the target show the significant fraction of neutrons which are lost by returning up the proton beam pipe.

To complete the target production Figs. II 7.7 to II 7.11 show the angular distribution for neutrons (intensity vs equal interval bins for the directional cosine to the Z axis), and the energy and angular distributions for protons and mesons. In the case of mesons, insufficient data is available to allow a break-down into the constituent $\pi^{\pm}$ and $\mu^{\pm}$ spectra.

7.2 Full System Production

The high energy escapes from the target produce a further 1.7 n° per proton incident at the target. The distribution of this production is shown in Fig. II 7.12. A very coarse bin structure of radial annulli of width 9 cm and a Z direction bin width of 4 cm is used. The majority of the production is in the Zircaloy and target pressure vessel. The forward nature of the high energy cascade is visible.

The sub-15 MeV energy neutrons will also lead to production, particularly by (n,2n) reactions in the reflector beryllium. This type of production is locked within the transport calculation and excepting for the numbers quoted within section 4 is not considered further.

7.3 Particle Escapes from the Full System

The intensities for escape particles are quoted in subsection 4.6 and the moderator fluxes considered in chapter 5, section 3.

The spectra and angular distributions (Z axis directional cosine) for high energy neutrons and protons are shown in Fig. II 7.13 to Fig. II 7.16. The probability of meson escape is too low to allow a meaningful spectrum to be constructed. The forward peaking of the proton spectrum is clearly visible.

The distribution for the low energy neutrons escaping the assembly are shown in Figs. II 7.17 and II 7.18. These distributions are from the MERCAT analysis routine (chapter 1, section 3.2) using a 60cm radius sphere about the centre of the full system. The results have been translated into units of neutrons/proton incident at the target/sr. These distributions show the voids penetrating the reflector for the proton beam to enter and for the neutrons escaping the moderators. The neutron flux returning up the proton beam is $\sim$ 5 n°/proton/sr. This will cause damage to components such as the final quadrupoles in the proton beam.

TABLE 2 - I

CALCULATED VOLUMES AND MASSES IN SYSTEM STUDIED

COMPONENT	MATERIALS	VOLUME (litres)		DENSITY g cm^{-3}	Mass kg
REFLECTOR	Be + D_2O	a) Be	134.8	1.8	242.6
		b) D_2O	33.7	1.1	37.1
NEUTRON BEAM EXIT HOLES	VOID		24.7	-	-
TARGET	^{238}U + Zircaloy 2 + D_2O	a) D_2O	5.59	1.1	6.2
		b) ^{238}U	1.806	18.7	33.8
		c) Zircaloy 2	1.8	6.57	11.8
LINER/DECOUPLER	B_4C (Powder)		8.47	1.1	9.3
PROTON BEAM ENTRANCE AND FORWARD EXIT	VOID		3.01	-	-
TARGET PRESSURE VESSEL	INCONEL+ CADMIUM		2.74	8.19	22.4
MODERATORS	H_2O		2.52	1.0	2.52
TARGET/MODERATOR VOID	VOID		1.3	-	-
		TOTAL VOL.	220.4 litres		TOTAL MASS 365.7 kg

TABLE 2 -II

NUCLEAR DENSITIES IN VARIOUS COMPONENTS

(units of nuclei $\mathring{A}^{-3}$)

1.	'Target' Geometry	(a) Uranium	^{238}U	0.0475
		(b) Coolant + Cladding#		
			^{2}H ‡	0.0515
			^{16}O	0.0258
			^{91}Zr	0.0095
			^{118}Sn	0.0001
2.	Full System			
		(a) Target Mixture	^{238}U	0.0390
			^{2}H‡	0.0091
			^{16}O	0.0045
			^{91}Zr	0.0017
		(b) Cladding#+ Coolant	^{91}Zr	0.0368
			^{16}O	0.0045
			^{2}H‡	0.0091
		(c) Coolant	Inconel*	0.013
		(Includes water flow guides to Inconel)	^{16}O	0.028
			^{2}H‡	0.056
		(d) Pressure Vessel	Inconel*	0.0843
			^{112}Cd	0.0093
		(e) Reflector	^{9}Be	0.0962
			^{16}O	0.0066
			^{2}H‡	0.0132
		(f) Moderator	^{1}H	0.0669
			^{16}H	0.0335
		(g) Liner/Decoupler	^{11}B	0.04
			^{10}B	0.01
			^{12}C	0.0125

*Inconel taken to be with following proportions by weight, ^{58}Ni 51.74%; ^{52}Cr 19.0%; ^{56}Fe 18.5%; ^{98}Mo 3.05%; ^{93}Cb 2.57%; ^{181}Ta 2.57%; ^{59}Co 1.0%; ^{48}Ti 0.9%; ^{27}Al 0.5%; ^{55}Mn 0.17%

‡For HET calculations the ^{2}H nucleus is replaced by ^{1}H.

#Cladding material taken as Zircaloy 2 with following proportions by weight, Zr 98.5%, Sn 1.5% (Fe .12%, Ni .05% and Cr .1% have been neglected).

Neutron cross sections were taken from ENDF/BIV MAT = 1284.

TABLE 2 - III

AN APPROXIMATE OVERALL ENERGY BALANCE

	MeV/proton	kW @ 200 μA
Input		
(a) 2.5×10^{13}, 800 MeV protons/pulse 50 pulses per second	800	160
(b) 3.3 fissions per proton liberate ~180 MeV per fission	594	118.8
(c) 3.6 $^{238}U(n,\gamma)^{239}U$ liberate ~4 MeV/event	14	2.8
(d) 9 $^{10}B(n,\alpha)$ liberate 2.7 MeV/event	24	4.8
	1432	286.4
Rounded	1400 MeV	290 kW
Output		
(a) Target coolant circuit (i) ^{238}U	996	
(ii) Cladding	31.9	
(iii) Can	31.8	
(iv) Coolant	25.6	
(v) Decay	45.0	
	1130.3	226.06
(b) Reflector	36	7.2
(c) Moderators	3.35	0.67
(d) Decoupler	44.55	8.91
(e) Escapes: (i) 9.88 LE n° escapes	6.9	
(ii) .83 HE n° escapes	69.0	
(iii) .022 protons	3	
(iv) .002 mesons	0.09	
	78.99	15.8
(f) Binding energy (16 escapes + thermal region, 2 evaps @ 7.5 Mev)	135	27.0
	1428.19	285.64
Rounded	1400 MeV	290 kW

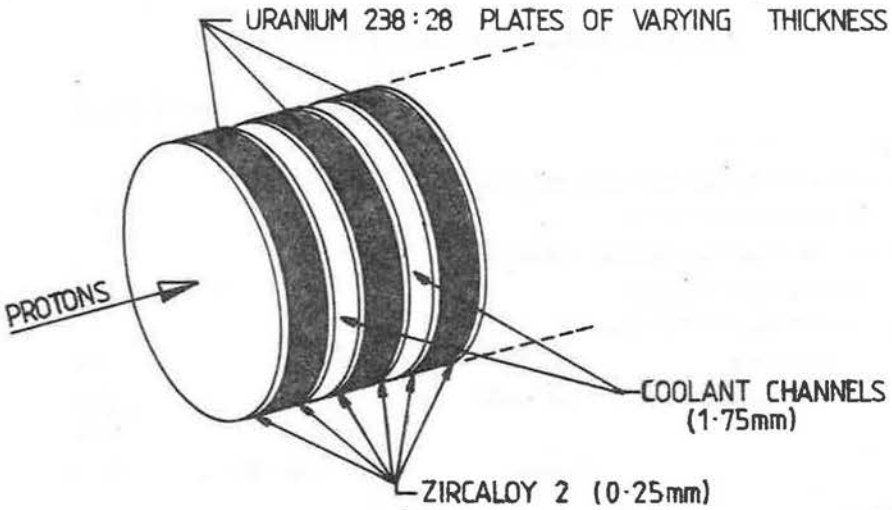

Fig II 2.1 (a): Sketch of 'Target' calculation geometry.

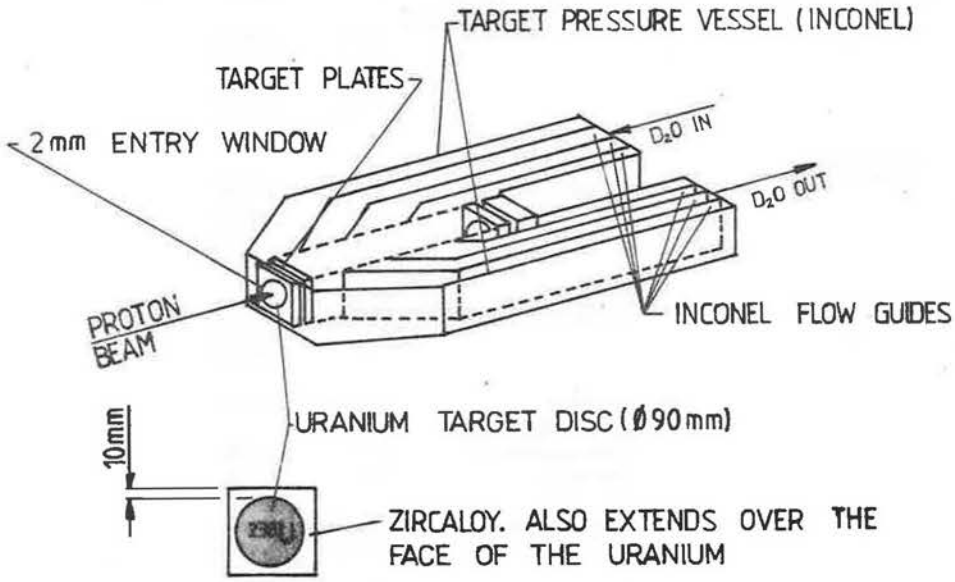

Fig II 2.1 (b): Perspective view of target assembly used in the full system calculations. This assembly fits between the upper and lower moderators in Fig II 2.2.

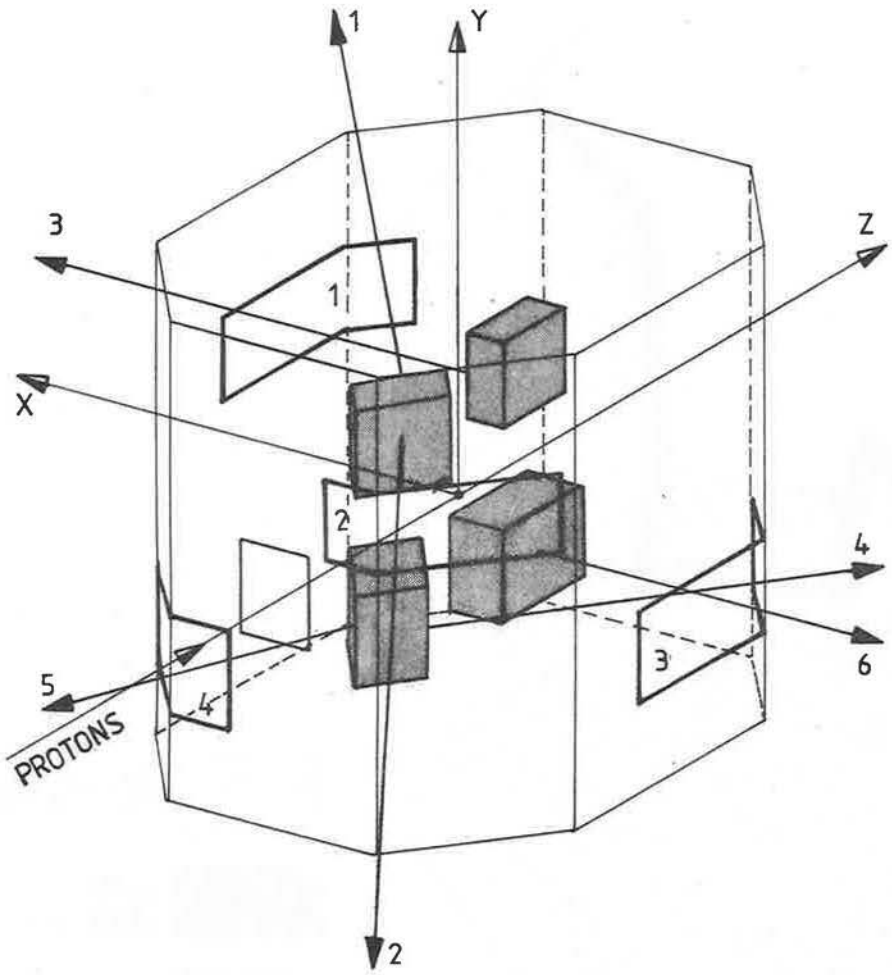

Fig II 2.2: *Perspective view of full system. The target assembly of Fig II 2.1 (b) fits between the two moderator layers; it has been omitted to aid clarity. Also included on the diagram are the coordinate system and identification numbers for moderator faces and neutron beam exit ports.*

33.925	TOP REFLECTOR LAYER FIG II 2.4 + NOTE A	13
21.425		
20.425	TOP MODERATORS UPPER LINER, FIG II 2.4 + NOTE B	12
	UPPER MODERATOR LAYER FIG II 2.4	11
7.825		
	TOP MODERATORS LOWER LINER, FIG II 2.4 + NOTE B	10
6.825		
	2MM AIR GAP (VOID)	9
6.625		
	TARGET PRESSURE VESSEL LID, FIG II 2.5 + NOTE A	8
5.525		
0.0	TARGET LAYER FIG II 2.5 DETAILS OF TARGET VESSEL ARE SHOWN IN FIG II 2.6	7
-5.525		
	TARGET PRESSURE VESSEL BASE, FIG II 2.5 + NOTE A	6
-6.625		
	2MM AIR GAP (VOID)	5
-6.825		
	LOWER MODERATORS UPPER LINER, FIG II 2.4 + NOTE B & C	4
-7.825		
	LOWER MODERATOR LAYER FIG II 2.4 + NOTE C	3
-20.425		
	LOWER MODERATORS LOWER LINER, FIG II 2.4 + NOTES B & C	2
-21.425		
	LOWER REFLECTOR LAYER FIG II 2.4 + NOTE A	1
-33.925		

Fig II 2.3: *Arrangement of vertical layers of full system geometry. The figures II 2.4 and 2.5 give details in conjunction with notes.*

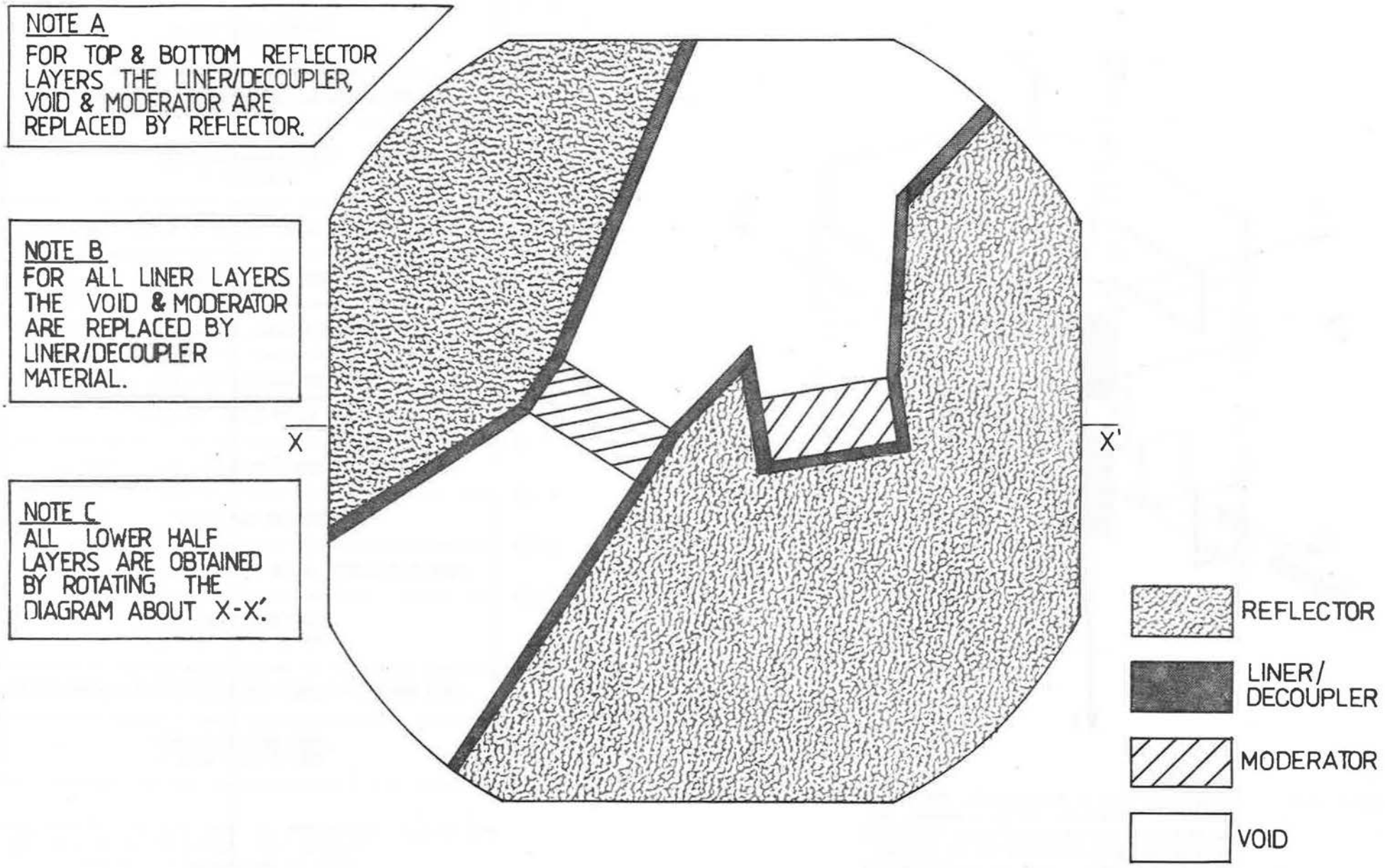

Fig II 2.4: *Layout of moderator, reflector and liner layers. This Diagram in conjunction with the notes is used to show 8 of the layers of Fig II 2.3.*

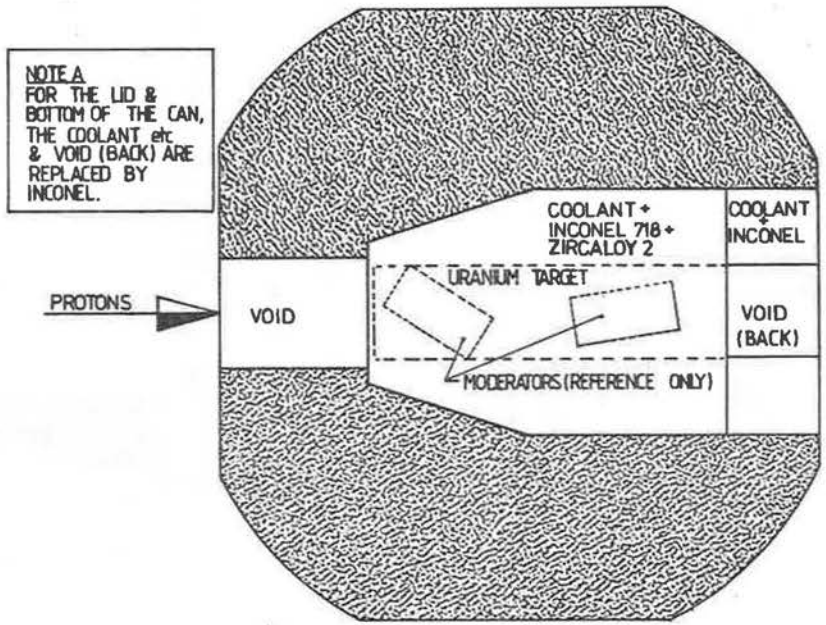

Fig II 2.5: *Layout of target level layers. The upper level moderators positions are shown for reference. Details of the target pressure vessel are shown in Fig II 2.6.*

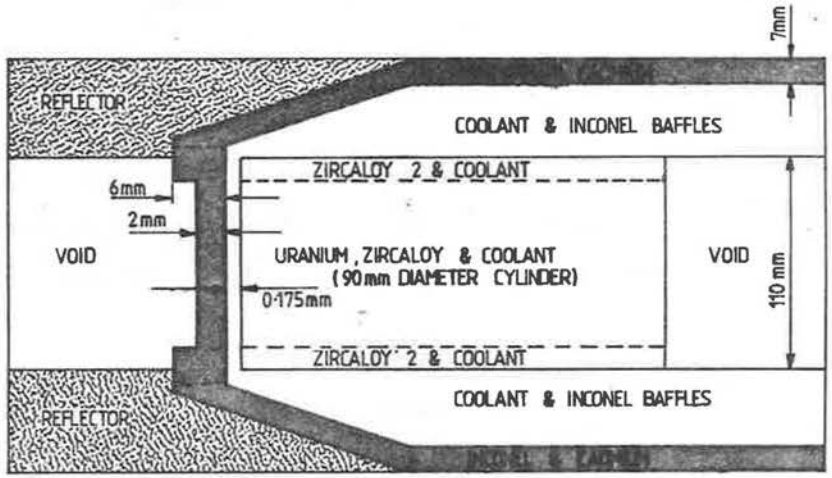

Fig II 2.6: *Sketch (not to scale) to show details of target pressure vessel.*

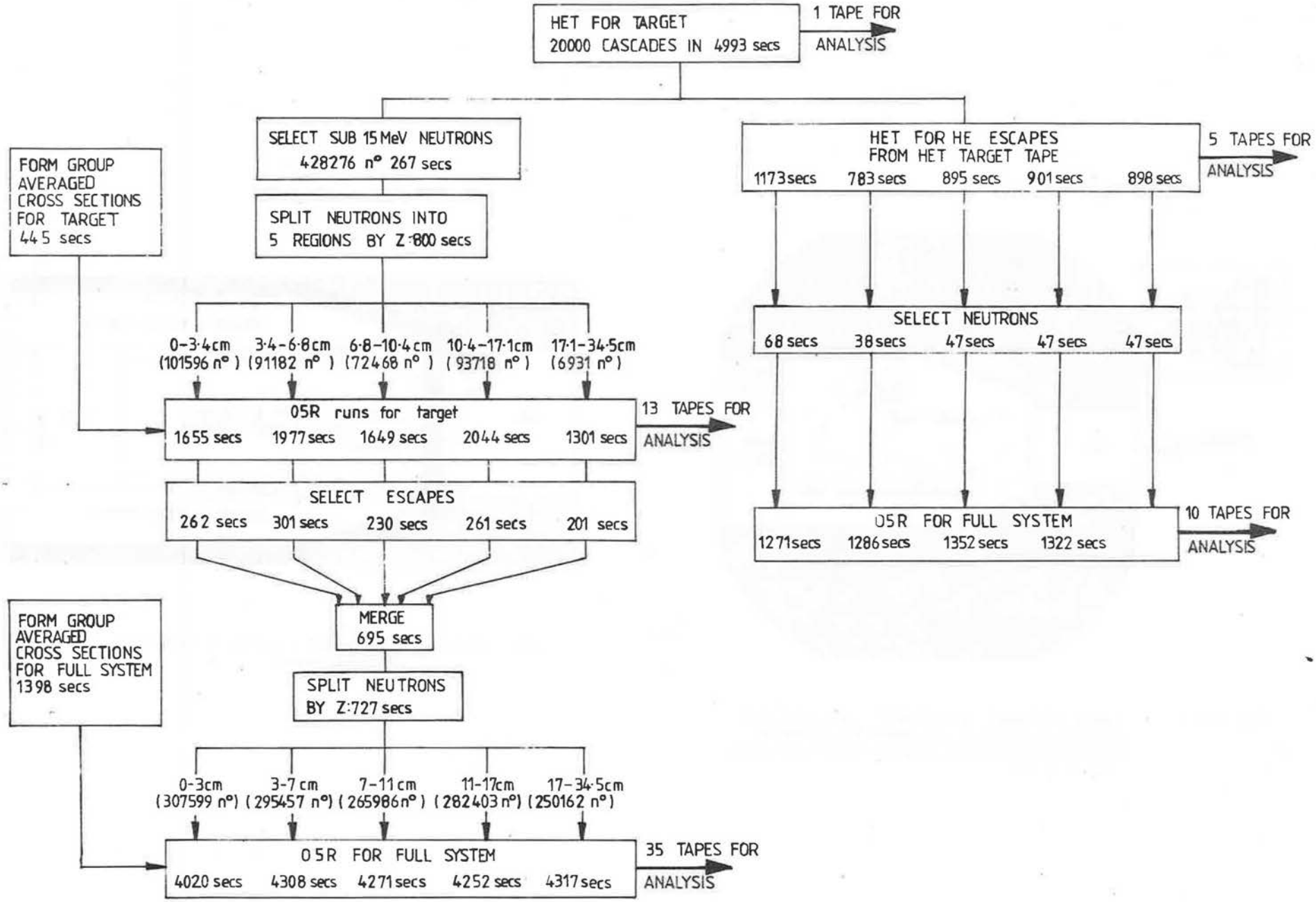

Fig II 3.1: A schematic flow diagram for the various stages of the transport calculation.

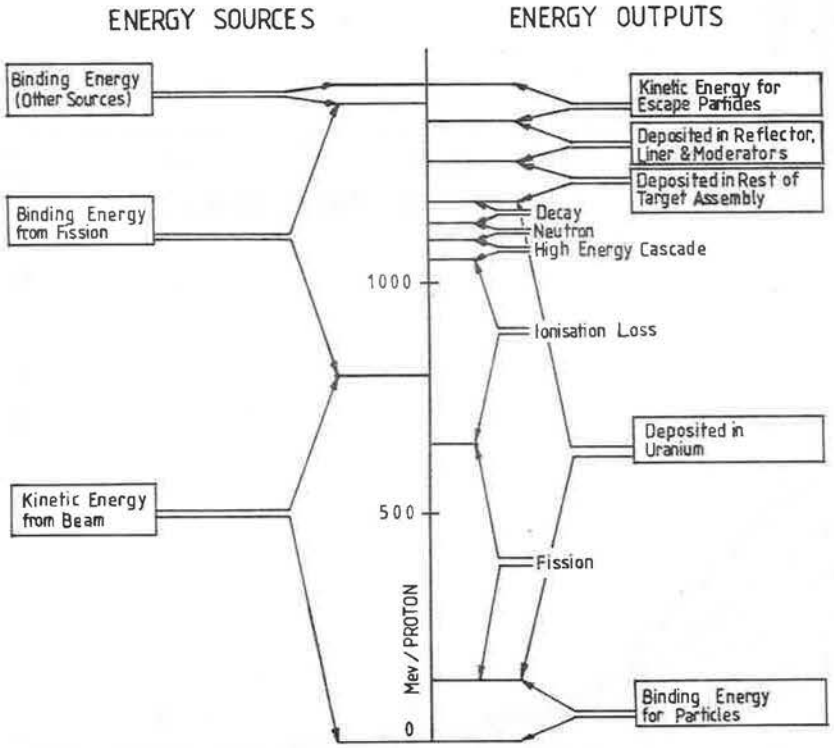

Fig II 4.1: Energy balance for the Target, reflector, moderator assembly.

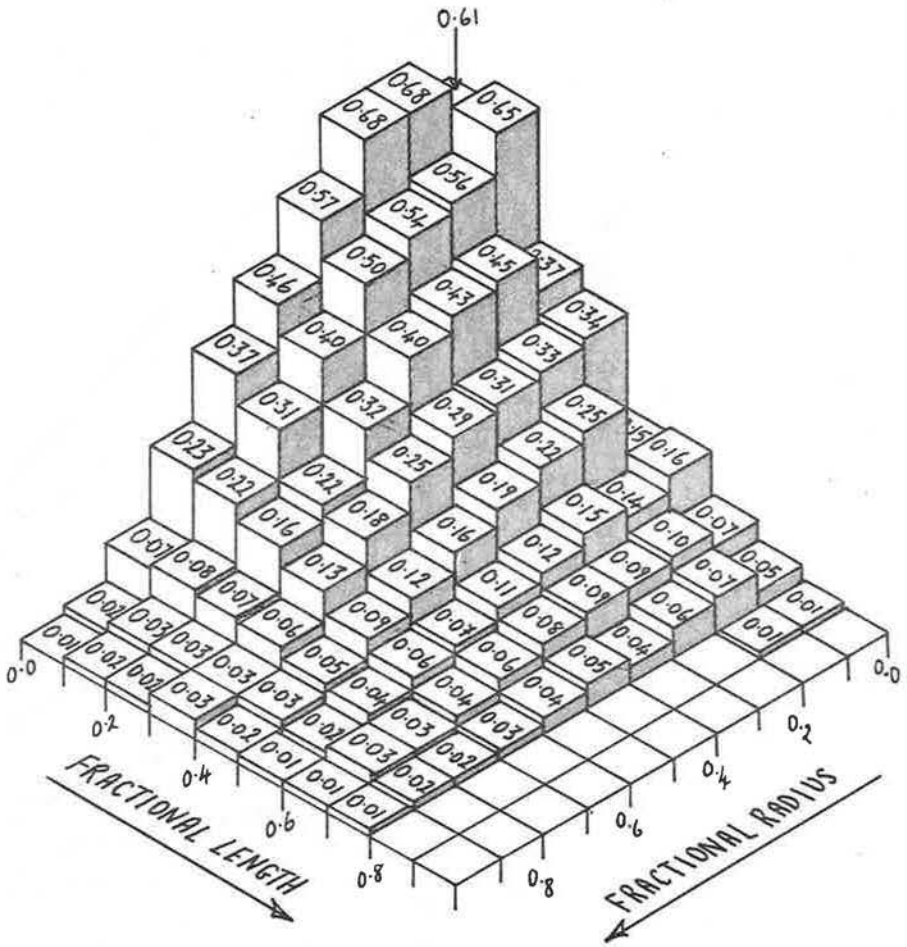

Fig II 7.1: Sub 15 MeV neutron production by primary incident 800 MeV protons and the cascade in the 'Target'. Numerical values are neutrons/10cm^3/incident proton. The 'Target' radius is 45mm amd length 347mm.

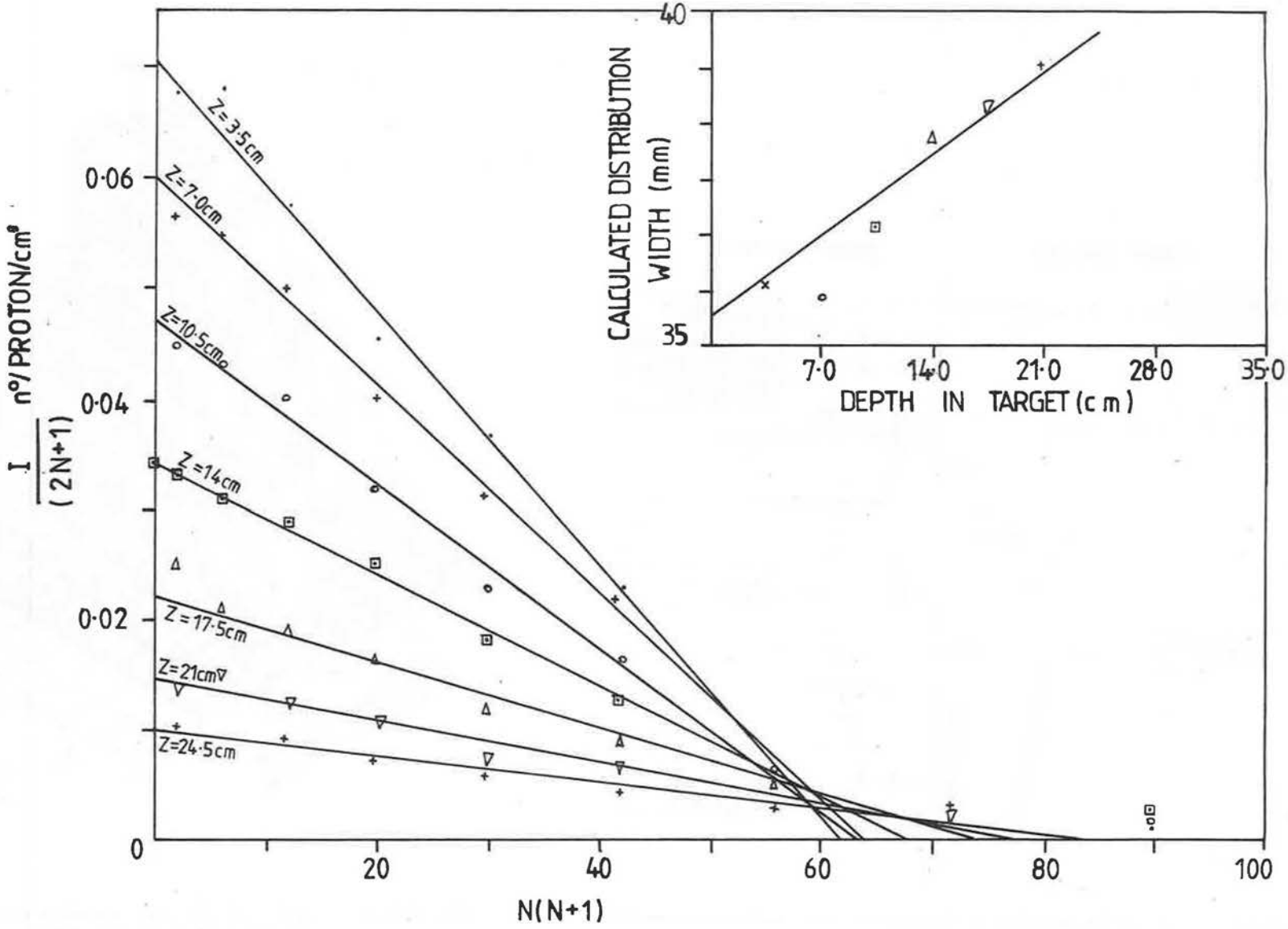

Fig II 7.2: *Comparison of transverse distribution of sub 15 MeV neutron production, with a parabolic type. N is the radial bin number for uniform radial intervals. The lines are marked with the upper limit of depth for 3.5cm bins in Z direction. Inset shows calculated distribution widths with depth from fits.*

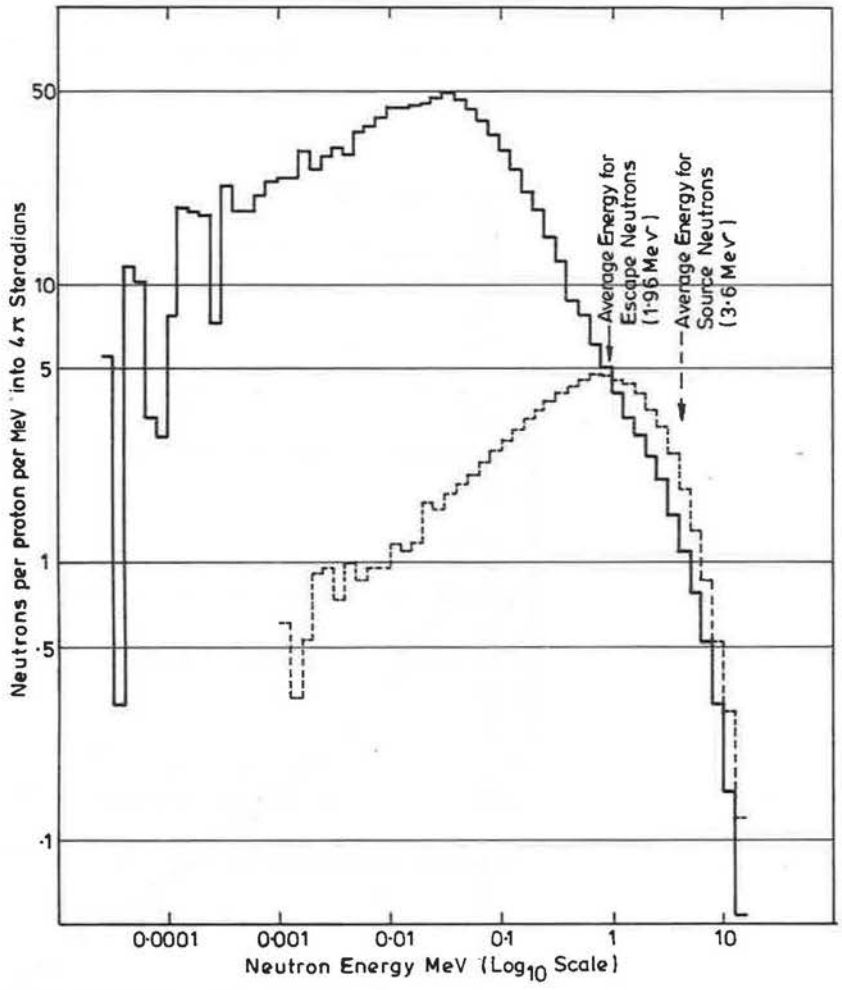

Fig II 7.3: *Energy spectra for sub 15 MeV neutrons produced (dashed histogram) and escapes from 'Target' (full line): Note the logarithmic energy scale and the scaling to unit energy bin.*

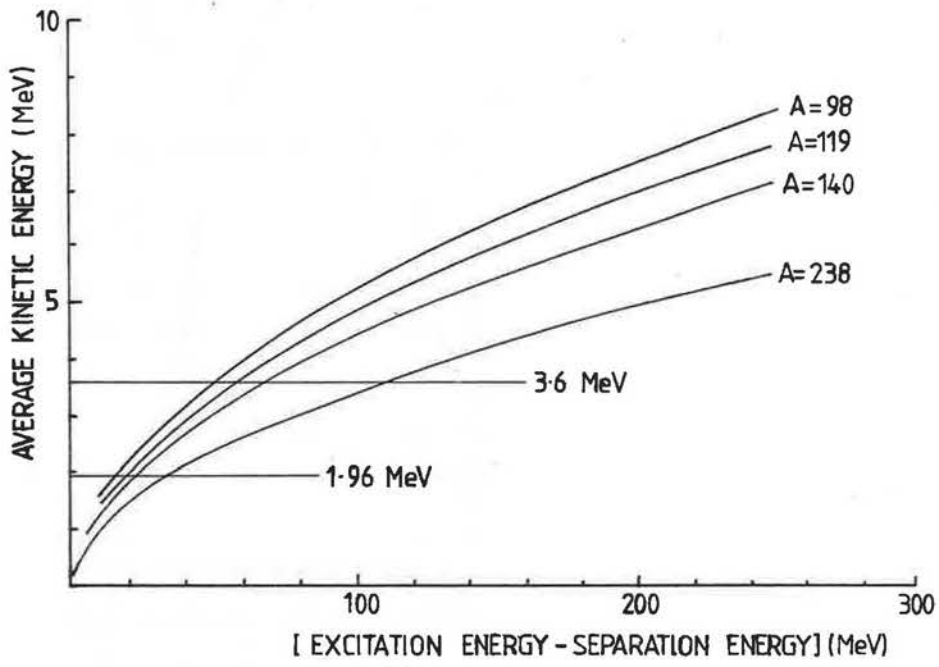

Fig II 7.4: *Average kinetic energies for evaporated neutrons as a function of nuclear excitation minus separation energy for masses typical of uranium interactions. The two horizontal lines at 3.6 and 1.96 MeV show the mean energy for cascade production and target escape neutrons.*

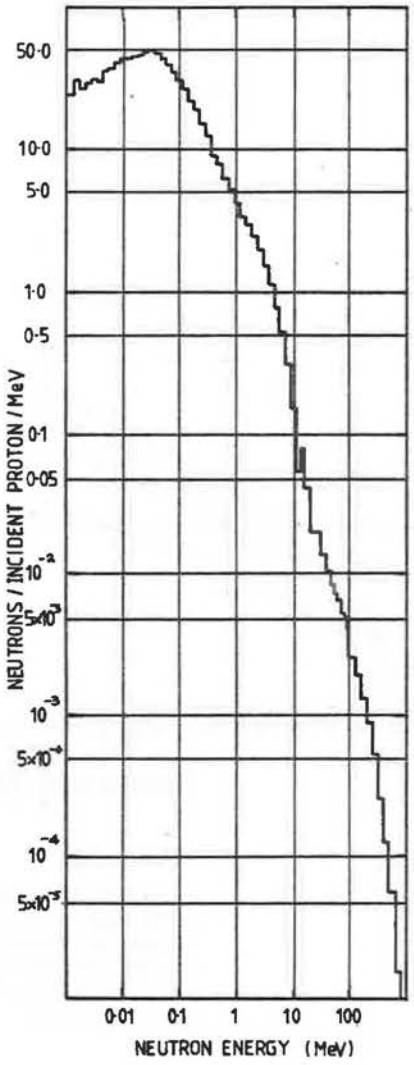

Fig II 7.5 (a): Log-log spectrum for 'Target' escape neutrons in energy region 1 KeV to 800 MeV.

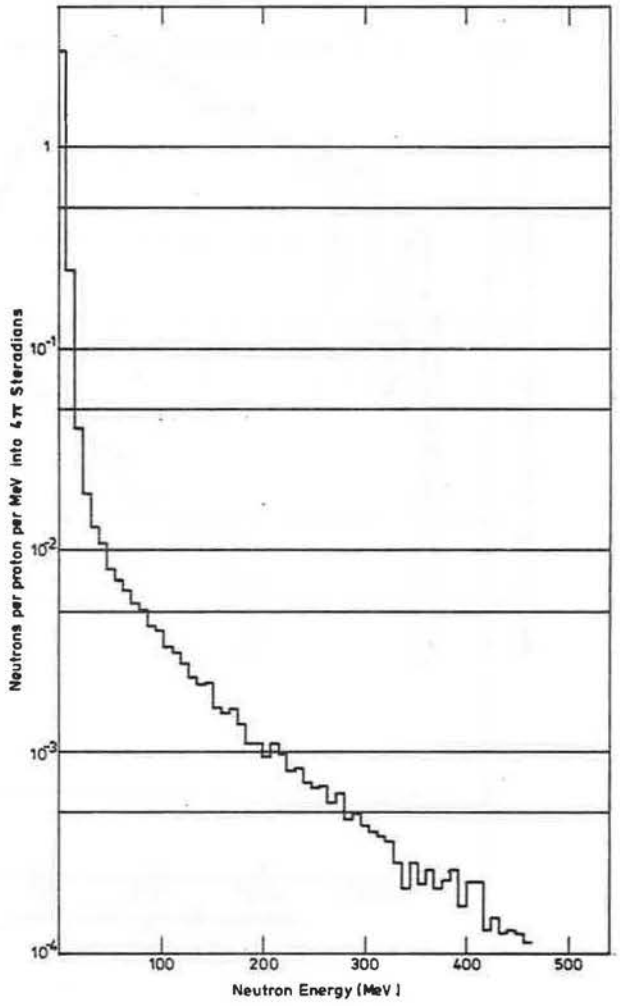

Fig II 7.5 (b): 'Target' escape neutrons of Fig II 7.5 (a) on a linear energy scale.

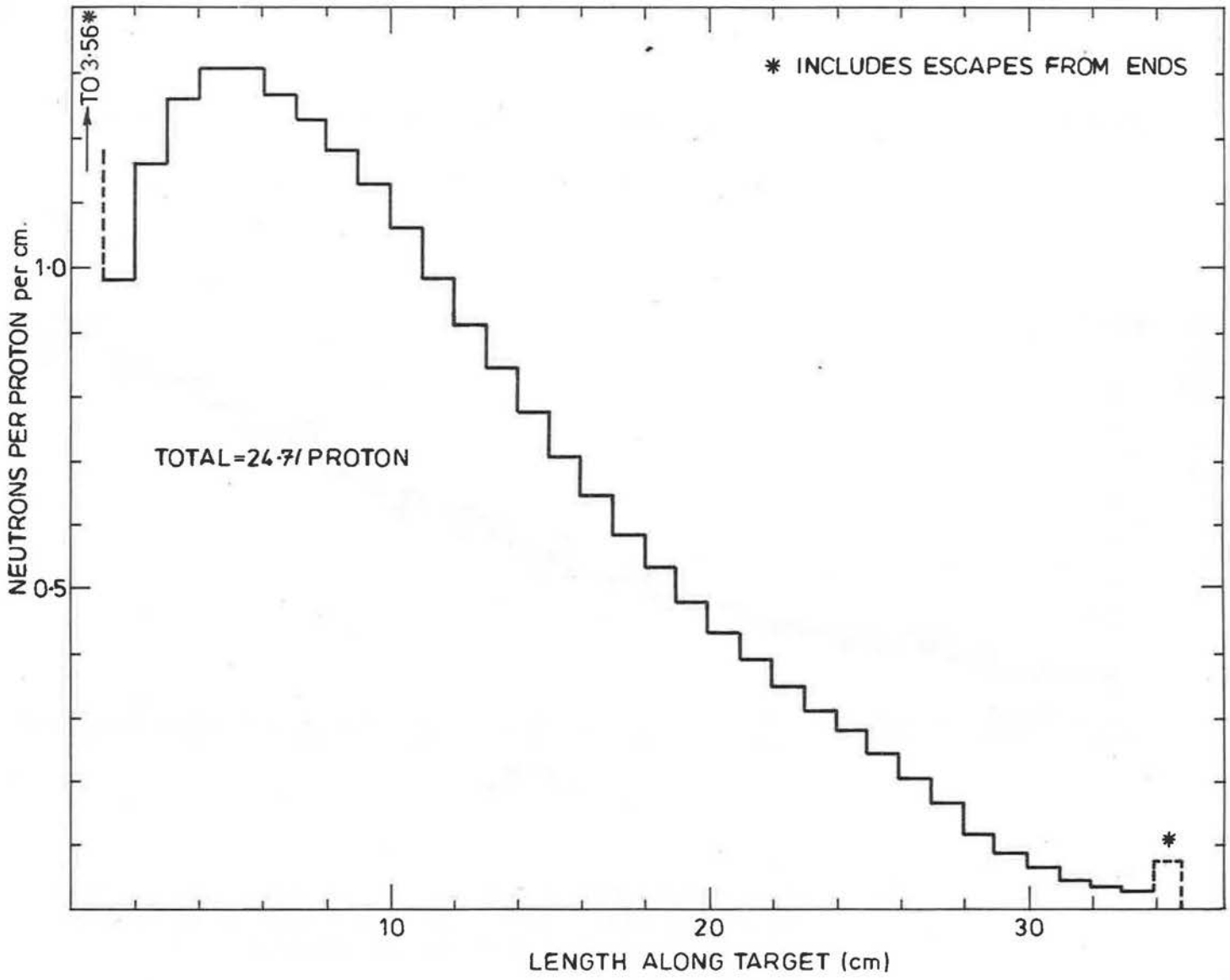

Fig II 7.6: *Sub 15 MeV escapes from target surface. Note the first and last bins include the end escapes.*

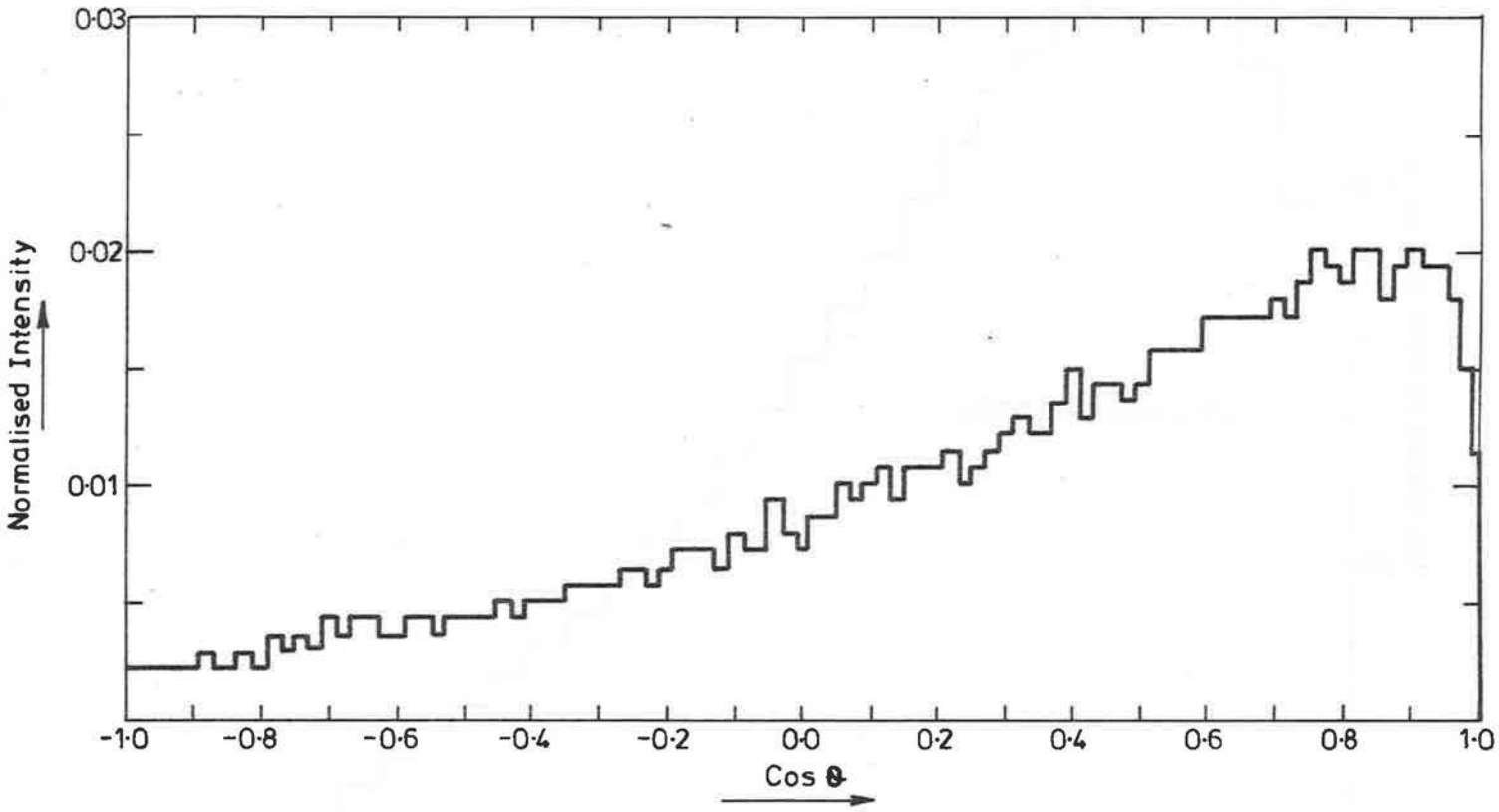

Fig II 7.7: *Angular distribution for high energy neutron escapes from 'Target' cylinder. The total intensity is normalised to 1.0. Cos Θ is the directional cosine to the Z axis (proton beam direction).*

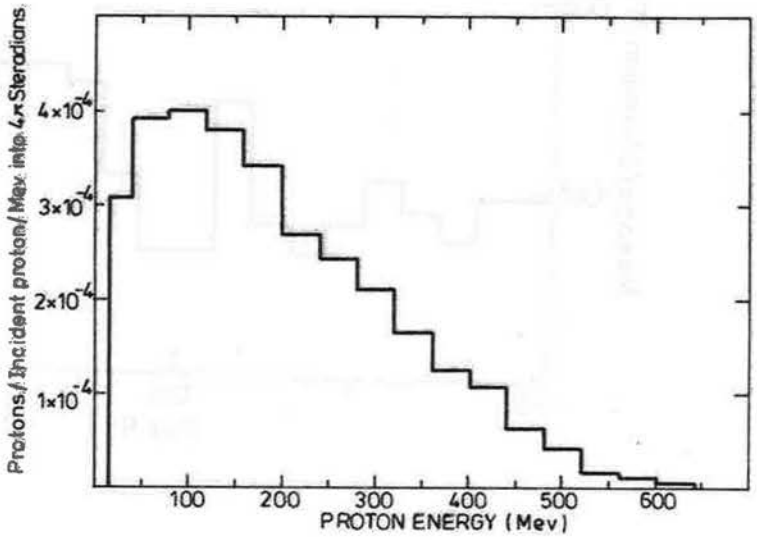

Fig II 7.8: *Energy distribution for proton escapes from the 'Target'.*

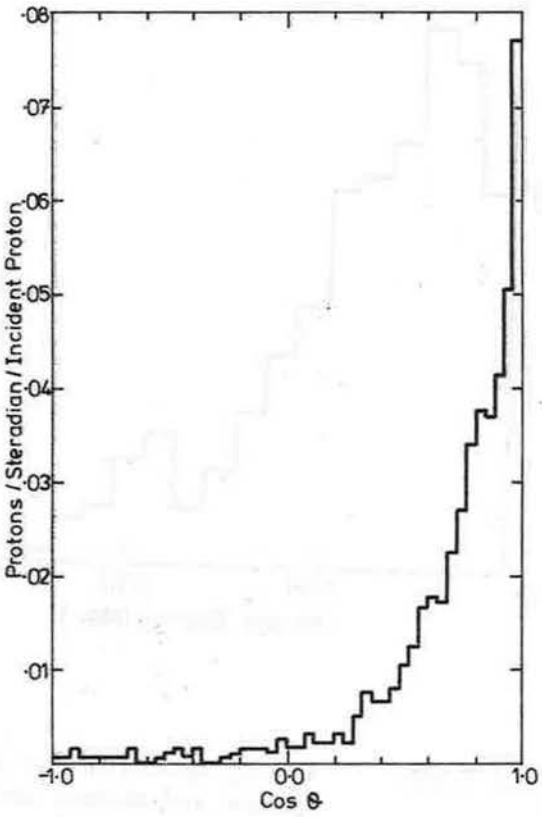

Fig II 7.9: *Angular distribution for proton escapes from the 'Target'. Cos θ is the directional cosine to the Z axis.*

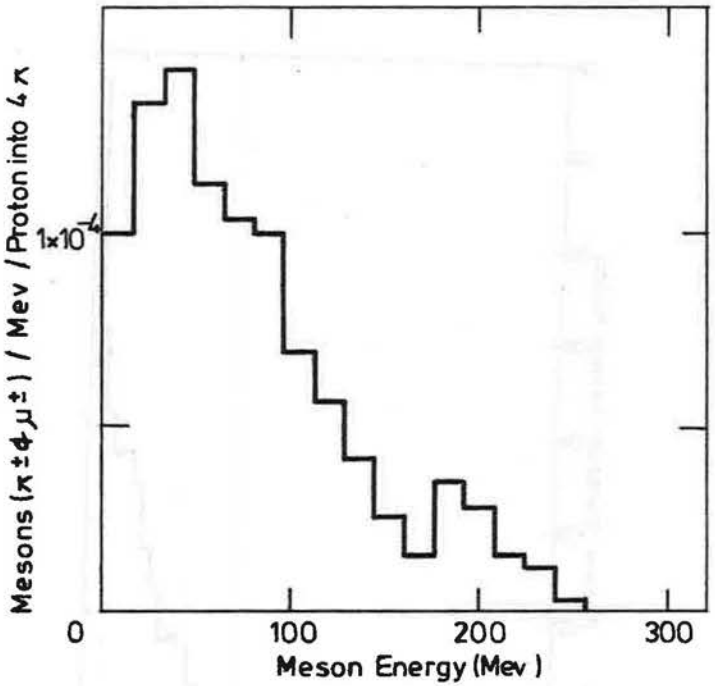

Fig II 7.10: *Energy spectrum for meson (pions and muons) escapes from the 'Target'.*

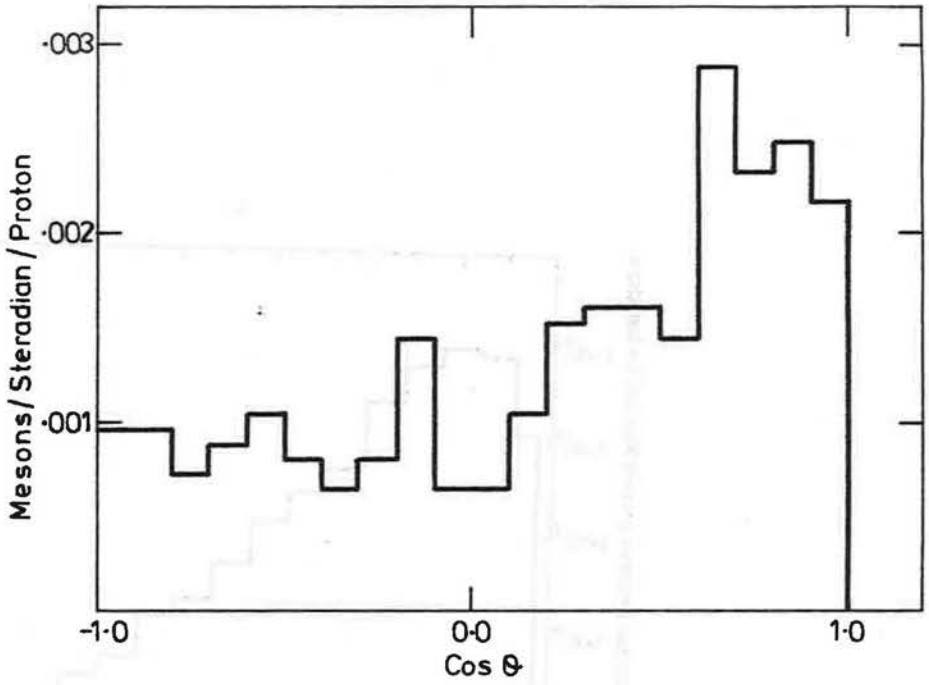

Fig II 7.11: *Angular distribution for meson escapes from the target. Cos Θ is the directional cosine to the Z axis.*

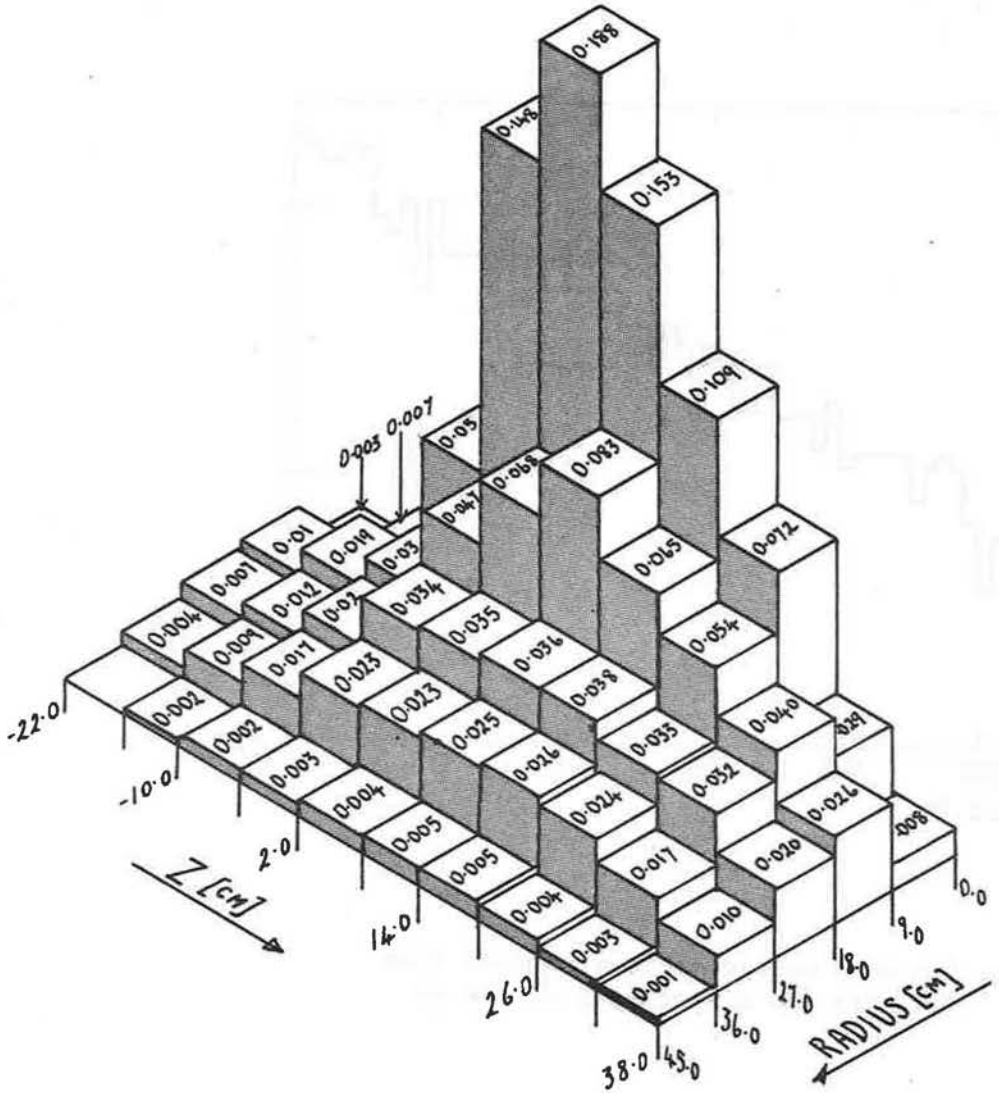

Fig II 7.12: *Neutron production by high energy escapes from the 'Target' in the full system. Intensities are neutrons per proton. Bins are (large) cylindrical annuli about the Z axis.*

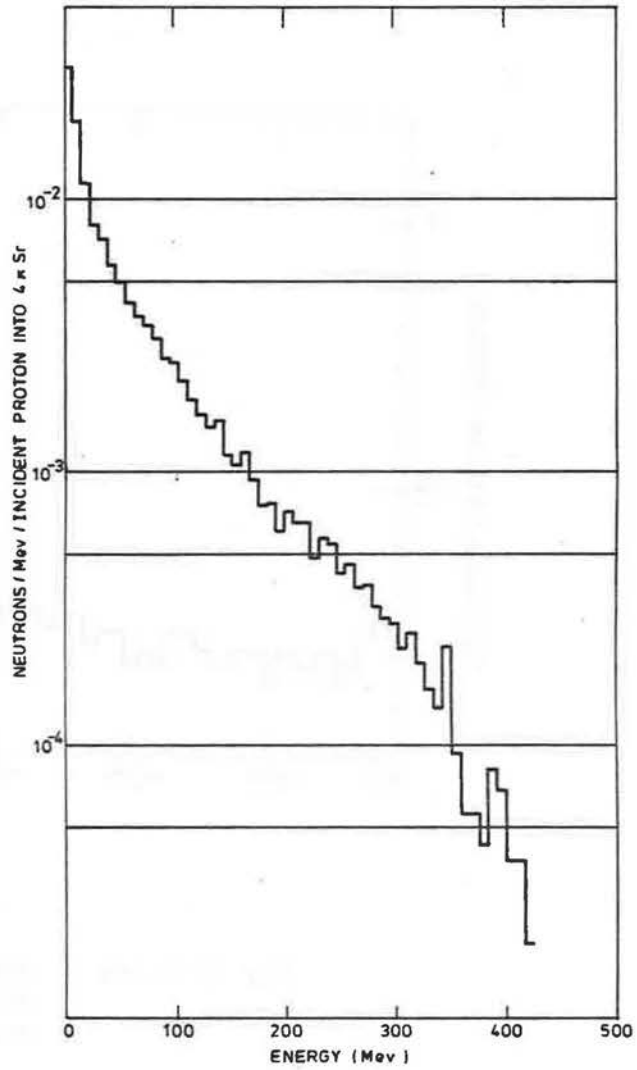

Fig II 7.13: *Energy spectrum for high energy neutron escapes from full system.*

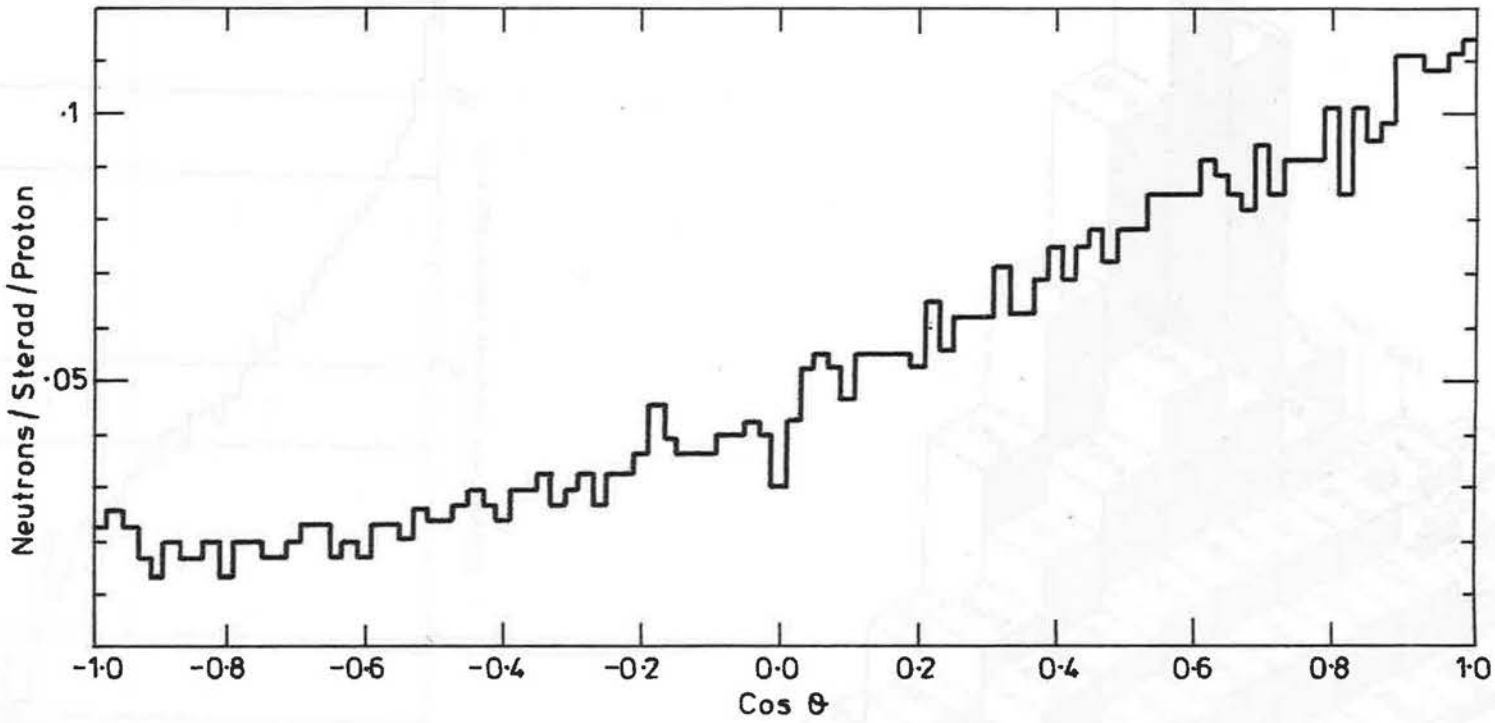

Fig II 7.14: *Angular distribution for high energy neutron escapes from full TRAM assembly. Cos θ is the directional cosine to the Z axis.*

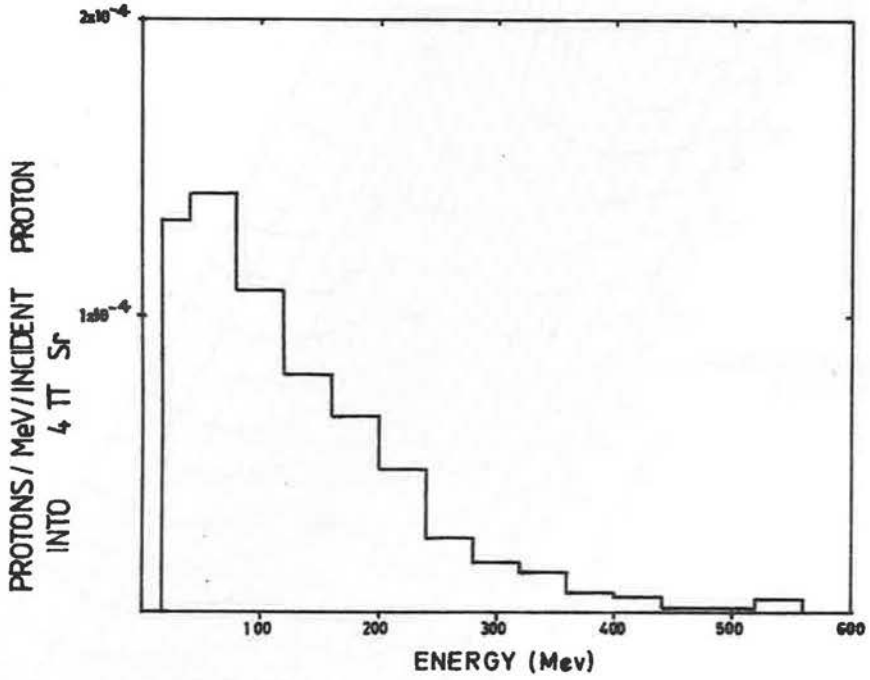

Fig II 7.15: *Energy distribution for proton escapes from the full TRAM assembly.*

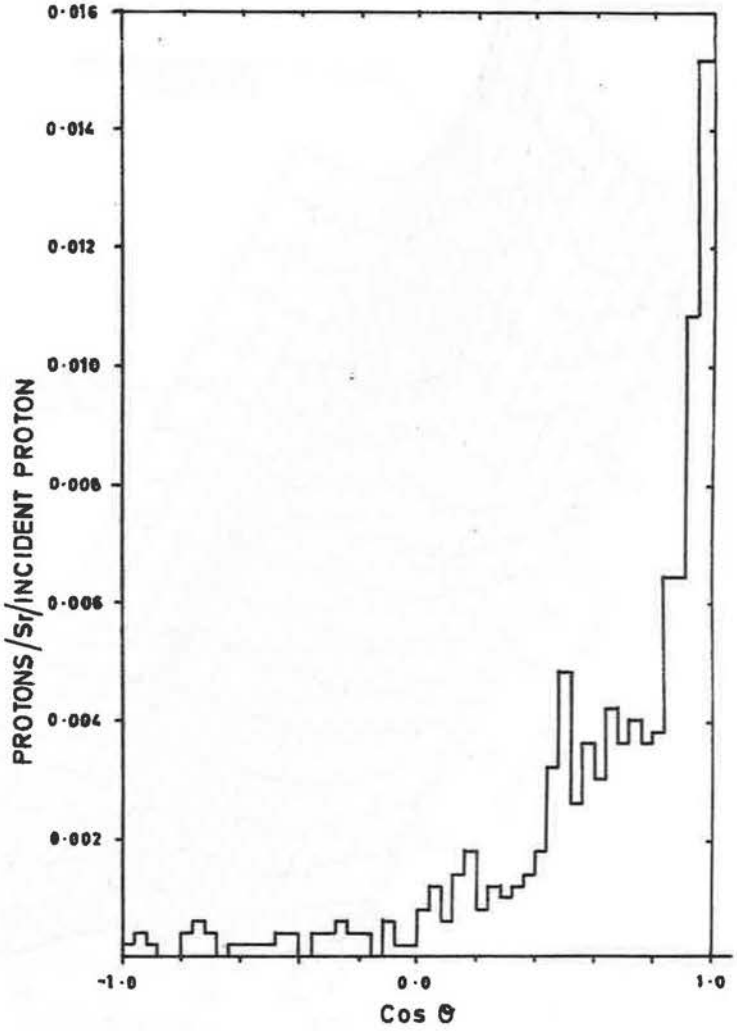

Fig II 7.16: *Angular distribution of proton escapes from TRAM assembly, Cos Θ is the directional cosine to the Z axis.*

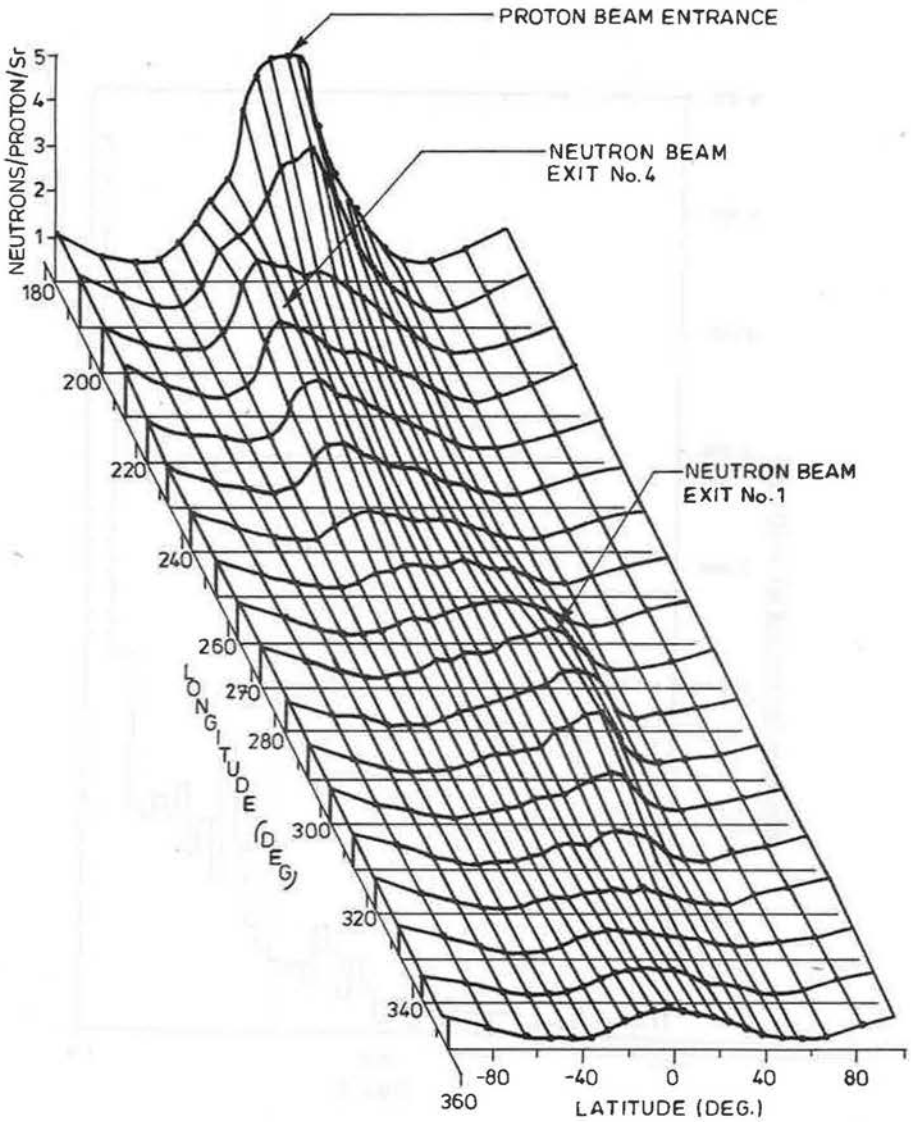

Fig II 7.17: Distribution of neutron escapes from TRAM assembly for energies ≲ 15 MeV and positive X hemisphere. Results are for MERCAT (qv Chapter 1 Section 3.2) with a 60cm diameter sphere.

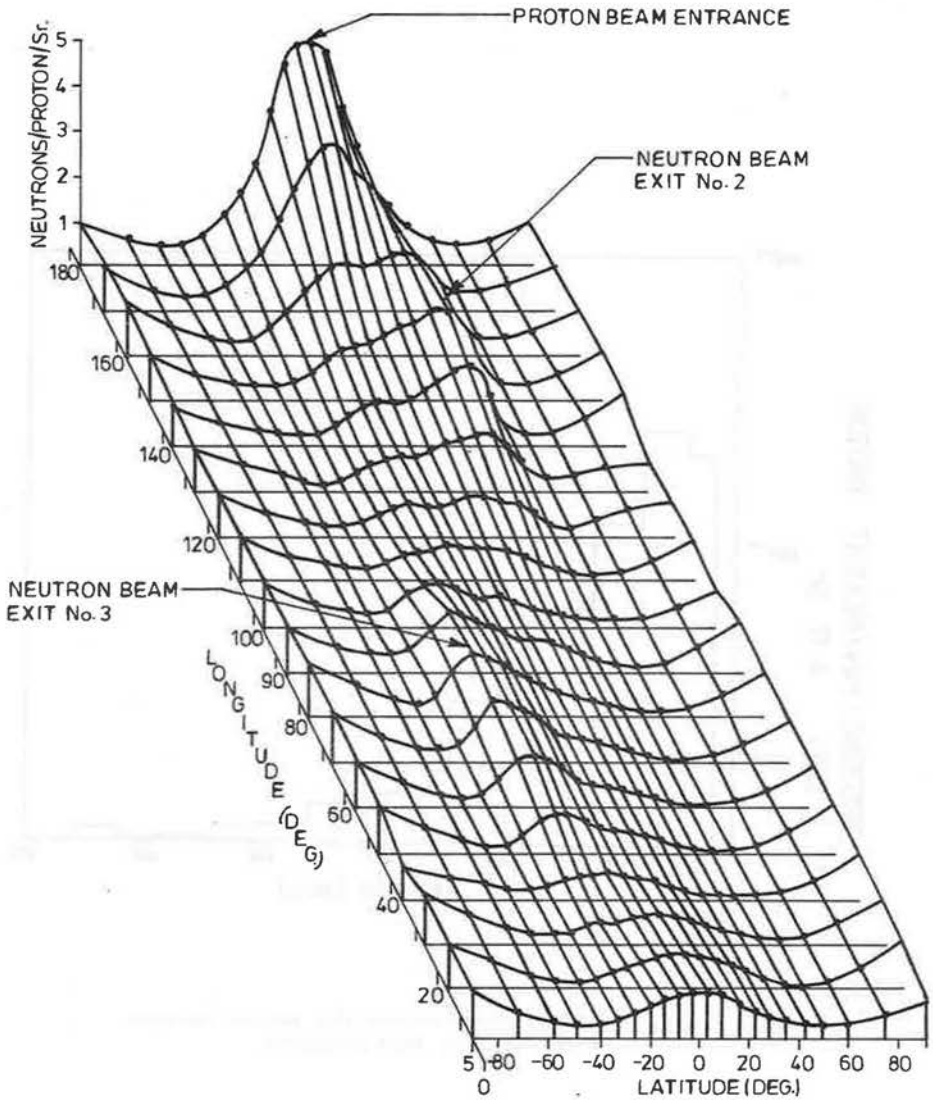

Fig II 7.18: As for Fig II 7.17 but for the negative-X hemisphere.

CHAPTER 3

TARGET RESULTS

1. INTRODUCTION

For the purpose of the modelling the target is taken to be the 9 cm diameter by 34.7cm long cylinder containing all the uranium. Part of the cladding and coolant channels will also be included. The layout of the target may be seen in the perspective view of Fig. II 2.1(a). The parameters for the target are now listed.

Target material	100% ^{238}U of density 18.7 g cm^{-3}	
Cladding material	Zircaloy 2 (98.3% Zr + 1.7% Sn) density 8.87 g cm^{-3}	
Coolant	D_2O of density	1.1 g cm^{-3}
Uranium disk diameter	9.0 cm	
Uranium disk thickness	(i) 12 @ 0.65 cm	
	(ii) 4 @ 0.85 cm	
	(iii) 4 @ 0.95 cm	
	(iv) 4 @ 1.25 cm	
	(v) 2 @ 1.75 cm	
	(vi) 2 @ 2.45 cm	

Total number of plates	28
Total length of uranium	28.4 cm
Thickness of cladding on each surface	0.025 cm
Total length of Zircaloy	1.4 cm
Width of coolant channels	0.175 cm
Total length of D_2O	4.9 cm
Total length of 'Target'	34.7 cm
Total volume of uranium	1.806 litres
Total mass of uranium	33.8 kg

The target is made up from 28 plates consisting of Zircaloy 2 clad uranium disks of six different thicknesses. These thicknesses were calculated using energy densities from an earlier study[16]. It is not certain that the thickest plates can be manufactured and they may be replaced by thinner ones; the effect of this will require separate consideration.

In the next few subsections, the results from the transport calculation relevant to the target are collected together and some of their consequences presented.

2. SPECIFIC POINTS CONCERNING TRANSPORT CALCULATIONS

Although these have been raised elsewhere, some specific points about the transport calculation are relevant to the target.

(1) For high-energy transport the plate structure is modelled with two materials; U and a mixture of Zr, Sn, H & O. Code limitations in HET do not allow for treatment of collisions with deuterium and the deuterons are replaced by protons, or in other words the D_2O is replaced by ordinary water of density 1.1 g cm^{-3} .

(2) For neutron transport the deuterium is restored. The ^{238}U cross sections were obtained by unfolding ENDF/BIV resonance data. The resonances were NOT Doppler broadened.

(3) For all runs with the target in the full system, the plate structure is not included and the target replaced by a cylinder containing a uniform mixture of ^{238}U, Zr, ^{2}H (or ^{1}H for HET runs) and O nuclei. The plate structure gives a systematic variation of the relative proportions of these nuclei which has been ignored.

3. RESULTS FROM TRANSPORT CALCULATION

3.1 HET for target

800 MeV protons incident on the first plate started assuming a uniform density in 4-D ellipsoidal phase space of 300 x 250 (mm mrad)^2, with a double waist configuration of width 70 mm in both planes. All results are normalised to per proton incident at the target.

High energy particle induced fissions	1.3
^{238}U spallation events	.42
Coolant and cladding spallations	.11
Total energy deposited in ^{238}U	630 Mev
Total energy deposited in coolant and cladding	16 Mev
Sub-15 MeV neutrons produced	21.4
Total kinetic energy for sub-15 MeV neutrons	77 MeV
HE neutron escapes from target cylinder	1.4
Kinetic energy of these neutron escapes	110 MeV
Proton escapes	0.12
Kinetic energy of the proton escapes	23 MeV
π^0 production	.088
Kinetic energy of π^0's	5.7 MeV
Meson escapes ($\pi\pm$ & $\mu\pm$)	.017
Kinetic energy of meson escapes	1.4 MeV
Cascade protons ranged out	1.5
Spallation fragments (i) Protons	.48
(ii) Deuterons	.13
(iii) Tritons	.06
(iv) ^3He	.004
(v) ^4He	.12

3.2 05R for Target

The 21.4 neutrons of sum energy 77 MeV (per incident proton) created during the

HET run of Section 3.1 are transported from their production point to the surface of the target. All numbers are normalised to per 800 MeV incident proton.

Neutron escapes from surface of target	24.7
Total kinetic energy of neutron escapes	48.3 MeV
Neutron account	
(a) Created by fission	5.5
(b) Created by (n,xn) reactions	0.7
(c) Lost by absorption and inducing fission	2.9
Total energy deposited in ^{238}U	330 MeV
Total energy deposited in coolant and cladding	7.3 MeV
Neutron events in ^{238}U	
(a) ^{238}U (n,n) ^{238}U	55.2
(b) ^{238}U (n,n´) ^{238}U	11.1
(c) ^{238}U (n,(xn)f)	1.8
(d) ^{238}U (n,γ) ^{239}U	1.1
(e) ^{238}U (n,2n) ^{237}U	0.51
(f) ^{238}U (n,3n) ^{236}U	0.02

3.3 Transport through the Full System

These results are the combination of three separate calculations. (i) The transport of low energy neutron escapes from the target run of section 3.2. (ii) The transport of the high energy escapes from the target run of section 3.1. (iii) The transport of Sub 15 MeV neutrons created by the extension of the high energy cascade outside the target. All numbers are normalised to per 800 MeV proton incident at the target.

Total energy deposited within the target cylinder	37 MeV
High energy particle induced fissions	4×10^{-3}
Neutron induced events	
(a) ^{238}U (n,n) ^{238}U	52
(b) ^{238}U (n,n´) ^{238}U	3
(c) ^{238}U (n,γ) ^{239}U	2.6
(d) ^{238}U (n,(xn)f)	0.16
(e) ^{238}U (n,2n) ^{237}U	0.03
(f) ^{238}U (n,3n) ^{236}U	6×10^{-4}

4. ENERGY DEPOSITION

4.1 Total Energy

The contributions come from sections 3.1, 3.2 and 3.3; for the last one we have a value for the target cylinder and the energy is apportioned between the three sections, ^{238}U, cladding and coolant in the following way. Fission leads to an average deposition of 160 MeV, hence the 0.16 fissions will be responsible for 26 MeV. The remaining 11 MeV is split according to the collision densities which are 58 in ^{238}U, 2 in ^{16}O, 3.4 in ^{2}H and 2 in Zr; that is ~ 90%, or 10 MeV assigned to ^{238}U.

Hence the ^{238}U deposited energy is:

(i)	HET for target	630 MeV/proton
(ii)	05R for target	330 MeV/proton
(iii)	Full system transport	36 MeV/proton
(iv)	Nuclide decay	45 MeV/proton
	Total	1041 MeV/proton

The nuclide decay contribution is estimated from the (rounded) value of 9 kW after ~ 6 months irradiation at 200 μA (see subsection 5.6)

For 200 μA proton beam the power in the uranium (rounded to 2 figures) is:

210 kW

N.B. There are more contributions to add to obtain the total thermal load on the coolant system. q.v chapter 4, section 2.3

4.2 Energy Distribution

Sufficient information is available to estimate the distribution of energy throughout the target volume for the two 'target' runs: These

contribute 92% of the total energy. The remaining energy is distributed on the following basis:-

The main contribution (∿ 33 Mev/proton) from the full system calculation comes from the target neutron escapes. The bulk of these should come from reflection by material close to the target and will therefore have a longitudinal distribution following the longitudinal distribution of neutron escapes. The radial distribution should be reasonably uniform. Hence the full system contribution is distributed according to the total energy deposition in each plate and the energy per unit volume assumed uniform across each plate.

The decay power should follow the 'target' runs energy deposition.

The calculated peak depositions in MeV cm^{-3} proton $^{-1}$ are shown in Fig.III 4.1. Also shown in this figure are the peak power densities used in the original plate thickness computation (these include a safety factor). In Fig. III 4.2 is shown the total energy deposition for each plate expressed as MeV cm^{-1} proton $^{-1}$. The peak values of Fig. III 4.1 show considerable fluctuations and a smoothed set of values obtained by the following procedure. On the assumption of a parabolic distribution, we may estimate distribution widths - these are plotted in Fig. III 4.3. From the earlier bins a linear growth rate for the distribution is estimated and these widths then used to re-estimate the peak values. The results of this smoothing are shown in Fig. III 4.1.

The energy distribution should reflect the distribution of other quantities of interest and two useful quantities are the peak to average for both the volume and depth variations. The peak to average energy density is 7.5 and the peak to average of energy per cm 2.3.

4.3 Temperatures

The plate thicknesses were estimated [17] on the basis of energy depositions calculated in a 10 x 10 x 30 cm^3 solid and isolated ^{238}U block [16]. The main criterion was to limit the maximum temperature

reached by the uranium to 400°C. The final choice being based on attempting to maximise the overall uranium density in the divided target whilst allowing for practicality of plate manufacture and coolant system design. The uranium disk diameter was selected on the basis of an overall optimisation [16] and the smaller dimensions have led to a reduction of total energy deposition.

The centre-line uranium temperatures for each plate have been recalculated using the smoothed peak energy deposition values (Fig. III 4.1). These temperatures along with other relevant information are given in Table 3-I, with the details of the calculation given in Appendix 3 - A at the end of this chapter. Plates 2 and 3 reach the maximum centreline temperature of 348°C. The increase of energy deposition by ~ 30% would result in the maximum reaching 400°C; this could also be caused by a 15% decrease of the distribution width were the total energy in the plate to remain constant.

Note added in proof.

Tests carried out recently, indicate that the heat transfer mechanism for the target plate to the coolant will be 'forced-convection' rather than 'nucleate-boiling' as assumed in Appendix 3-A. The consequence of this is that the temperature estimates in Table 3-I may be too high; the overestimates, ΔT_{oE}, are approximately given by:-

$$\Delta T_{oE} = T_{cool} + \Delta T_{sat} - Q/h$$

Where T_{cool} and ΔT_{sat} are defined in Appendix 3-A, Q is the power flux density and h the heat transfer coefficient for forced-convection.

The current estimates for h indicate that ΔT_{oE} is of the order of 70°C.

---

5. ACTIVATION

The activation has been calculated using the ORIHET code, a modified version of the ORNL code ORIGEN (qv chapter 1, section 3.3). This performs a build-up and a decay calculation using the production rates from the transport calculation. Collecting together the relevant

information from section 3, the channels leading to activation are:

High energy particle induced fissions	1.3 per incident proton
Neutron induced fissions	1.96 per incident proton
^{238}U spallations	0.42 per incident proton
^{238}U (n,2n) ^{237}U	0.54 per incident proton
^{238}U (n,3n) ^{236}U	0.021 per incident proton
^{238}U (n,γ) ^{239}U	3.61 per incident proton

For the ^{238}U spallations, the predictions of the nuclides from HET are used. These are illustrated in Fig. III 5.1 as a contour plot in the charge-mass plane. A cross denotes the position of the parent uranium nucleus. The contours represent a hill. The incident particle energies inducing the spallations are shown in Fig. III 5.2.

HET's direct predictions are used for the nuclide production by high energy fission. These masses are again represented by contours in the (Z -A) plane in Fig. III 5.3.

The nuclear excitations prior to the start of evaporation are shown in Fig. III 5.4.

For neutron induced fissions a different procedure has been adopted. The mass distribution in O5R is obtained by random sampling from a "known" distribution and with post scission nuclear de-excitation a more predictable process than in the case of high energy fission. The nuclide distribution function depends on the energy of the fission inducing neutron

The O5R history tapes have been analysed to give the energy spectrum for the neutrons inducing fission. This will in effect be the neutron spectrum weighted by the fission cross section, i.e.

$$\Psi(E) = \int_{E}^{E+\Delta E} \phi(E) \frac{\sigma_f(E)}{\sigma_t(E)} \, dE \qquad 3.5.1$$

where $\phi(E)$ is the neutron spectrum, and $\sigma_f(E)$ & $\sigma_t(E)$ the fission and total cross sections. This is shown in Fig. III 5.5. The mass distribution function is discussed in Appendix 3-B and the resulting mass plots for 0 MeV, 15 MeV and folded with the spectrum of equation 3.5.1 are shown in Fig III 5.6.

5.2 The ORIHET Calculation

The ORIHET code solves the N coupled equations:

$$\frac{dx_i}{dt} = \sum_{j=1}^{N} \ell_{ij} X_j - \lambda_i X_i + \alpha_i \quad i = 1 \text{ to } N$$

where X_i is the concentration of nuclide i which has a decay constant λ_i and a production rate α_i, and ℓ_{ij} is the fraction of nuclide j, which has a decay constant λ_j and concentration X_j, which leads to the production of X_i.

The ℓ and λ parameters are held as a data library. The original ORIGEN libraries were tailored to the needs of reactor calculations and have had to be expanded to accommodate the nuclide production from the transport calculation.

The α_i parameters are derived from the production rate per proton and are converted to g atoms sec $^{-1}$ (the required input unit) using a 200μA proton beam.

The calculation was made in three parts using the extended data libraries for mass chains 40 to 119 and 120 to 170 for the fission products and mass chains 207 to 250 for the spallation products. The calculation output was restricted to nuclides of activity $\geq 10^{-3}$ Ci for overall activity and a factor of 10 lower for α activities. Activities for 1172 nuclides contribute.

As a guide to the principal producers of activity there are 182 nuclides which have an activity at 6 months irradiation of ≥1kCi:-

Br 87 to 91; Kr 87 to 94; Rb 88 to 96; Sr 89 and 91 to 99; Y 91,91m and 92 to 101 Zr 95 and 97 to 104; Nb 95, 97 to 106, 97m 98m, 100m; Mo 99 and 101 to 107; Tc 100 to 109 Ru 103, 105 and 107 to 110; Rh 103m, 105 and 107 to 111; Pd 109, and 111 to 113; In 115m and 118; Ag 109m, 111m and 111 to 114; Cd 115; Sn 121, 127 and 128; Sb 128m and 129 to 132; Te 127, 129 and 131 to 135; I 131 to 138; Xe 133, 135 and 137 to 141; Cs 138 to 143; Ba 139 to 145; La 140 to 147; Ce 141 and 143 to 148; Pr 143 to 149; Nd 147 and 149; Pm 149; Pa 237; U 237, 239; Np 239.

The highest individual contributions came from ^{239}U and ^{239}Np at 122 kCi.

5.3 Activation Results

The build-up of gross activity averaged over the full target volume is shown in Fig. III 5.7; also included are the build-up of components of the activity.

The actinide and transuranic nuclides reach a nearly constant level of ~0.28 MCi after 1 month although there is a continuing rise of α activity at the kCi level. The fission products activity is still rising after 1 year's irradiation. A level of ~ 0.58 MCi is reached after 6 months. This means the activity averaged over the full target volume is ~ .86 MCi following 6 months irradiation.

The decay of activity following 6 months irradiation is shown in Fig. III 5.8. The activity drops by a factor of 2 after ~ ½ hour and by a factor of 10 in just over 1 week. After 1 year the activity has dropped to ~ 3.2 kCi. As the activitation is highly unlikely to be for a continuous 6 months period but is more likely to be for broken intervals the actual activity will probably not reach the 6 months level - a calculation using a more realistic irradiation/cooling cycle should be performed when details of the likely cycle are known.

5.4 Consequences of a Cladding Split

If a cladding split occurs an estimated 350 mg cm^{-2} h^{-1} of uranium may be corroded from the plates and into the D_2O coolant. The corrosion will bring with it the active nuclides. The activity following 6 months irradiation corresponds to 25 Ci g^{-1} averaged over the full volume.

Because the nuclide distribution should closely follow the energy distribution a peak activity ~ 7½ times higher should occur i.e. 190 Ci/g.

The corrosion rate at the peak plate would release ~1Ci/min/cm^2 in contact with the D_2O. If the cladding came away from the whole of the face of the peak plates (exposing the whole 9 cm diameter disk face) then the corrosion would release ~ 21 Ci/min (In this case the 2.3 factor for peak to average linear density is used)

For long corrosion times the decay of the products will reduce the effective build-up rates in the coolant. The activity A(t) after a period of corrosion t, may be expressed by

$$A(t) = C \times \underline{A} \times t \times f(t)$$

where C is the corrosion rate for uranium, $\underline{A}$ the activity of the uranium per unit of the corrosion rate, f(t) is a factor dependent on the irradiation time and t is the corrosion period.

The factor f(t) has been estimated from the decay curve (Fig. III 5.8) by numerical integration assuming that the decay curve over each decade of seconds may be represented by:

$$\underline{A} = D\, t^{\alpha} \qquad \text{with D and } \alpha \text{ constants}$$

The estimated function f(t) is shown in Fig. III 5.9.

This function indicates that for the whole face corrosion (i.e. 21 Ci/min build-up) after 1 hour we would have

$$\frac{21}{60} \times 3600 \times 0.53 \times \frac{1}{600} = 1.1 \text{ Ci/litre}$$

After 8 hours

$$\frac{21}{60} \times 8 \times 3600 \times 0.37 \times \frac{1}{600} = 6.2 \text{ Ci/litre}$$

5.5 Polonium

Polonium production is selected for special mention for three reasons: it may be one of the more serious potential hazards; it might provide

an effective monitor for a cladding failure; the HET fission/ spallation competition modifies the production rate from uranium spallation.

Polonium is produced in several decay chains and is also weakly produced by spallation. The production of polonium has been estimated also by an elaboration of Perry's [18] analysis using spallation cross section information quoted by Barbier [19] in an ORIHET calculation. The results from these two calculations are at 6 months irradiation:-

ISOTOPE	205	206	207	208	209	210	211	212	213	214	215	216	217	218	SUM
'HET'	80	80	70	7	.2	30	20	30	30	50	40	20	0	10^{-3}	450
'BARBIER'	4	17	270	7	.3	180	180	390	480	340	230	270	5	9	2100

The results are in general quite different. This will be discussed further in section 6.

The overall elemental build-up of polonium according to HET roughly follows:-

$$233t^{\,.1243} \text{ Ci with t in days } (t>1)$$

If ^{210}Po were considered as a monitor for a cladding split, we may estimate the build-up rate in the coolant.

For the 'Barbier' model the whole of the peak plate (21 Ci/min total) would lead to 4.5×10^{-3} Ci/min and the 'HET' model a factor of 6 lower.

This should be viewed in the terms of the total α-activity build-up, the total activity build-up, and the 'natural' activity of the coolant. (Chapter 4 Section 1.3).

5.6 Decay Power

The decay power after 6 months irradiation is estimated to be 8.3 kW. To this figure we must add a contribution for delayed neutron induced fissions.

On the assumption that the delayed neutron spectrum is not too dissimilar to the prompt neutron spectrum which induced fissions during the transport calculations then:

21.4 neutrons/proton created induced 2 fissions/proton, that is .09 fissions per neutron created in the target.

The equilibrium activity for delayed neutron emitters is 4.5 kCi, which is 1.7×10^{14} neutrons/sec or a fission rate of 1.5×10^{13}/sec. If we take 160 MeV/fission deposited energy, then this gives a contribution of 2.4×10^{15} MeV/sec which is ~0.4kW. Hence giving a total decay power of 8.7 kW.

The fall of decay power with time following 6 months irradiation is shown in Fig. III 5.10. The power drops by a factor of 2 in about 1 min. and is down to ~0.7 kW after 1 day.

5.7 Delayed Neutrons

The neutron activity is included in Fig. III 5.7. The saturation level of 4.5 kCi corresponds to 1.7×10^{14} neutrons/sec or ~0.6% of the primary neutron flux. It is probable that these neutrons will behave in a similar way to the primary produced ones and will act as a time independent background in SNS. This activity reaches saturation quickly (~ 100 secs) and also decays rapidly (by a factor of ~ 500 within 1 min. Fig. III 5.8).

5.8 Uranium Burn-up

In reactor terms, burn-up is related to loss by fission only; for our target, roughly half the loss of uranium nuclei comes from fission (3.26 by fission, 4.59 by other channels) and this higher 'total loss' figure is taken in this case. There are ~ 8 ^{238}U nuclei removed per incident proton averaged over the full target volume. This corresponds

to a removal rate of 4μg sec^{-1}. The total mass of uranium is 33.8 kg hence the removal of uranium takes place at a rate of 1.2×10^{-8}%/sec.

On the basis of the power density peak to average of 7½ to 1 this corresponds to a peak burn-up rate of 9×10^{-8}%/sec.

If the target lifetime was to be based on burn-up, it might be more appropriate to consider the average rate for the peak plate - i.e. to use the linear density peak to average factor of 2.3:1. This corresponds to 2.8×10^{-8} sec^{-1} or 1% burn-up in 1.1 years.

5.9 Gas Evolution

Discussion is limited to 'normal' gasses and elements such as bromine and Iodine which may be in the gaseous phase because of the temperature of the target not considered.

The sources of gas are:-

1) Stopped protons
2) Deuterons and tritons as evaporation fragments
3) ^{3}He and ^{4}He as evaporation fragments
4) Gaseous fission products - Kr, Xe and Ar
5) ^{4}He from α decay

The transport calculation indicates (in units of per incident proton):

2.0 protons brought to rest + 0.2 deuterons and tritons giving 2.2 hydrogen atoms/protons and 0.12 heliums.

From the activation calculation:

~2kCi of α emitters (≡ 9.4 x 10^{13}He atoms/sec), 4.4g per year of Xe, 0.6 g/year of Kr. Argon production is negligbly small.

This gives average gas evolutions of (units of litres (NTP)/sec)

Hydrogen	5.1 x 10^{-8}
Helium	9.1 x 10^{-9}
Xenon	2.4 x 10^{-8}
Krypton	5.1 x 10^{-9}

5.10 Damage

Damage is related to the displacement rate of atoms from the lattice. The primary collisions propogate a displacement cascade. The overall damage estimate requires calculation of the total lattice defects created; this is outside the scope of the present calculation. Here, as elsewhere in this report, only the primary displacement rate is calculated.

From section 5.3 we may expect 8 removals and 121 primary displacements per incident proton averaged over 1.806% of uranium.

This gives 1.9 x 10^{-9} primary displacements/atom/sec.

The peak to average from energy density is 7.5:1 giving a peak rate of

1.4 x 10^{-8} primary displacements/atom/sec.

This is negligible compared to the damage from the recoiling fission fragments.

6. Discussion of Target Results

A breakdown of the energy interchange in the high energy cascade is shown in Table 3-II. The total energy for sub-15MeV neutrons corresponds to rougly 30% of the incident 800 Mev proton's kinetic energy. The energy released by fission has contributed ~3 neutrons although ~ 15 are evaporated from fission fragments due to the transfer of excitation from the nucleus after the intranuclear cascade prior to scission. The average kinetic energy for evaporated neutrons as a function of excitation energy above threshold is shown in Fig III 6.1 for typical masses in uranium interactions. The lighter mass of the fission fragments will give a harder evaporation spectrum than for evaporations by uranium nuclei. Fig III 6.2 shows the neutron induced fission cross section as a function of energy for ^{238}U; A neutron energy of greater than 1 or 2 MeV is required to cause fission hence the harder evaporation spectrum for high energy fission leads to an increase of secondary fissions.

During transport of the high energy cascade-produced neutrons to the surface of the uranium an increase of 3.3 neutrons/proton occurs; 1.8n° are lost inducing fission, 1.1 are absorbed, 5.5 and 0.7 n° are created by fission and (n, xn) reactions respectively. The productive reactions will be caused by the higher energy end of the neutron spectrum and absorption by the lower; this suggests that approximately 80% of the neutrons escaping from the target uranium come from fission reactions.

The energy deposition corresponds to ~40 MeV per neutron. The high energy cascade gives ~30 Mev/n° whilst the neutron transport 100 MeV/n°. The uranium diameter used is smaller than required to give the best neutron production [16], being chosen on the basis of optimising the performance of SNS as a pulsed neutron source. The main cause of increased production with size will be secondary neutron induced fissions, and the energy deposition will tend towards 100 MeV/per extra neutron; the present calculated deposited energy is less than in previous estimates because of this.

Nuclide production is modified by the competition from fission in the high energy interactions. The spallation products [Fig III 5.1] show a reduction for the production of low mass isotopes of U, Pa and Th and for nuclides 'far removed' from the parent uranium [e.g. Polonium Section 5.5].

The energy spectrum for particles inducing spallation events (i.e. nuclear reactions which did not lead to fission) is shown in Fig III 5.2. Two components are present; the primary protons as they are slowed by ionisation loss and low energy cascade products (neutrons). As both the interaction cross section and the ionisation loss are insensitive to proton energy between 300 and 800 Mev, the logarithmic decrement ($200\ MeV^{-1}$) may be used to estimate a high energy interaction cross section of ~ 2 barns. Similarly, a spallation cross section of ~1/3 barn is indicated. The mean energy for 'high energy' interactions is ~600 MeV and there are 0.2 per Incident proton. (The other 0.22 spallations come from the 'low energy' cascade products).

The 'Barbier' [19] cross sections used in section 5.5 are equivalent to 0.22 spallations per proton.

The fission probability for a given isotope in the actinide region is independent of excitation energy once above a threshold of ~ 6MeV; the value of the fission probability is significantly less than 1 and increases as the isotope mass decreases, but decreases with proton emission. Evaporation is heavily biased toward neutron emission (particularly in the early stages) due to the neutron excess in heavy nuclei and also the inhibiting effect of the coulomb barrier to charged particle emission. The overall fission probability will increase with excitation of the nucleus because the chances of being able to fission will occur at more stages of the evaporation.

These factors taken in conjunction, mean that the fissioning nuclei will tend to be the low mass isotopes of U, Pa and Th and also the highly excited fragments which would have reached for example Polonium were fission not competing.

TABLE 3-I

ENERGY, POWER AND CENTRE LINE TEMPERATURES FOR EACH TARGET PLATE.

Plate Thickness	E_{max} Wcm^{-3}	Q_{max} Wcm^{-2}	Q_{tot} kW	ΔT_{SAT} °C	ΔT_{ZIRC} °C	ΔT_u °C	T_z °C	T_u °C
	720	234	4.9	31.4	42.4	124	214	338
	770	250	5.3	31.8	45.3	131	217	348
	770	250	5.4	31.8	45.3	131	217	348
	750	243	5.4	31.6	44.0	128	216	344
	730	237	5.4	31.5	42.9	125	214	339
0.65cm	720	234	5.2	31.4	42.4	124	214	338
	680	221	5.2	31.1	40.0	117	211	328
	620	202	4.8	30.7	36.6	108	207	315
	580	189	4.6	30.3	34.2	101	205	306
	560	182	4.5	30.1	33.0	98	203	301
	510	166	4.2	29.7	30.1	90	200	290
	490	159	4.1	29.5	28.8	86	198	284
	430	183	4.8	30.2	33.2	127	203	330
	390	166	4.4	29.7	30.1	116	200	316
0.85cm	340	145	3.9	29.0	26.3	102	195	297
	310	132	3.7	28.6	23.9	93	193	286
	270	128	3.7	28.4	23.2	101	192	293
0.95cm	250	119	3.4	28.1	21.6	94	190	284
	210	100	3.0	27.3	18.1	80	185	265
	190	90	2.7	26.8	16.3	73	183	256
	160	100	3.2	27.3	18.1	105	185	290
	140	88	2.8	26.7	15.9	92	183	275
1.25cm	120	75	2.4	26.0	13.6	80	180	260
	110	69	2.3	25.7	12.5	73	178	251
	90	79	2.8	26.2	14.3	115	181	296
1.75cm	54	47	1.7	24.1	8.5	71	173	244
2.45cm	7.4	9	0.4	18.3	1.6	20	160	180
	3	3.7	0.2	15.8	.7	8	157	165

Col. 2 E_{max} - The maximum power density (Wcm^{-3}) assumed constant over plate thickness.
3 Q_{max} - The maximum heat transfer rate to coolant (Wcm^{-2})
4 Q_{tot} - The total heat to be removed from ONE face (kW)
5 ΔT_{SAT} - The temperature above 140°C at Zircaloy 2 D_2O interface
6 ΔT_{ZIRC} - The temperature drop across the Zircaloy 2
7 ΔT_u - The temperature drop from the centre to the face of the uranium
8 T_z - The temperature of the Zircaloy 2 uranium interface
9 T_u - The temperature of the uranium at the centre of the plate

TABLE 3 - II

ENERGY DEPOSITION DURING HIGH ENERGY TRANSPORT
- UNITS ARE MEV/PROTON

	ENERGY SOURCE		ENERGY SINK		
PROCESS	INCIDENT PROTONS' KINETIC ENERGY	BINDING ENERGY	ESCAPE	DEPOSITED AS HEAT	NUCLEAR EXCITATION
IONISATION LOSS OF PRIMARY PROTON REACHING 1ST COLLISON	230	-	-	230	-
1.3 FISSIONS	171	239	-	204	206
0.5 SPALLATIONS	66	-	-	-	66
HIGH ENERGY ESCAPE PARTICLES	315	-	145	170	-
LOW ENERGY NEUTRONS	-	-	237		-237
RESIDUAL EXCITATION	-	-	-	18	- 18
γ PRODUCTION	18	-	-	18	-
OTHER EVAPORATION PRODUCTS	-	-	7	10	- 17
	800	239	389	650	0
	1039		1039		

Note - 'Particle' energies include a value of 7.5 MeV/nucleon for separation energy.

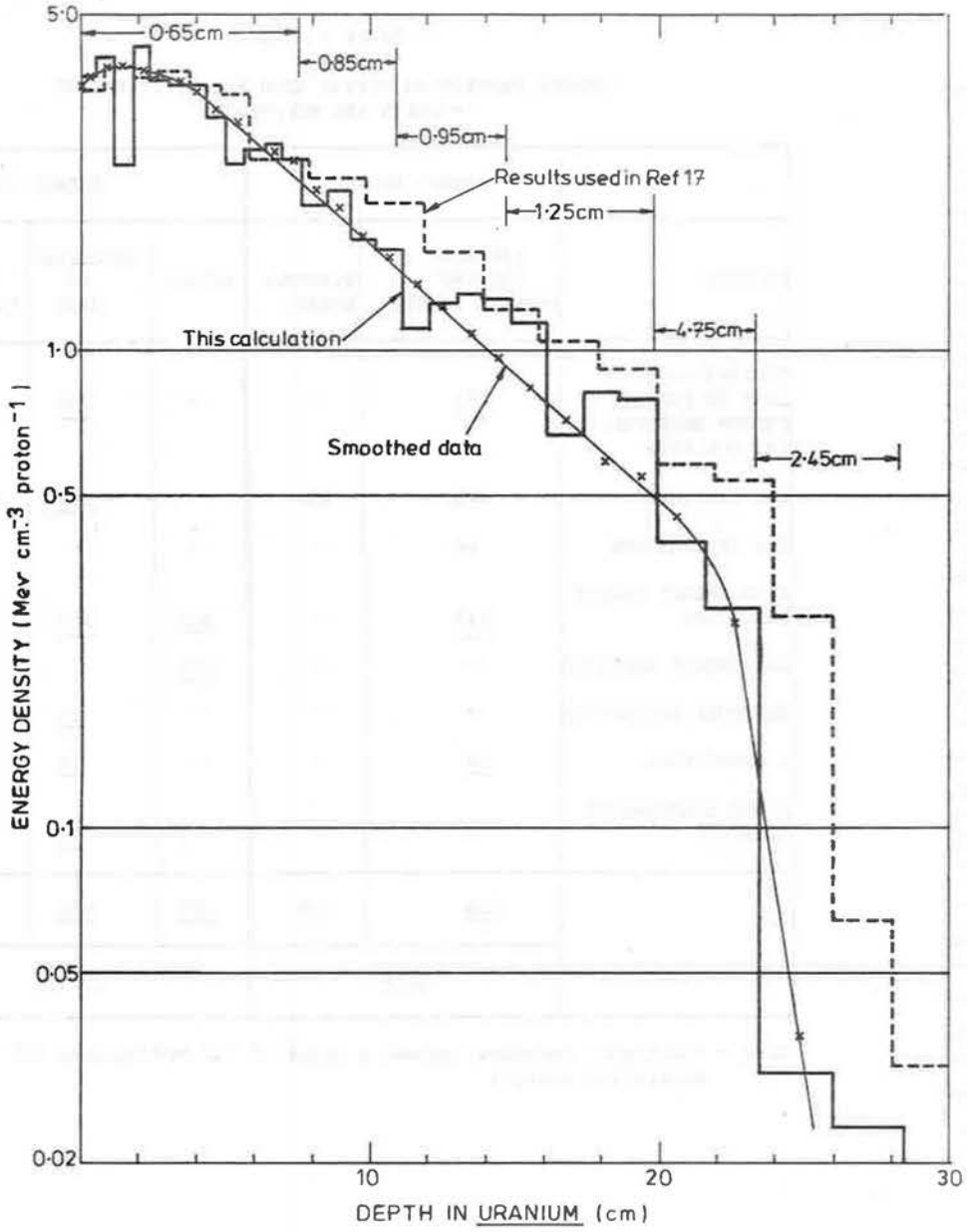

Fig III 4.1: *Centre line energy deposition in MeV cm^{-3} proton $^{-1}$ for 'Target' uranium only. Dimensions above curves show the plate thickness. Also shown are the values used in ref 17 temperature calculation and smoothed values (see Fig III 4.3).*

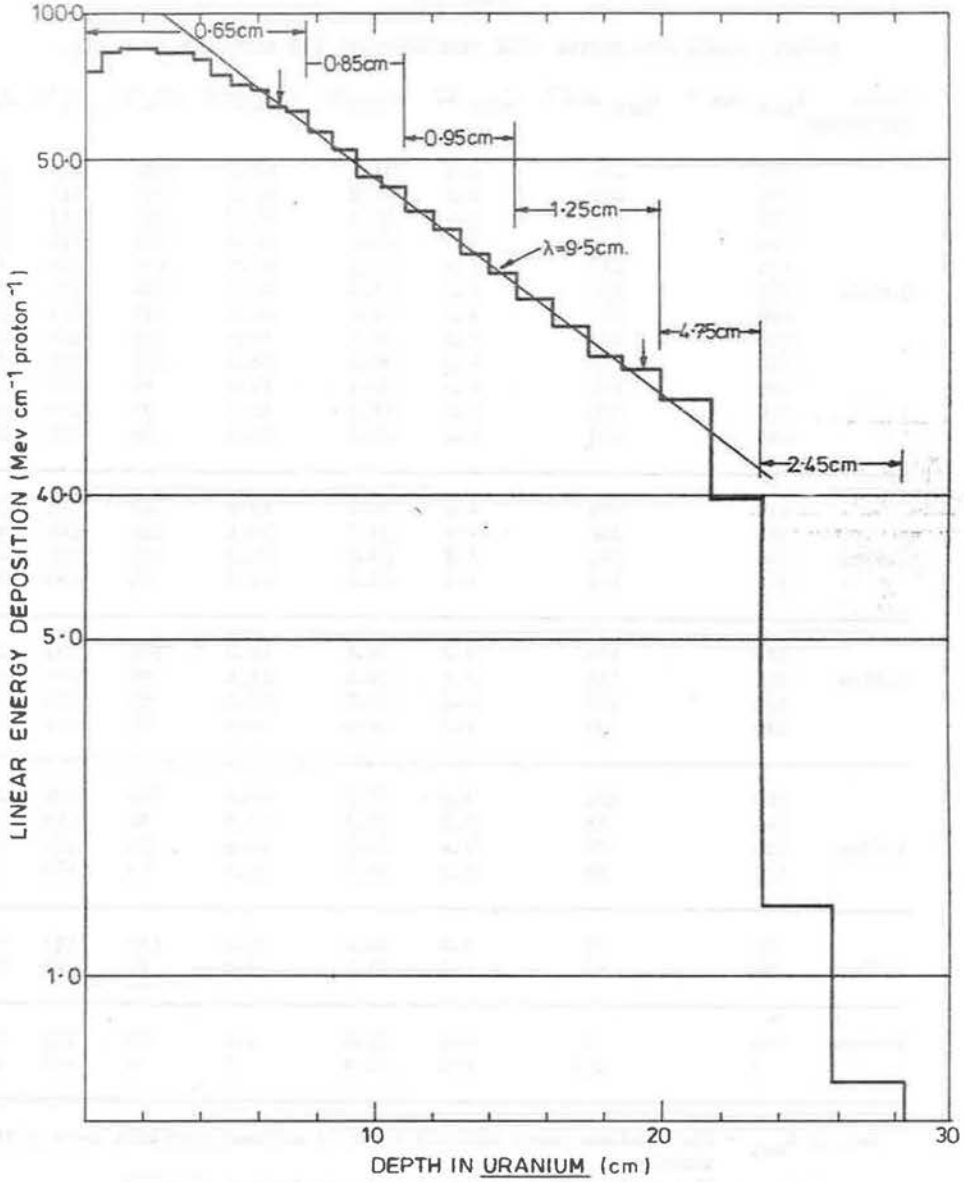

Fig III 4.2: *Energy deposition vs depth (Z direction) in 'Target' uranium. The exponential fit ($r^2 = .998_5$) is for the data between the 2 arrows.*

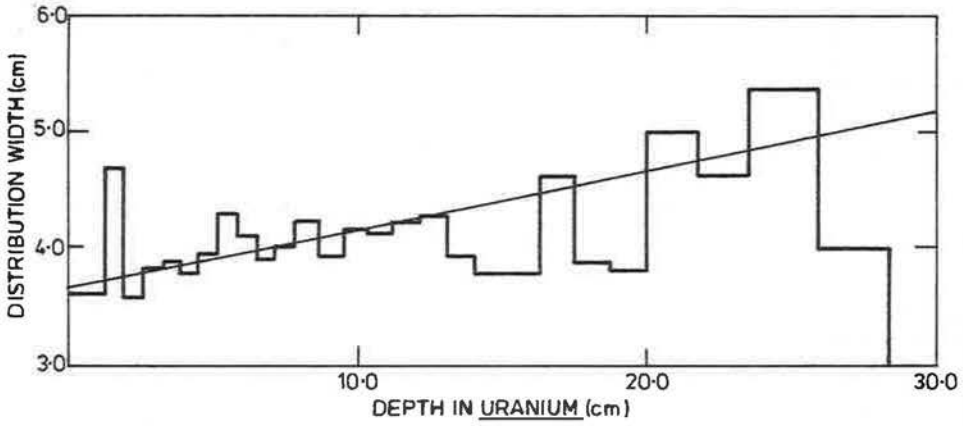

Fig III 4.3: *Calculated widths for a parabolic transverse energy distribution from the peak and total energies in the 'Target' uranium.*

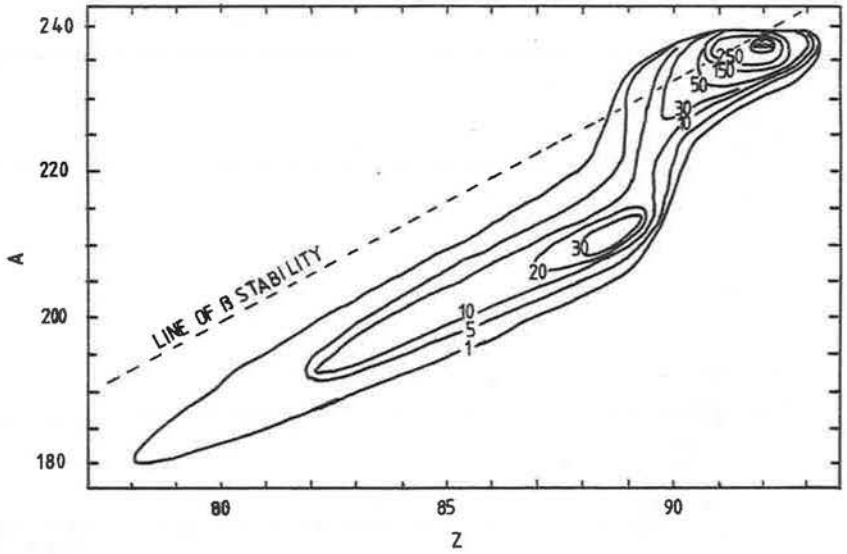

Fig III 5.1: *Products from ^{238}U high energy particle induced spallation reactions. Intensities are in arbitrary units. The parent nucleus $[^{238}U_{92}]$ is marked with an x.*

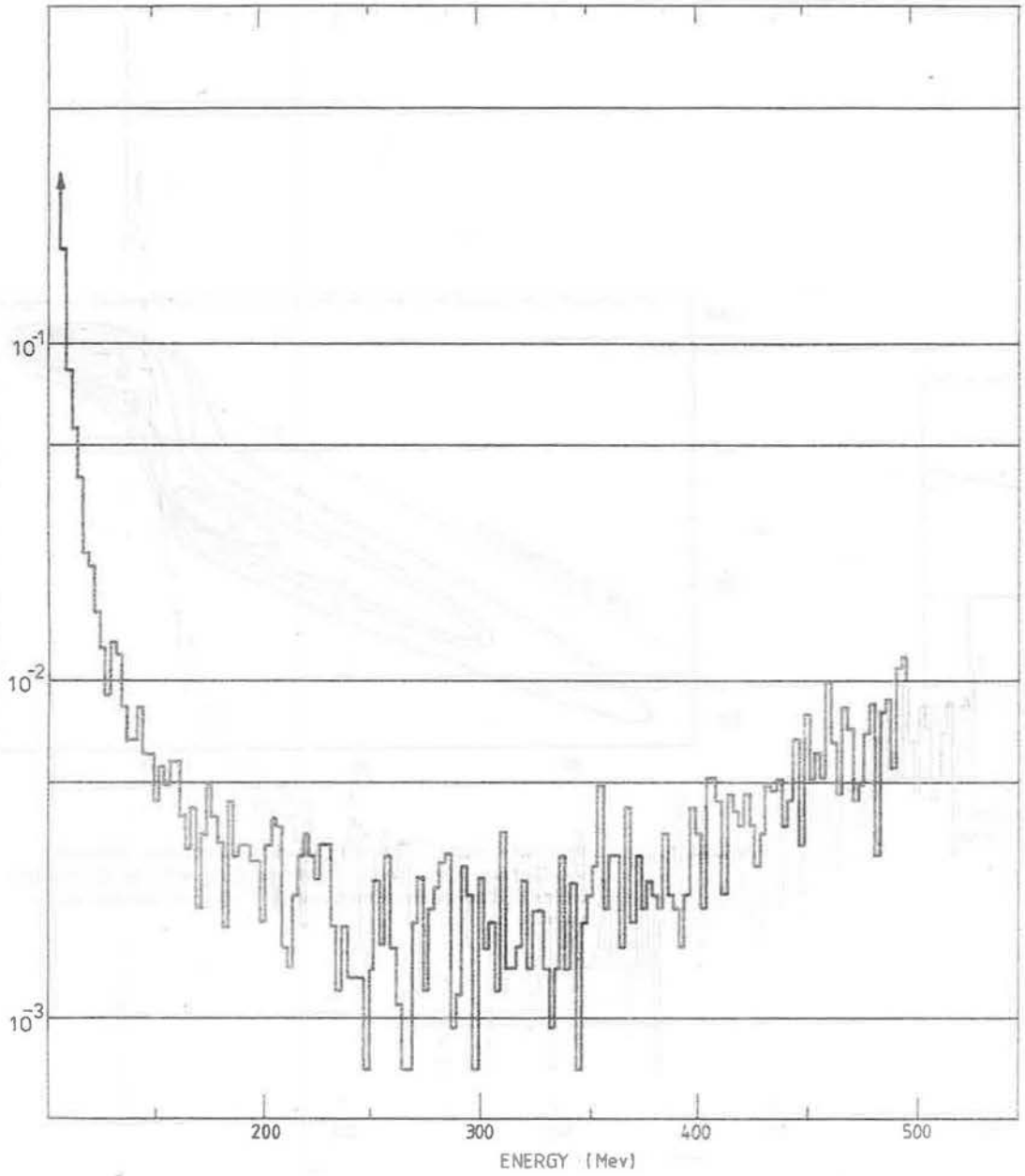

Fig III 5.2: Distribution for energies of particles inducing ^{238}U spallation reactions. Incident energies in range 15 to 800 MeV. Distribution is normalised to 1.0.

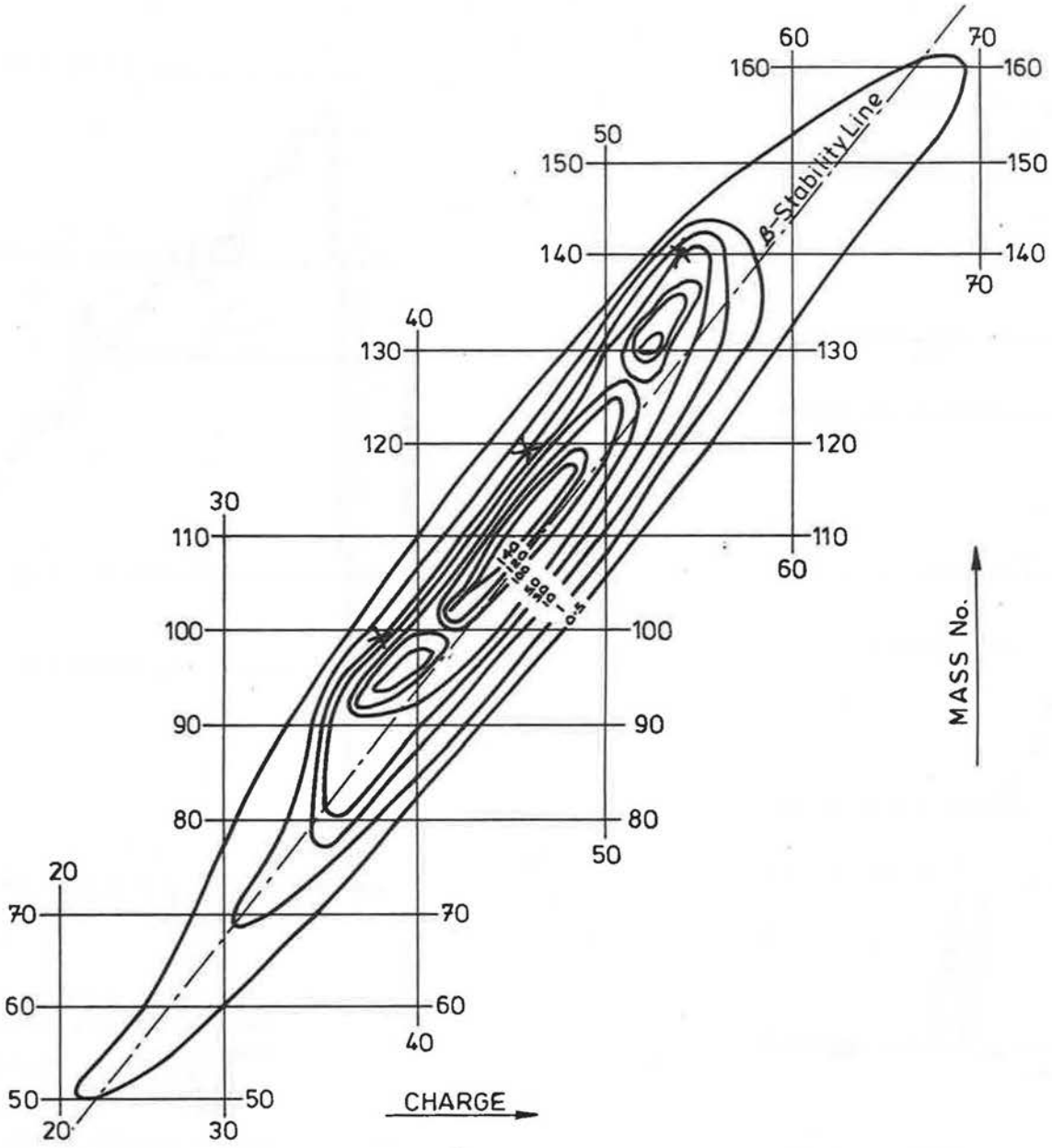

Fig III 5.3: *Nuclide distribution in high energy particle induced fission of ^{238}U. Contour intensities are for an arbitary linear scale. Crosses denote the position of A/2 and 140 mass-split nuclides.*

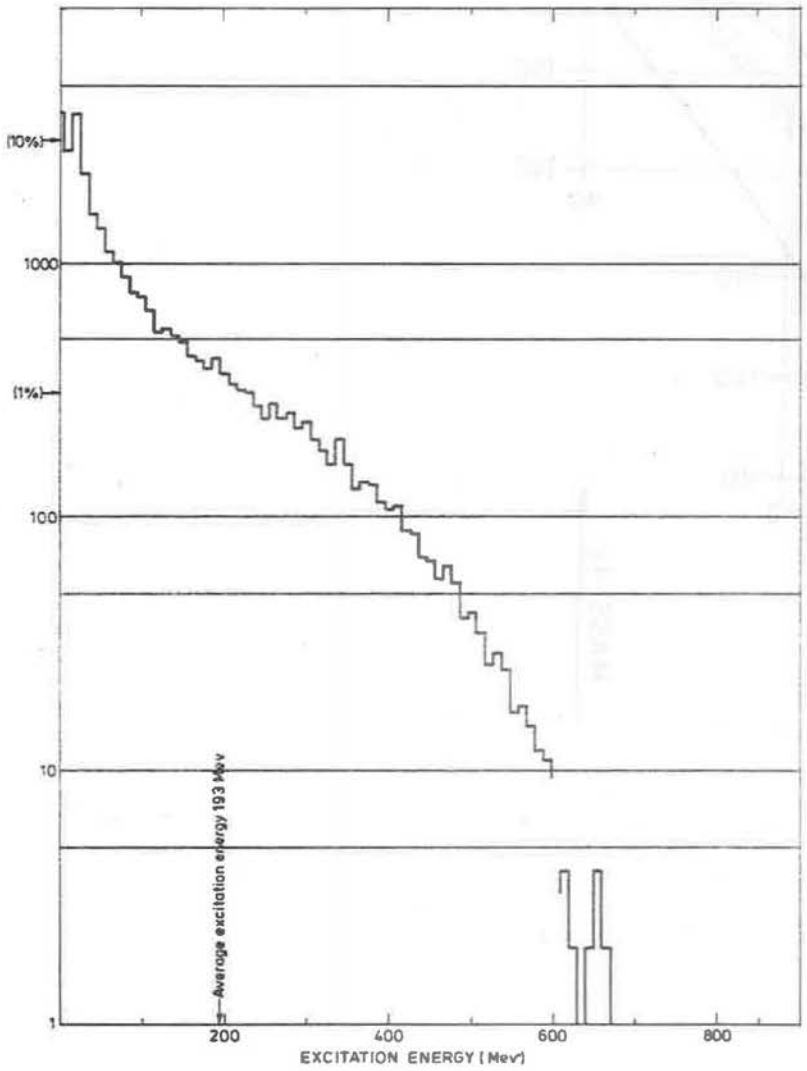

Fig III 5.4: *Distribution of excitation energies for nuclei after the intranuclear cascade 'Target' interactions. 30160 events, 27880 ^{238}U collisions, 2280 ^{16}O collisions.*

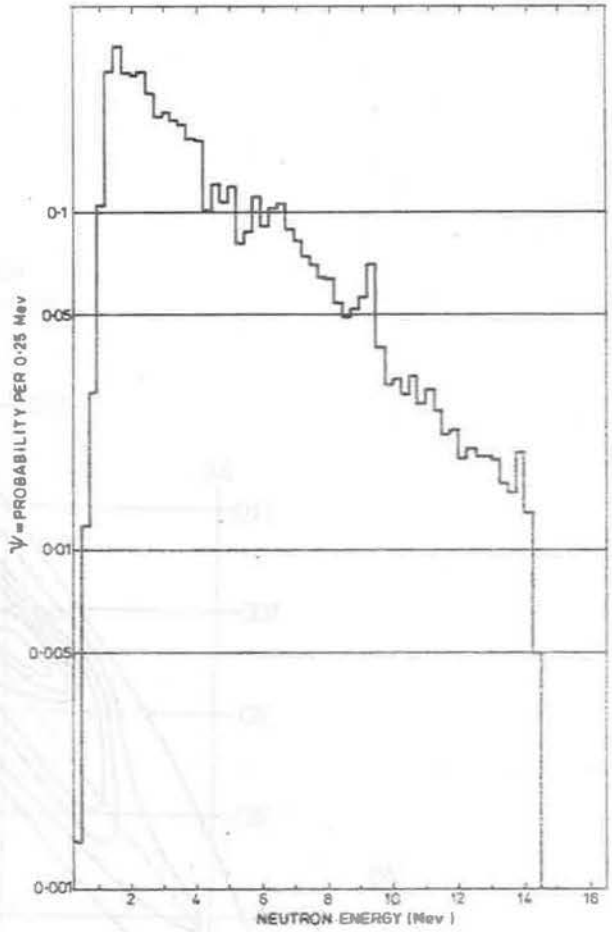

Fig III 5.5: *Distribution of energies of sub 15 MeV neutron induced fissions.*

$$\psi = \int_{E}^{E+.25} \phi(E) . \frac{\sigma_f(E)}{\sigma_r(E)} \, dE$$

$\phi(E)$ is incident neutron spectrum σ_f & σ_r the fission and total cross sections. ψ is normalised to 5.0.

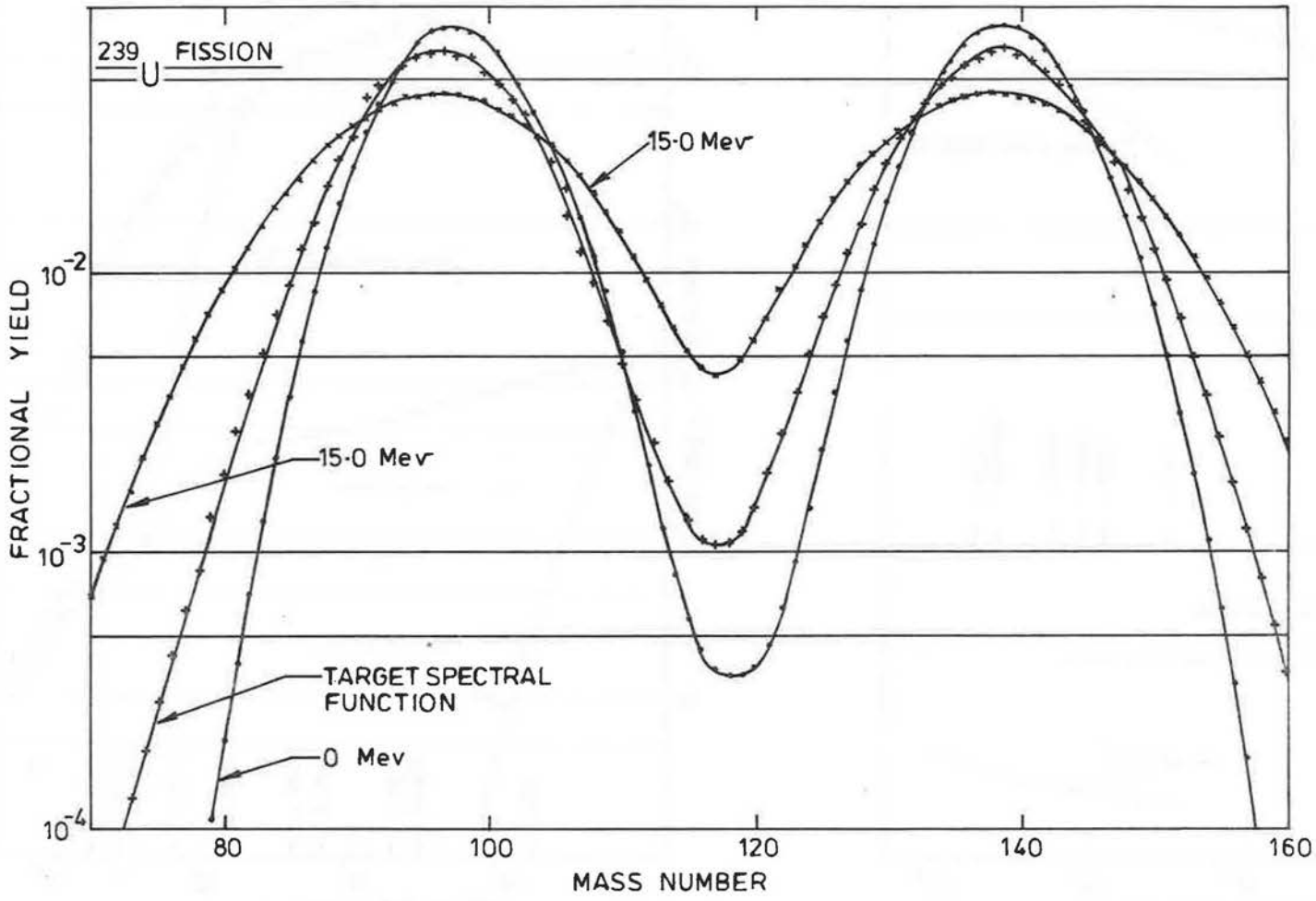

Fig III 5.6: *Mass yield in neutron induced fission of ^{238}U. Results are for spontaneous, 15 MeV and folding of spectral function of Fig III 5.5 and calculated using the function discussed in Appendix 3.B.*

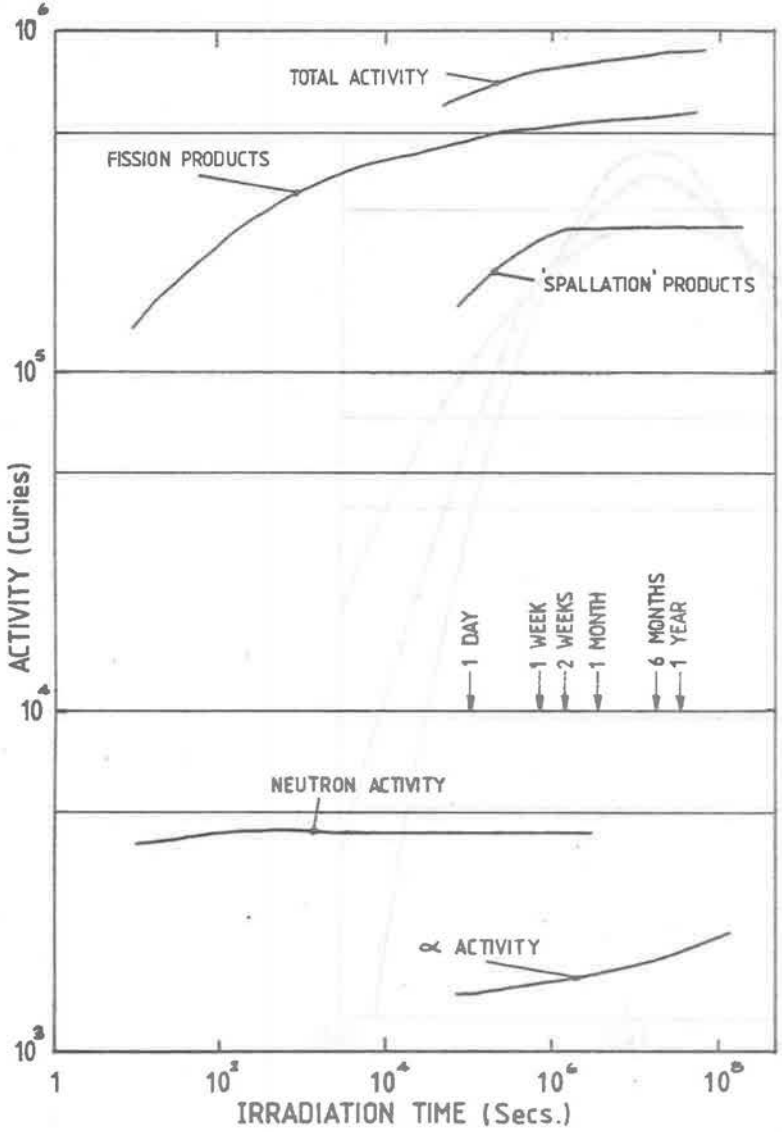

Fig III 5.7: Buildup of activity of target uranium vs irradiation time at 200μA proton current.

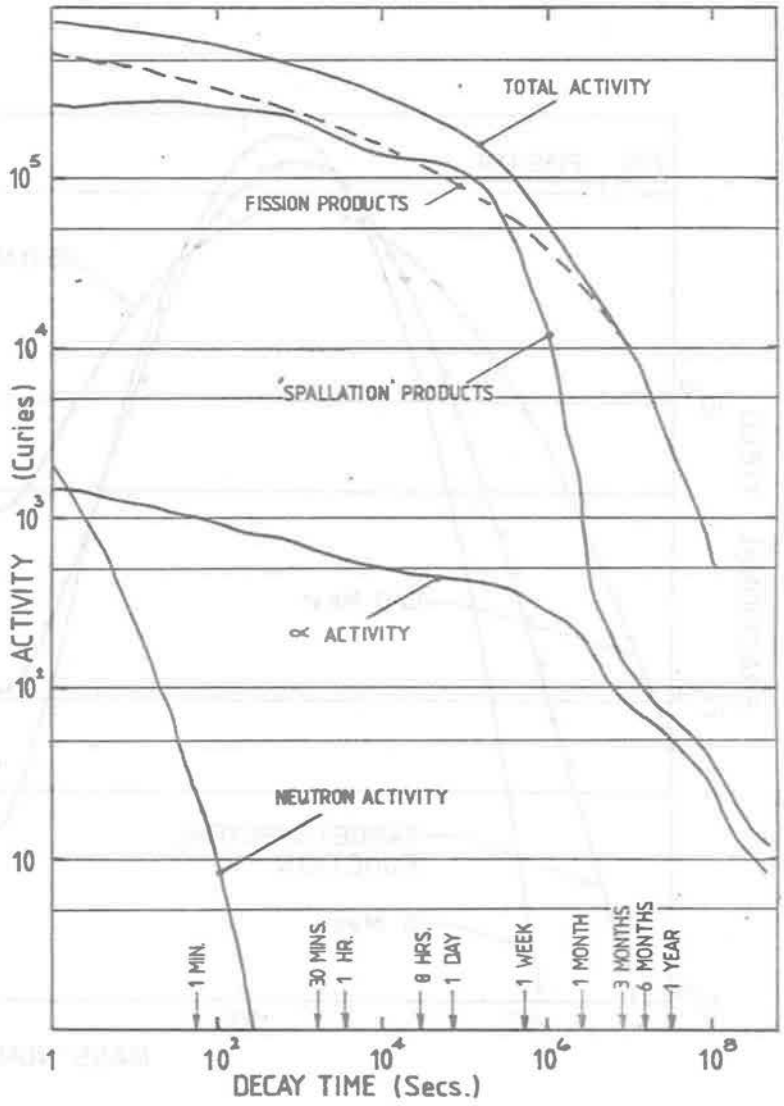

Fig III 5.8: Decay of activity in target uranium following 6 months irradiation at 200μA (continuous).

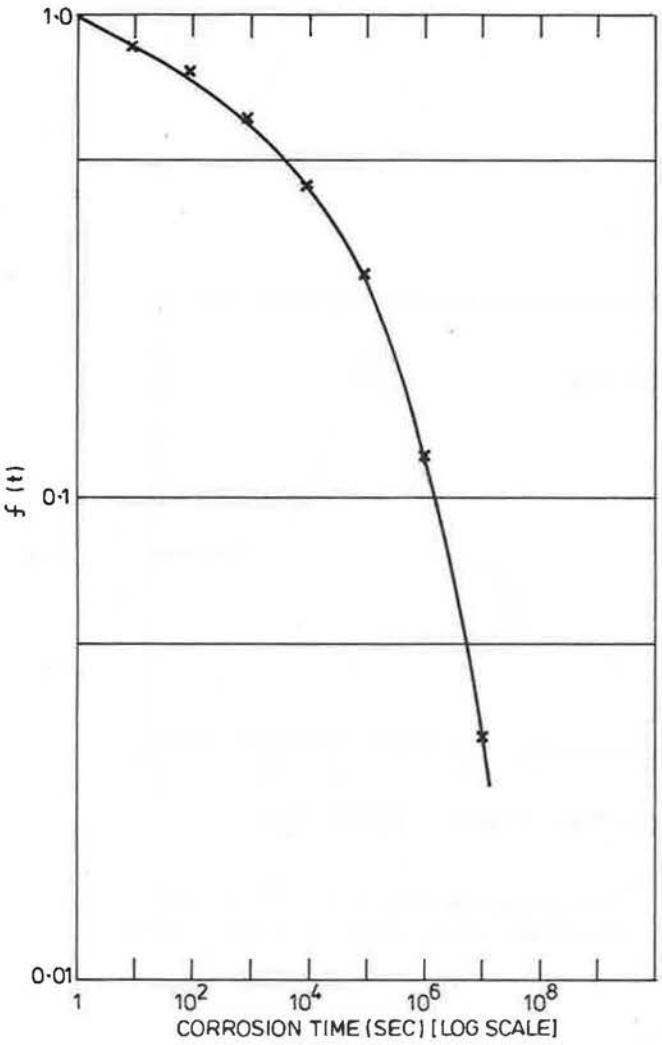

Fig III 5.9: Activation buildup function for coolant due to uranium corrosion (see Text in Section 5.4).

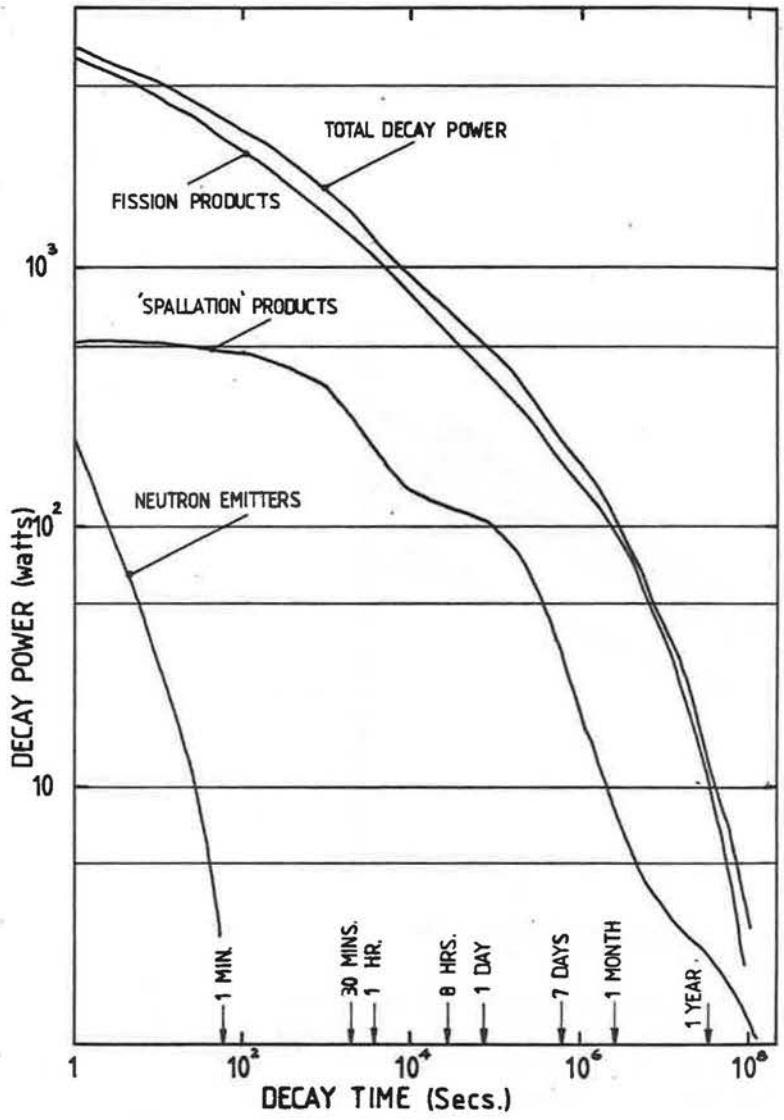

Fig III 5.10: Decay power as a function of decay time following 6 months irradiation of target uranium by 200μA proton beam.

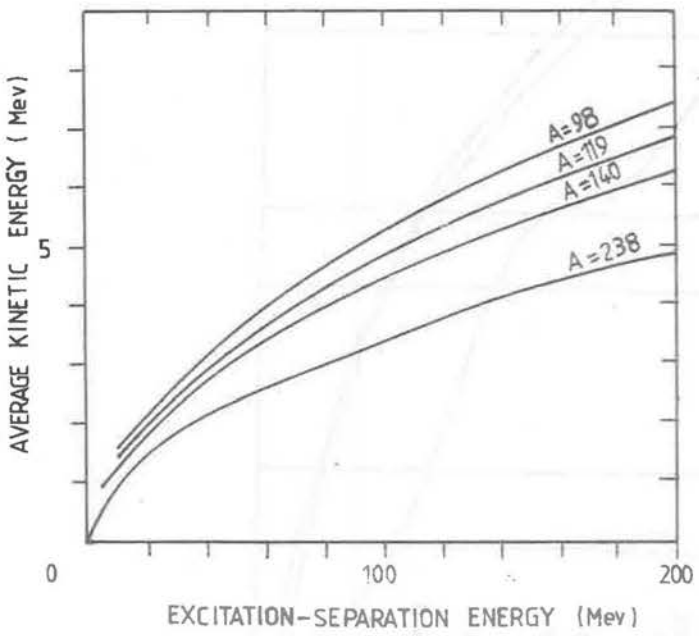

Fig III 6.1: The average Kinetic Energy for neutrons evaporated from mass 238, 140 and 98 AMU nuclei, as a function of excitation minus separation energy.

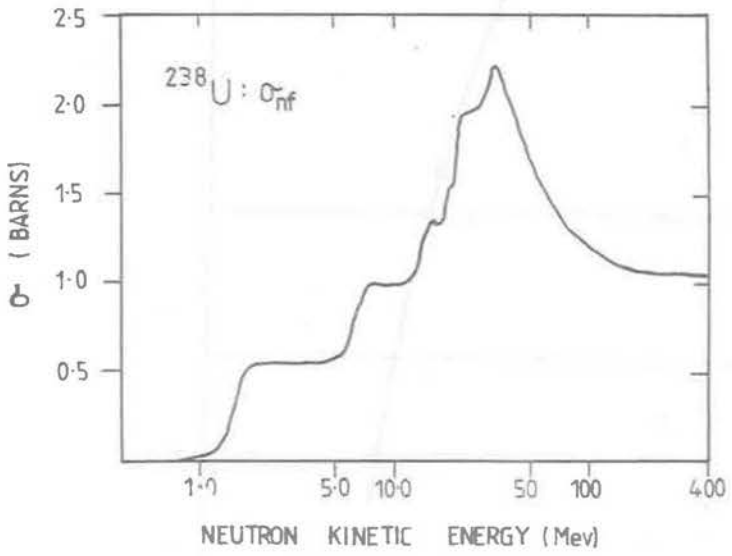

Fig III 6.2: The cross-section for ^{238}U (n,xnf) as a function of incident neutron energy.

APPENDIX 3-A

We require a formula to estimate the centre line temperature for the uranium/Zircaloy 2 sandwich.

The following assumptions are made:

1. The heat flow is one-dimensional

2. The energy deposition is constant

As usual, consider an element of thickness δx at some distance x. The temperatures are T and $T + \frac{dT}{dx}\delta x$. The thermal conductivity is a function of temperature. Considering unit area perpendicular to direction of flow then:-

(1) Heat into the element = $\xi\delta x$, ξ the energy deposited per unit volume per unit time

(2) Heat conducted into the element = $\left(K + \frac{dK}{dT}\delta T\right)\frac{d}{dx}\left(T+\frac{dT}{dx}\delta x\right)$

K the thermal conductivity

(3) Heat conducted out of the element = $K\frac{dT}{dx}$

For steady state then

$$K\frac{dT}{dx} = \xi\delta x + \left(K + \frac{dK}{dT}\delta T\right)\frac{d}{dx}\left(T + \frac{dT}{dx}\right)\delta x$$

neglecting the term dkd^2T then the balance equation gives

$$K\frac{d^2T}{dx^2} + \left(\frac{dK}{dT}\right)\left(\frac{dT}{dx}\right)^2 + \xi = 0$$

This equation may be straightforwardly solved under the following conditions:

(1) The thermal conductivity is a linear function of temperature $K = K_o + \alpha T$

(2) At the plate centre ($x = t_u$) $T = T_\psi$ and $\frac{dT}{dx} = o$ (symetry)

(3) The temperature at $x = o$ is T_x

to give

$$\xi t_u^2 = 2\,(T_\psi - T_x)\,\{K_o + \tfrac{1}{2}\alpha(T_\psi + T_x)\}$$

N.B. t_u is the plate HALF thickness.

The Zircaloy 2 layer will raise the temperature T_x above the surface temperature of the uranium.

On the assumption of no energy deposition in the Zircaloy then the energy balance will give:

$$\frac{K_z}{t_z}\,(T_x - T_s) = \xi\, t_u$$

Where t_z is the Zircaloy cladding thickness and K_z the (constant) thermal conductivity.

T_s is the surface temperature of the clad plate and is related to the temperature of the coolant by

$$T_s = T_{cool} + \Delta T_{sat}$$

Where ΔT_{sat} is the heat load dependent saturation temperature, increasing the surface temperature above the boiling point of the coolant.

Experimental data suggests that:

$$\Delta T_{sat} = Cl\,(\xi\, t_u)^{c2}$$

Hence collecting together these relations, the maximum uranium temperatures T_ψ, the plate (half) thickness t_u, the energy deposition ξ are connected by:

$$\xi t_u^2 = 2(T_\psi - T_x)\,\{K_o + \tfrac{1}{2}\alpha(T_\psi + T_x)\}$$

$$T_x = T_{cool} + Cl(\xi t_u)^{c2} + \xi\, t_u\,\frac{t_z}{K_z}$$

The entries in Table 3 - II are evaluated using

Uranium thermal conductivity = $.2443 + 2.3 \times 10^{-4}T$ Wcm^{-1} (T in °C)

$\Delta T_{sat} = 12.7\,(\xi t_u)^{0.1661}$ °C (ξt_u in watts)

Zircaloy thermal conductivity = .138 Wcm^{-1} $°C^{-1}$

$T_{cool} = 140°C$

Zircaloy thickness $t_z = 0.025cm$

Appendix 3-B

The nuclide distribution function is very closely a bivariate gaussian with two components - a symmetric mass split and an asymmetric mass split. The asymmetric mass split has a heavy mass component of ~ 140 AMU independent of fissioning system.

The Z, A distribution function is taken as:

$$P(Z, A, E_n) = \frac{1}{2\pi\sigma_z} \exp\frac{-(Z-\bar{Z})^2}{2\sigma_z^2} \left\{ \frac{2f_s}{\sigma_s} \exp\frac{-(A-\frac{1}{2}[A_0-\bar{\nu}])^2}{2\sigma_s^2} + \frac{(1-f_s)}{\sigma_a} \left[\exp\frac{-(A-[140-\frac{\bar{\nu}}{2}])^2}{2\sigma_a^2} + \exp\frac{-(A-[A_0-140-\frac{\bar{\nu}}{2}])^2}{2\sigma_a^2} \right] \right\}$$

where En is the kinetic energy of the nucleus inducing fission

$\bar{\nu}$ is the average neutrons per fission and is a function of fissioning neutron energy.

$\bar{Z}$ is the mean charge, which is taken on an equal charge to mass ratio of parent and daughter basis.

A_0 & Z_0 are the fissioning nucleus (A_0 = 239, Z_0 = 92 in our case)

f_s is the probability of symmetric fission and a function of the fissioning neutrons' energy.

σ_z, σ_s & σ_a the standard deviation for the charge, symmetric and asymmetric mass distributions.

For $\bar{\nu}$, the values from ENDF/BIV for ^{238}U neutron induced fission are used. These fit the relationship:

$$\bar{\nu} = 2.27_4 + 0.153E_n$$

E_n is the neutron inducing-fission's kinetic energy.

Very little data exists for the probability of symmetric fission, values of the peak to trough ratio after spontaneous fission and for an energy of 14.7 MeV [20] are available. A relationship based on the statistical model has been derived to give a variation with neutron energy:

$$\text{Peak to trough} = 3607\ e^{-1.315\sqrt{E^*}}$$

Where E* is the excitation of the nucleus being fissioned. This relationship has no firm basis but provides a plausible means of interpolation.

Experimental data [21, 22] suggests $\sigma_z = 0.6$ and $\sigma_s = \sigma_a = 5.2 + 0.27E_n$.

The frequency distribution of Fig III 5.5 gives us:

$$F(E_m) = \int_{E_m}^{E_m + \Delta E} \Psi(E) \frac{\sigma_f(E)}{\sigma_T(E)} dE$$

in bins of width ΔE for a 'target' neutron spectrum $\Psi(E)$ and a fission cross section $\sigma_f(E)$ and total cross section $\sigma_T(E)$, and then the probability of a given nuclide produced, is formed by the relation:

$$\text{PROB}(Z, A) = \text{Constant} * \sum_m F(E_m) * P(Z, A, E_m)$$

CHAPTER 4

ZIRCALOY CLADDING, TARGET COOLANT AND TARGET CONTAINER

1. ZIRCALOY AND COOLANT

1.1 Energy Deposition in Zircaloy and Coolant

1.1.1 Total Energy
1.1.2 Distribution of Energy

1.2 Activation of Zircaloy

1.2.1 Collision Information
1.2.2 Activation Calculation and Results
1.2.3 Interaction with Coolant
1.2.4 Damage

1.3 Activation of D_2O Coolant

1.3.1 Collision Information
1.3.2 Activation Calculation
1.3.3 Long Lived Products
1.3.4 Short Lived Products
1.3.5 Overall Activity Estimates
1.3.6 Loss and Contamination of D_2O

2. TARGET VESSEL

2.1 Energy Deposition
2.2 Activation and Damage
2.3 Total heat load on Coolant Circuit for target

Zircaloy Cladding, Target Coolant and Target Container

These sections of the system are taken together as the amount of information is rather less and in the transport calculation some parts have not been isolated.

All five sections of the calculation contribute. The quantities of prime interest are activation of the Zircaloy and (with special emphasis on tritiation) coolant plus data to enable damage estimates for the Zircaloy. Energy deposition will provide an additional thermal load on the target cooling system.

1.1 Energy Deposition in Zircaloy and Coolant

1.1.1 Total Energy

The contributions to the energy depositions in Zircaloy and coolant are as follows:

(i)	HET for target cylinder		16 Mev/proton incident
(ii)	05R for target cylinder		7.3 MeV/proton incident
(iii)	All full system running	(a) Zircaloy	18.2 MeV/proton incident
		(b) Coolant	16.0 MeV/proton incident

This gives a total thermal load of 58 MeV/proton incident which corresponds to 11.6 kW at 200 μA.

To apportion the energy between Zircaloy and coolant the following assumptions are made: (i) For HE transport ionisation loss will dominate and hence split according to equal energy deposition per gram. (ii) For neutron transport nuclear recoil will be the major contribution hence split this part according to the collision density. This gives:

Total energy deposited in Zircaloy	32 MeV
Total energy deposited in the D_2O coolant	26 MeV

1.1.2 Distribution of Energy

No direct calculation of the energy distribution has been made - as far as the coolant is concerned the energy is insignificant compared to the thermal load from the uranium and will be considered no further.

For the Zircaloy 14 MeV is deposited in the fifty six .025 cm face claddings within the 9 cm 'target' cylinder. The radial and longitudinal distributions should follow the energy deposition in the uranium (Fig. III 4.1 and Fig. III 4.2 in chapter 3).

On this basis the peak linear energy density should correspond to 17 MeV/cm (i.e. a total deposition of .43 MeV in the complete face cladding). Taking a 3.5 cm width parabolic distribution this gives a maximum energy deposition rate of ~ 0.9 MeV/cm^3. This is negligible compared to the energy from the uranium and hence energy deposition in the cladding may be ignored in the temperature calculation.

The volume of Zircaloy in the target cylinder is ~ 89 cm^3 hence the average energy deposition is 0.19 MeV cm^{-3} and the peak to average 4.7.

The remaining 15 MeV deposited in the thick frames should again follow the target uranium distribution in the axial direction. It is most probable that the radial distribution is uniform. On this basis a peak deposition rate of 0.02 MeV cm^{-3} is estimated.

For the total amount of Zircaloy (1800 cm^3) we can calculate an overall average of .018 MeV cm^{-3}, giving a peak to average of 50 for the face cladding at the most critical position or for the frames alone a peak to average of 2.3.

1.2 Activation of Zircaloy

1.2.1 Collision Information

The interactions with the various nuclei are as follows:-

(i)	High energy spallations	0.21
(ii)	Neutron elastic scattering	50 (+ .03 with Sn)
(iii)	Neutron non-elastic scattering	1.3 (+ .002 with Sn)
(iv)	(n,2n) on Zr	3.4×10^{-2}
(v)	(n,γ) on Zr	0.22
(vi)	(n,γ) on Sn	4×10^{-4}
(vii)	(n,p) on Zr	2.4×10^{-3}
(viii)	(n,d) on Zr	9.4×10^{-5}

Natural zirconium has five stable isotopes; ^{90}Zr 51.6%, ^{91}Zr 11.0%, ^{92}Zr 17.1%, ^{94}Zr 17.5% and ^{96}Zr 2.8%. For the high energy spallations this mixture of isotopes was included in the calculation but in the case of neutron transport ENDF/BIV cross sections for Zircaloy 2 were used and it is assumed the fractions of the channels taken by each isotope follow the natural abundance.

1.2.2 Activation Calculation and Results

The calculation was made using ORIHET as discussed in section 3.3 of chapter 1.

The build-up results are shown in Table 4-I for individual nuclides and summed over isotopes in Table 4-II. The total activity vs irradiation time is shown in Fig. IV 1.1. The activity after 1 month irradiation is 5.4 kCi, and follows a rise for further irradiation of $10.7\ t^{.185}$ kCi - t in years. The decay power is ~ 25 watts after 3 months activation rising to 33 watts after 1 year. This is small compared to the prompt power.

The decay of activity following 6 months irradiation is listed by nuclides and summed over isotopes in Table 4-III and 4-IV respectively.

The total activity is plotted vs decay time in Fig. IV 1.2

The Zircaloy contributes a further 10% at most, compared to the uranium, to the total activity during decay.

1.2.3 Interaction with Coolant

A corrosion rate of 4.2×10^{-14} g sec^{-1} cm^{-2} of Zircaloy by the D_2O at the proposed operating temperature, has been estimated [23]. This corresponds to ~ 4 mg of Zircaloy entering the D_2O over a 6 month operating period.

The activity averaged over all the Zircaloy is 9.5 kCi after 6 months continuous irradiation, with an average activity of ~ 7 kCi. This average activity corresponds to ~ 0.6 Ci/g or over a 6 month period ~ 3 mCi of products entering the coolant. A significant proportion of these will be lost by decay over this time period; neglecting these losses and relative radiotoxicity, these products should represent an insignificant contribution to coolant activation (cf Section 1.3.5 below.

1.2.4 Damage

52 Zircaloy nuclear collisions occur per incident proton. This corresponds to an average primary displacement rate of 6×10^{-10} per atom per second. Taking the 50 value for peak to average this gives a peak rate of 3×10^{-8} primary displacements per atom per second.

1.3 Activation of Coolant (D_2O)

1.3.1 Collision Information

The transport calculation gives the following collision information. (Normalised to per incident proton):

(i)	High energy collisions with deuterons	.038
(ii)	^{2}H (n,n) ^{1}H	48.5
(iii)	^{2}H (n,2n) ^{1}H	6.1×10^{-2}
(iv)	^{2}H (n,γ) ^{3}H	9.2×10^{-5}
(v)	High energy oxygen spallations	0.1
(vi)	Neutron elastic scatters with oxygen	28
(vii)	Neutron non elastic scatters with oxygen	.04
(viii)	Neutron (n,γ) interactions with oxygen	1×10^{-5}
(ix)	Neutron (n,p) interactions with oxygen	1.5×10^{-3}
(x)	Neutron (n,d) interactions with oxygen	3.3×10^{-4}
(xi)	Neutron (n,p) interactions with oxygen	3.8×10^{-2}

The natural isotopic composition for oxygen is 99.76% ^{16}O, 0.04% ^{17}O and 0.2% ^{18}O. It will be assumed that the oxygen reactions take place with these proportions and that the cross sections do not vary significantly over the isotopes. Cross section information for the individual isotopes has not been found.

1.3.2 Activation Calculation

The overall activity in the coolant will be made up of a short lived component and some long lived isotopes (^{7}Be, ^{3}H, ^{10}Be and ^{14}C)

The coolant system has been considered in five parts:

(i) An irradiation volume (the target assembly) containing 5.6 litres of D_2O and having a mean irradiation time of 0.65 sec.

(ii) Pipe work connecting target to heat exchanger which introduces a delay of 7.2 secs between irradiation and entry to heat exchanger.

(iii) A heat exchanger of volume 70 litres having an area of ~ 37 m^2 in contact with a secondary cooling circuit. The traversal time for the coolant is taken as 8.1 secs.

(iv) An external volume of 518 litres which takes 43.4 secs to traverse, and represents the rest of the coolant system outside the target station.

(v) A delay of 10 secs to return to the target.

This is illustrated in Fig. IV 1.3

A total circulation time of 69.4 secs is assumed. These numbers are to allow an estimate to be made and do not necessarily correspond to the coolant circuit which may be installed.[23]

The activity at the exit of the target irradiation volume will be proportional to

$$\alpha\{1 - e^{-t_i/\lambda}\}\{1 - e^{-Nt_c/\lambda}\}\{1 - e^{-t_c/\lambda}\}^{-1}$$

Where α is the nuclide production rate, λ the decay constant, t_i the irradiation time (0.65s), t_c the circulation time (69.4s) and N the number of irradiation cycles.

The average activity for the heat exchanger and the external volume is estimated from the delays of 7.2 and 15.3 secs and traversal times of 8.1 and 43.4 secs respectively.

The overall activity is considered in two parts - firstly long lived isotopes and then the short.

1.3.3. Long Lived Products

Four contributions are considered ^{7}Be (53.29d), ^{3}H (12.346y), ^{10}Be (1.6×10^{6}y) and ^{14}C (5730y).

(a) ^{7}Be: HET predicts no production of ^{7}Be. Yiou et.al. [24] have measured a cross section of 6.5 ± 2 mb for 600 MeV protons on oxygen. 600 MeV is a reasonable average energy for interaction and hence we use this cross section to estimate a production rate of ^{7}Be of 1.7×10^{-3} proton $^{-1}$. This gives a saturation activity of .096 Ci/litre with a build-up rate of 1.5×10^{-8} Ci/litre/sec both at 200 μA incident proton current. 10% of saturation will be reached in ~ 8 days, 90% in ~ 6 months.

(b) ^{3}H: Oxygen spallation will dominate. Experimental data suggests ~ 10% of the oxygen cross section will lead to tritium production. This indicates ~ .01 tritons per proton from oxygen spallation. Neutron capture by deuterium leads to a production rate ~ 100 times lower.

The production rate corresponds to a saturation activity of .57 Ci/litre, with a build-up rate of ~ 10^{-9} Ci/litre/sec. 10% of the saturation activity will be reached in ~ 1.9 years and 90% in 41 years.

(c) ^{10}Be: HET predicts a production rate of 1.1×10^{-4}/proton. This gives a build-up rate of 8.5×10^{-17} Ci/litre/sec to a saturation activity of 6×10^{-3} Ci/litre. This will always be a negligible activity.

(d) ^{14}C: Contributions from both oxygen spallation and $^{17}O\ (n,\alpha)\ ^{14}C$ give a total production rate of 1.2×10^{-3}/proton, which leads to a saturation activity of .068 Ci/litre and a build-up rate of 2.6×10^{-13}Ci/litre/sec.

1.3.4 Short Lived Products

26 channels are considered to contribute to the activity; these are given in Table 4-V along with estimated production rates and saturated activity at the exit of the irradiation volume.

Only a few of the nuclides contribute to the activity in the heat exchanger and external volumes. These are shown in Table 4-VI. The activity in the heat exchanger is estimated to be 79 Ci and in the external volume 430 Ci. These levels should be reached after about a ½ hour's operation.

1.3.5 Overall Activity Estimates

The contributions to the activity in the system from the long lived isotopes are listed in Table 4-VII as a function of irradiation time. This table also shows the total estimated activity for the heat exchanger and ballast volume. The long lived isotopes make an ~ 10% contribution after about ½ year. The short lifetime products will decay rapidly, but for the long lived products there will be a gradual accumulation without much decay over the lifetime of the coolant.

Attention is drawn to the presence of ^{17}N. The contributions to ^{17}N production are from the two isotopes ^{17}O and ^{18}O. ^{17}N decays by βn hence the .34 Ci equivalent in the heat exchanger corresponds to 1.3×10^{10} n°/sec, or taking an area of $37m^2$, 3.4×10^{8} n°/m^2/sec irradiating the secondary coolant. The build-up of activity in the secondary coolant has not been estimated.

The activity levels should also be considered in relation to the activity following a cladding failure. Particularly, there exist contributions to all decay modes which will represent background levels against which any detection system so based will have to operate.

1.3.6 Loss and Contamination of D_2O

If we assume every collison will disrupt the D_2O molecule, then a loss of 77 molecules of D_2O per proton will occur - this corresponds to 1.7×10^{-6}%/hour.

Most of the nuclides produced are displaced by one mass unit from a stable isotope and also have short lifetimes. This will lead to a build-up of foreign nuclei in the system. No speculation about the form of these products is made.

ELEMENT	PRODUCTION/PROTON	PERCENT/HOUR
Fluorine	2×10^{-8}	4.5×10^{-16}
Oxygen	9.5×10^{-3}	2.2×10^{-10}
Nitrogen	5.1×10^{-2}	1.2×10^{-9}
Carbon	6.1×10^{-2}	1.4×10^{-9}
Boron	3.9×10^{-3}	8.8×10^{-11}
Beryllium	3.2×10^{-4}	7.2×10^{-12}
Lithium	2.5×10^{-3}	5.7×10^{-11}
Helium	1.1×10^{-2}	2.5×10^{-10}
Hydrogen	8.8×10^{-4}	2.0×10^{-11}

2. TARGET VESSEL

2.1 Energy Deposition

The transport calculation indicates 31.8 MeV/proton is deposited in the Inconel can. To this must be added the contribution from the passage of the proton beam through the window: as this should be subject to special study an estimate of 3 Mev/proton is taken at this stage.

This gives a total estimated energy deposition of 34.8 MeV/proton.

The distribution of the energy deposition in the various parts of the can is illustrated in Fig. IV 2.1. The symmetry in the system has been exploited by showing only half the full can. All quoted energies except for regions No's 2 and 4 will occur twice.

2.2 Activation Damage

Inconel is made up from many different nuclei - activation channels cannot be estimated in detail because of code limitations. The collision information we have may serve as a normalisation basis for a separate calculation.

Total high energy spallations	0.17
Total neutron scatters	93
Neutron absorptions by Inconel	1.0
High energy interactions with cadmium	.023
Total neutron scatters in cadmium	5.9
Total neutron absorptions in cadmium	0.81

The spallations will be with 31 nuclear species and the neutron interactions spread over some 230 channels. Only some of these will lead to a build-up of activity.

To further this calculation, the spectrum of particles inducing spallations and of the incident neutrons is illustrated in Figs. IV 2.2 and IV 2.3.

The cadmium is included to try and reduce the low energy neutrons returned to the uranium and coolant. The cross sections for $^{238}U(n,\gamma)^{239}U$ and $^{2}H(n,\gamma)^{3}H$ are shown in Fig IV 2.4. As may be seen both cross sections show a marked rise at low energies with the direct tritation being 2 to 3 orders of magnitude higher. Our transport calculation only follows neutrons to 0.1eV, and so it is difficult to estimate how effective the cadmium is in reducing these contributions. The cadmium absorptions should be at low energies, and hence if we assume these are neutrons which would have produced (n,γ) reactions in ^{238}U, the cadmium has reduced ^{239}Pu production by some 20%.

For damage estimation the calculation predicts 93 primary displacements per proton incident. This corresponds to 5.1×10^{-10} primary Inconel atom displacements per second. On the basis of energy deposition, local rates ~ 3½ times higher may occur. As stated above, the beam window should be the subject of a separate study.

2.3 Total Heat Load in the Target Coolant Circuit

The contributions are

(1)	Target uranium	(Chapter 3, Section 4.1)	1041 MeV/proton
(2)	Zircaloy	(This Chapter, Section 1.1.1)	32 MeV/proton
(3)	Coolant	(This Chapter, Section 1.1.1)	26 MeV/proton
(4)	Inconel vessel		35 MeV/proton
		Total Heat Load	1134 MeV/proton

That is at 200 μA proton current 226.8 kW - which rounds to 230 kW

TABLE 4 - I (SHEET 1)

BUILDUP OF ACTIVITY (CURIES) IN ZIRCALOY 2 , SUM OVER ALL TARGET ASSEMBLY
200 μA 800 MeV PROTON IRRADIATION OF TARGET URANIUM

	INITIAL	10s	1 min.	1 hour	8 hours	1 day	1 week	4 weeks	12 weeks	26 weeks	1 year
CO 56	0.0	6.50E-06	3.90E-05	2.34E-03	1.87E-02	5.59E-02	3.82E-01	1.50E+00	3.52E+00	5.10E+00	6.12E+00
CO 57	0.0	1.88E-06	1.13E-05	6.91E-04	6.22E-03	2.27E-02	2.73E-01	1.43E+00	4.04E+00	7.23E+00	1.17E+01
CO 58	0.0	1.45E-05	8.68E-05	5.20E-03	4.16E-02	1.24E-01	8.47E-01	3.29E+00	7.54E+00	1.06E+01	1.24E+01
NI 57	0.0	6.82E-04	4.09E-03	2.43E-01	1.82E+00	4.72E+00	1.23E+01	1.28E+01	1.28E+01	1.28E+01	1.28E+01
CU 61	0.0	7.20E-03	4.32E-02	2.35E+00	1.02E+01	1.27E+01	1.28E+01	1.28E+01	1.28E+01	1.28E+01	1.28E+01
CU 62	0.0	2.26E-01	1.32E+00	1.89E+01	1.91E+01	1.91E+01	1.91E+01	1.91E+01	1.91E+01	1.91E+01	1.91E+01
CU 64	0.0	9.67E-04	5.80E-03	3.39E-01	2.26E+00	4.66E+00	6.38E+00	6.38E+00	6.38E+00	6.38E+00	6.38E+00
CU 65	0.0	1.43E-01	8.10E-01	6.38E+00	6.38E+00	6.38E+00	6.38E+00	6.38E+00	6.38E+00	6.38E+00	6.38E+00
ZN 63	0.0	1.94E-02	1.15E-01	4.24E+00	6.38E+00	6.38E+00	6.38E+00	6.38E+00	6.38E+00	6.38E+00	6.38E+00
ZN 65	0.0	1.05E-05	6.38E-05	5.27E-03	4.83E-02	1.46E-01	1.01E+00	4.23E+00	1.17E+01	2.06E+01	3.29E+01
GA 65	0.0	1.45E-01	8.53E-01	1.79E+01	1.91E+01	1.91E+01	1.91E+01	1.91E+01	1.91E+01	1.91E+01	1.91E+01
GA 66	0.0	3.90E-03	2.34E-02	1.35E+00	8.49E+00	1.58E+01	1.91E+01	1.91E+01	1.91E+01	1.91E+01	1.91E+01
GA 67	0.0	9.41E-04	5.65E-03	3.37E-01	2.62E+00	7.33E+00	2.97E+01	3.82E+01	3.83E+01	3.83E+01	3.83E+01
GA 68	0.0	2.15E-02	1.29E-01	5.82E+00	1.27E+01	1.28E+01	1.33E+01	1.50E+01	1.90E+01	2.41E+01	3.14E+01
GE 68	0.0	8.89E-06	5.33E-05	3.20E-03	2.56E-02	7.67E-02	5.34E-01	2.25E+00	6.29E+00	1.13E+01	1.86E+01
GE 69	0.0	4.09E-03	2.46E-02	1.53E+00	1.18E+01	3.10E+01	8.48E+01	8.93E+01	8.93E+01	8.93E+01	8.93E+01
GE 71	0.0	4.59E-05	2.76E-04	1.82E-02	2.36E-01	1.26E+00	2.60E+01	9.78E+01	1.21E+02	1.21E+02	1.21E+02
AS 69	0.0	4.93E-02	2.90E-01	5.99E+00	6.38E+00	6.38E+00	6.38E+00	6.38E+00	6.38E+00	6.38E+00	6.38E+00
AS 70	0.0	8.33E-02	4.97E-01	2.08E+01	3.82E+01	3.83E+01	3.83E+01	3.83E+01	3.83E+01	3.83E+01	3.83E+01
AS 71	0.0	2.83E-03	1.72E-02	1.30E+00	1.00E+01	2.75E+01	9.79E+01	1.15E+02	1.15E+02	1.15E+02	1.15E+02
AS 72	0.0	3.31E-03	1.98E-02	1.18E+00	8.64E+00	2.16E+01	5.33E+01	6.83E+01	7.02E+01	7.02E+01	7.02E+01
AS 73	0.0	1.91E-05	1.15E-04	8.06E-03	1.16E-01	5.34E-01	5.25E+00	2.09E+01	4.90E+01	7.12E+01	8.57E+01
AS 74	0.0	5.75E-05	3.45E-04	2.07E-02	1.65E-01	4.87E-01	3.05E+00	8.86E+00	1.24E+01	1.27E+01	1.28E+01
SE 71	0.0	5.91E-01	3.35E+00	2.55E+01	2.55E+01	2.55E+01	2.55E+01	2.55E+01	2.55E+01	2.55E+01	2.55E+01
SE 72	0.0	2.44E-04	1.46E-03	8.76E-02	6.92E-01	2.02E+00	1.12E+01	2.34E+01	2.55E+01	2.55E+01	2.55E+01
SE 73	0.0	1.88E-02	1.13E-01	6.46E+00	3.78E+01	6.35E+01	7.54E+01	9.10E+01	1.19E+02	1.41E+02	1.56E+02
SE 75	0.0	1.73E-05	1.04E-04	8.28E-03	1.13E-01	4.09E-01	2.85E+00	1.15E+01	2.91E+01	4.61E+01	6.19E+01
BR 74	0.0	1.16E-01	6.90E-01	2.06E+01	2.55E+01	2.55E+01	2.55E+01	2.55E+01	2.55E+01	2.55E+01	2.55E+01
BR 75	0.0	5.40E-02	3.23E-01	1.58E+01	4.33E+01	4.47E+01	4.46E+01	4.46E+01	4.46E+01	4.46E+01	4.46E+01
BR 76	0.0	8.39E-03	5.03E-02	3.01E+00	2.30E+01	6.01E+01	1.21E+02	1.21E+02	1.21E+02	1.21E+02	1.21E+02
BR 77	0.0	1.51E-03	9.10E-03	7.01E-01	8.31E+00	2.59E+01	8.91E+01	1.02E+02	1.02E+02	1.02E+02	1.02E+02
BR 78	0.0	5.65E-01	3.25E+00	3.18E+01	3.19E+01	3.19E+01	3.19E+01	3.19E+01	3.19E+01	3.19E+01	3.19E+01
KR 76	0.0	6.63E-03	3.98E-02	2.33E+00	1.59E+01	3.44E+01	5.10E+01	5.10E+01	5.10E+01	5.10E+01	5.10E+01
KR 77	0.0	8.87E-02	5.30E-01	2.45E+01	5.67E+01	5.74E+01	5.74E+01	5.74E+01	5.74E+01	5.74E+01	5.74E+01
KR 79	0.0	4.21E-03	2.54E-02	1.84E+00	1.59E+01	4.12E+01	1.05E+02	1.08E+02	1.08E+02	1.08E+02	1.08E+02
RB 79	0.0	1.60E-01	9.47E-01	2.67E+01	3.19E+01	3.19E+01	3.19E+01	3.19E+01	3.19E+01	3.19E+01	3.19E+01
RB 80	0.0	2.35E+01	9.00E+01	1.28E+02	1.28E+02	1.28E+02	1.28E+02	1.28E+02	1.28E+02	1.28E+02	1.28E+02
RB 81	0.0	4.29E-02	2.58E-01	1.57E+01	8.52E+01	1.18E+02	1.21E+02	1.21E+02	1.21E+02	1.21E+02	1.21E+02
RB 82	0.0	5.07E+00	2.44E+01	5.76E+01	5.89E+01	6.18E+01	8.56E+02	1.48E+02	2.04E+02	2.16E+02	2.17E+02
RB 83	0.0	4.75E-05	2.85E-04	1.79E-02	1.85E-01	7.99E-01	1.18E+01	5.97E+01	1.45E+02	2.14E+02	2.61E+02
RB 84	0.0	9.37E-05	5.62E-04	3.37E-02	2.69E-01	8.01E-01	5.28E+00	1.82E+01	3.27E+01	3.75E+01	3.82E+01
RB 85	0.0	2.74E-05	1.65E-04	9.87E-03	7.85E-02	2.33E-01	1.46E+00	4.32E+00	6.16E+00	6.37E+00	6.38E+00
SR 81	0.0	8.48E-02	5.03E-01	1.53E+01	1.91E+01	1.91E+01	1.91E+01	1.91E+01	1.91E+01	1.91E+01	1.91E+01

TABLE 4 - I (SHEET 2)

	Initial	10s	1 min.	1 hour	8 hours	1 day	1 week	4 weeks	12 weeks	26 weeks	1 year
SR 82	0.0	5.12E-04	3.07E-03	1.84E-01	1.47E+00	4.36E+00	2.82E+01	9.08E+01	1.47E+02	1.58E+02	1.59E+02
SR 83	0.0	1.25E-02	7.53E-02	4.68E+00	3.51E+01	8.97E+01	2.17E+02	2.23E+02	2.23E+02	2.23E+02	2.23E+02
SR 85	0.0	1.03E-04	6.18E-04	4.81E-02	7.54E-01	2.88E+00	2.21E+01	8.53E+01	1.91E+02	2.63E+02	3.00E+02
SR 89	0.0	3.04E-05	1.82E-04	1.09E-02	8.72E-02	2.61E-01	1.76E+00	6.56E+00	1.38E+01	1.79E+01	1.95E+01
SR 91	0.0	1.41E-03	8.44E-03	4.89E-01	3.07E+00	5.73E+00	6.93E+00	6.93E+00	6.93E+00	6.93E+00	6.93E+00
SR 93	0.0	1.36E-03	7.85E-03	8.86E-02	8.89E-02	8.89E-02	8.89E-02	8.89E-02	8.89E-02	8.89E-02	8.89E-02
Y 83	0.0	2.07E-01	1.19E+00	1.27E+01	1.28E+01	1.28E+01	1.28E+01	1.28E+01	1.28E+01	1.28E+01	1.28E+01
Y 84	0.0	4.20E-01	2.50E+00	9.27E+01	1.40E+02	1.40E+02	1.40E+02	1.40E+02	1.40E+02	1.40E+02	1.40E+02
Y 85	0.0	1.33E-01	8.03E-01	4.94E+01	1.95E+02	2.23E+02	2.23E+02	2.23E+02	2.23E+02	2.23E+02	2.23E+02
Y 86	0.0	1.84E-02	1.11E-01	9.25E+00	7.41E+01	1.61E+02	2.36E+02	2.36E+02	2.36E+02	2.36E+02	2.36E+02
Y 87	0.0	6.27E-03	3.77E-02	2.49E+00	2.46E+01	7.65E+01	3.14E+02	4.07E+02	4.08E+02	4.08E+02	4.08E+02
Y 88	0.0	1.58E-04	9.51E-04	5.70E-02	4.57E-01	1.37E+00	9.83E+00	4.51E+01	1.43E+02	2.77E+02	4.43E+02
Y 90	0.0	3.64E-03	2.18E-02	1.30E+00	1.00E+01	2.77E+01	1.02E+02	1.21E+02	1.21E+02	1.21E+02	1.21E+02
Y 91	0.0	1.22E-04	7.34E-04	4.41E-02	3.57E-01	1.09E+00	7.64E+00	2.91E+01	6.35E+01	8.51E+01	9.49E+01
Y 91M	0.0	9.42E-07	3.38E-05	9.18E-02	1.56E+00	3.36E+00	3.99E+00	3.99E+00	3.99E+00	3.99E+00	3.99E+00
Y 92	0.0	3.13E-02	1.88E-01	1.02E+01	4.55E+01	5.69E+01	5.74E+01	5.74E+01	5.74E+01	5.74E+01	5.74E+01
Y 93	0.0	1.20E-02	7.22E-02	4.20E+00	2.68E+01	5.14E+01	6.39E+01	6.39E+01	6.39E+01	6.39E+01	6.39E+01
Y 94	0.0	3.87E-02	2.28E-01	5.66E+00	6.38E+00	6.38E+00	6.38E+00	6.38E+00	6.38E+00	6.38E+00	6.38E+00
Y 95	0.0	6.98E-02	4.07E-01	6.26E+00	6.38E+00	6.38E+00	6.38E+00	6.38E+00	6.38E+00	6.38E+00	6.38E+00
ZR 85	0.0	5.59E-01	3.23E+00	3.81E+01	3.83E+01	3.83E+01	3.83E+01	3.83E+01	3.83E+01	3.83E+01	3.83E+01
ZR 86	0.0	6.68E-01	3.94E+00	8.80E+01	9.57E+01	9.57E+01	9.57E+01	9.57E+01	9.57E+01	9.57E+01	9.57E+01
ZR 87	0.0	1.80E-01	1.08E+00	5.24E+01	1.42E+02	1.47E+02	1.47E+02	1.47E+02	1.47E+02	1.47E+02	1.47E+02
ZR 88	0.0	3.01E-04	1.81E-03	1.15E-01	9.35E-01	2.80E+00	1.92E+01	7.55E+01	1.80E+02	2.64E+02	3.22E+02
ZR 89	0.0	3.43E-02	2.06E-01	1.23E+01	9.68E+01	2.72E+02	1.11E+03	1.43E+03	1.43E+03	1.43E+03	1.43E+03
ZR 93	0.0	3.93E-10	2.36E-09	1.42E-07	1.14E-06	3.46E-06	2.47E-05	1.07E-04	3.21E-04	6.43E-04	1.28E-03
ZR 95	0.0	1.67E-03	1.00E-02	6.04E-01	4.83E+00	1.44E+01	9.82E+01	3.77E+02	8.49E+02	1.17E+03	1.34E+03
ZR 97	0.0	2.39E-02	1.43E-01	8.42E+00	5.86E+01	1.31E+02	2.08E+02	2.08E+02	2.08E+02	2.08E+02	2.08E+02
NB 88	0.0	3.75E-01	2.17E+00	2.54E+01	2.55E+01	2.55E+01	2.55E+01	2.55E+01	2.55E+01	2.55E+01	2.55E+01
NB 89	0.0	3.02E-02	1.81E-01	9.23E+00	2.98E+01	3.19E+01	3.19E+01	3.19E+01	3.19E+01	3.19E+01	3.19E+01
NB 90	0.0	1.22E-02	7.35E-02	4.32E+00	3.01E+01	6.64E+01	9.92E+01	9.93E+01	9.93E+01	9.93E+01	9.93E+01
NB 95	0.0	1.89E-09	6.80E-08	2.45E-04	1.57E-02	1.40E-01	6.53E+00	9.79E+01	5.07E+02	9.86E+02	1.31E+03
NB 95M	0.0	2.23E-10	8.03E-09	2.89E-05	1.82E-03	1.56E-02	5.36E-01	3.84E+00	1.03E+01	1.43E+01	1.62E+01
NB 96	0.0	1.86E-04	1.12E-03	6.61E-02	4.78E-01	1.15E+00	2.25E+00	2.26E+00	2.26E+00	2.26E+00	2.26E+00
NB 97	0.0	3.26E-06	2.17E-04	1.96E+00	4.69E+01	1.31E+02	2.08E+02	2.08E+02	2.08E+02	2.08E+02	2.08E+02
NB 97M	0.0	1.27E-03	3.74E-02	7.26E+00	5.05E+01	1.13E+02	1.79E+02	1.80E+02	1.80E+02	1.80E+02	1.80E+02
MO 90	0.0	2.17E-03	1.30E-02	7.34E-01	3.98E+00	6.04E+00	6.38E+00	6.38E+00	6.38E+00	6.38E+00	6.38E+00
MO 93	0.0	3.79E-10	2.28E-09	1.52E-07	1.71E-06	6.00E-06	4.59E-05	2.00E-04	5.98E-04	1.20E-03	2.39E-03
TC 93	0.0	4.46E-03	2.67E-02	1.42E+00	5.53E+00	6.36E+00	6.38E+00	6.38E+00	6.38E+00	6.38E+00	6.38E+00
RH100	0.0	6.63E-09	2.57E-07	1.67E-03	9.77E-02	7.13E-01	8.39E+00	1.28E+01	1.28E+01	1.28E+01	1.28E+01
PD100	0.0	1.44E-04	9.61E-04	1.01E-01	7.89E-01	2.22E+00	9.42E+00	1.27E+01	1.28E+01	1.28E+01	1.28E+01
AG100	0.0	3.12E-01	1.66E+00	6.38E+00	6.38E+00	6.38E+00	6.38E+00	6.38E+00	6.38E+00	6.38E+00	6.38E+00
CD107	0.0	3.36E-06	1.20E-04	2.86E-01	3.69E+00	5.99E+00	6.38E+00	6.38E+00	6.38E+00	6.38E+00	6.38E+00
IN107	0.0	2.27E-02	1.35E-01	4.61E+00	6.38E+00	6.38E+00	6.38E+00	6.38E+00	6.38E+00	6.38E+00	6.38E+00
SN113	0.0	8.89E-06	5.34E-05	3.20E-03	2.56E-02	7.66E-02	5.28E-01	2.14E+00	5.39E+00	8.51E+00	1.13E+01
SB114	0.0	2.06E-01	1.14E+00	6.38E+00	6.38E+00	6.38E+00	6.38E+00	6.38E+00	6.38E+00	6.38E+00	6.38E+00
TOTAL	0.0	3.44E+01	1.48E+02	9.32E+02	2.01E+03	2.99E+03	5.29E+03	6.68E+03	8.27E+03	9.58E+03	1.05E+04

TABLE 4-II

ACTIVITIES FROM TABLE 4-I SUMMED OVER ISOTOPES

	INITIAL	10s	1min	1 hour	8 hours	1 day	1 week	4 weeks	12 weeks	26 weeks	1 year
MN	0.0	7.49E-13	4.49E-12	2.70E-10	2.16E-09	6.47E-09	4.54E-08	1.97E-07	5.91E-07	1.18E-06	2.36E-06
CO	0.0	2.28E-05	1.37E-04	8.23E-03	6.65E-02	2.03E-01	1.50E+00	6.21E+00	1.51E+01	2.29E+01	3.02E+01
NI	0.0	6.82E-04	4.09E-03	2.43E-01	1.82E+00	4.72E+01	1.23E+01	1.28E+01	1.28E+01	1.28E+01	1.28E+01
CU	0.0	3.77E-01	2.17E+00	2.79E+01	3.80E+01	4.28E+01	4.46E+01	4.46E+01	4.46E+01	4.46E+01	4.46E+01
ZN	0.0	1.94E-02	1.15E-01	4.25E+00	6.43E+00	6.52E+00	7.39E+00	1.06E+01	1.80E+01	2.70E+01	3.93E+01
GA	0.0	1.71E-01	1.01E+00	2.54E+01	4.29E+01	5.51E+01	8.12E+01	9.15E+01	9.56E+01	1.01E+02	1.08E+02
GE	0.0	4.14E-03	2.49E-02	1.55E+00	1.21E+01	3.23E+01	1.11E+02	1.89E+02	2.17E+02	2.22E+02	2.29E+02
AS	0.0	1.39E-01	8.25E-01	2.93E+01	6.35E+01	9.48E+01	2.04E+02	2.57E+02	2.91E+02	3.14E+02	3.28E+02
SE	0.0	6.10E-01	3.46E+00	3.21E+01	6.41E+01	9.15E+01	1.15E+02	1.51E+02	1.99E+02	2.39E+02	2.69E+02
BR	0.0	7.45E-01	4.32E+00	7.19E+01	1.32E+02	1.88E+02	3.12E+02	3.25E+02	3.25E+02	3.25E+02	3.25E+02
KR	0.0	9.95E-02	5.95E-01	2.87E+01	8.85E+01	1.33E+02	2.13E+02	2.17E+02	2.17E+02	2.17E+02	2.17E+02
RB	0.0	2.88E+01	1.16E+02	2.28E+02	3.04E+02	3.41E+02	3.85E+02	5.11E+02	6.69E+02	7.54E+02	8.03E+02
SR	0.0	1.01E-01	5.99E-01	2.08E+01	5.97E+01	1.22E+02	2.95E+02	4.32E+02	6.01E+02	6.89E+02	7.28E+02
Y	0.0	9.41E-01	5.57E+00	1.94E+02	5.44E+02	7.68E+02	1.18E+03	1.35E+03	1.49E+03	1.64E+03	1.82E+03
ZR	0.0	1.47E+00	8.61E+00	2.00E+02	4.37E+02	7.01E+02	1.71E+03	2.37E+03	2.95E+03	3.35E+03	3.58E+03
NB	0.0	4.19E-01	2.46E+00	4.82E+01	1.83E+02	3.69E+02	5.54E+02	6.49E+02	1.06E+03	1.55E+03	1.87E+03
MO	0.0	2.17E-03	1.30E-02	7.34E-01	3.98E+00	6.04E+00	6.38E+00	6.38E+00	6.38E+00	6.38E+00	6.38E+00
TC	0.0	4.46E-03	2.67E-02	1.42E+00	5.53E+00	6.36E+00	6.38E+00	6.38E+00	6.38E+00	6.38E+00	6.38E+00
RH	0.0	6.63E-09	2.57E-07	1.67E-03	9.77E-02	7.13E-01	8.39E+00	1.28E+01	1.28E+01	1.28E+01	1.28E+01
PD	0.0	1.44E-04	9.61E-04	1.01E-01	7.89E-01	2.22E+00	9.42E+00	1.27E+01	1.28E+01	1.28E+01	1.28E+01
AG	0.0	3.12E-01	1.66E+00	6.38E+00	6.38E+00	6.38E+00	6.38E+00	6.38E+00	6.37E+00	6.37E+00	6.38E+00
CD	0.0	3.36E-06	1.20E-04	2.86E-01	3.69E+00	5.99E+00	6.38E+00	6.38E+00	6.38E+00	6.38E+00	6.38E+00
IN	0.0	2.27E-02	1.35E-01	4.61E+00	6.38E+00	6.38E+00	6.38E+00	6.38E+00	6.38E+00	6.38E+00	6.38E+00
SN	0.0	8.89E-06	5.34E-05	3.20E-03	2.56E-02	7.66E-02	5.28E-01	2.14E+00	5.39E+00	8.51E+00	1.13E+01
SB	0.0	2.06E-01	1.14E+00	6.38E+00	6.38E+00	6.38E+00	6.38E+00	6.38E+00	6.38E+00	6.38E+00	6.38E+00
TOTALS	0.0	3.44E+01	1.48E+02	9.32E+02	2.01E+03	2.99E+03	5.29E+03	6.68E+03	8.27E+03	9.58E+03	1.05E+04

TABLE 4 - III (SHEET 1)

DECAY OF ZIRCALOY 2 ACTIVITY (CURIES) FOLLOWING SIX MONTHS IRRADIATION
BY 200μA 800 MeV PROTON BEAM ON TARGET URANIUM

	INITIAL	1s	10s	10^2s	10^3s	10^4s	10^5s	10^6s	10^7s	3 x 10^7s	10^8s
CO 56	5.10E+00	5.10E+00	5.10E+00	5.10E+00	5.10E+00	5.09E+00	5.05E+00	4.60E+00	1.84E+00	2.40E-01	1.92E-04
CO 57	7.23E+00	7.23E+00	7.23E+00	7.23E+00	7.23E+00	7.23E+00	7.24E+00	7.09E+00	5.43E+00	3.01E+00	3.81E-01
CO 58	1.06E+01	1.06E+01	1.06E+01	1.06E+01	1.06E+01	1.06E+01	1.05E+01	9.48E+00	3.42E+00	3.54E-01	1.27E-04
NI 57	1.28E+01	1.28E+01	1.28E+01	1.27E+01	1.27E+01	1.21E+01	7.47E+00	6.06E-02	7.44E-23	0.0	0.0
CU 61	1.28E+01	1.28E+01	1.27E+01	1.27E+01	1.21E+01	7.25E+00	4.49E-02	0.0	0.0	0.0	0.0
CU 62	1.91E+01	1.91E+01	1.89E+01	1.70E+01	5.84E+00	1.34E-04	0.0	0.0	0.0	0.0	0.0
CU 64	6.38E+00	6.38E+00	6.38E+00	6.37E+00	6.28E+00	5.48E+00	1.40E+00	1.66E-06	0.0	0.0	0.0
CU 66	6.38E+00	6.36E+00	6.24E+00	5.09E+00	6.62E-01	9.28E-10	0.0	0.0	0.0	0.0	0.0
ZN 63	6.38E+00	6.38E+00	6.36E+00	6.19E+00	4.71E+00	3.05E-01	4.00E-13	0.0	0.0	0.0	0.0
ZN 65	2.06E+01	2.06E+01	2.06E+01	2.06E+01	2.06E+01	2.06E+01	2.06E+01	2.00E+01	1.49E+01	7.70E+00	7.71E-01
GA 65	1.91E+01	1.91E+01	1.90E+01	1.77E+01	8.95E+00	9.69E-03	0.0	0.0	0.0	0.0	0.0
GA 66	1.91E+01	1.91E+01	1.91E+01	1.91E+01	1.87E+01	1.56E+01	2.49E+00	2.71E-08	0.0	0.0	0.0
GA 67	3.83E+01	3.83E+01	3.83E+01	3.83E+01	3.82E+01	3.73E+01	2.99E+01	3.27E+00	7.91E-10	3.38E-31	010
GA 68	2.41E+01	2.41E+01	2.41E+01	2.39E+01	2.21E+01	1.37E+01	1.13E+01	1.10E+01	8.58E+00	4.92E+00	7.00E-01
GE 68	1.13E+01	1.13E+01	1.13E+01	1.13E+01	1.13E+01	1.13E+01	1.13E+01	1.10E+01	8.58E+00	4.92E+00	7.00E-01
GE 69	8.93E+01	8.93E+01	8.93E+01	8.92E+01	8.89E+01	8.50E+01	5.46E+01	6.45E-01	3.45E-20	0.0	0.0
GE 71	1.21E+02	1.21E+02	1.21E+02	1.21E+02	1.21E+02	1.21E+02	1.20E+02	7.41E+01	1.15E-01	6.45E-08	0.0
AS 69	6.38E+00	6.37E+00	6.33E+00	5.90E+00	2.94E+00	2.74E-03	0.0	0.0	0.0	0.0	0.0
AS 70	3.83E+01	3.83E+01	3.82E+01	3.74E+01	3.08E+01	4.33E+00	1.31E-08	0.0	0.0	0.0	0.0
AS 71	1.15E+02	1.15E+02	1.15E+02	1.15E+02	1.14E+02	1.11E+02	8.38E+01	4.89E+00	2.25E-12	0.0	0.0
AS 72	7.02E+01	7.02E+01	7.02E+01	7.01E+01	6.98E+01	6.70E+01	4.61E+01	1.13E+01	2.09E-03	1.06E-11	0.0
AS 73	7.12E+01	7.12E+01	7.12E+01	7.12E+01	7.12E+01	7.12E+01	7.14E+01	6.55E+01	2.68E+01	3.64E+00	3.36E-03
AS 74	1.27E+01	1.27E+01	1.27E+01	1.27E+01	1.27E+01	1.27E+01	1.22E+01	8.12E+00	1.40E-01	1.70E-05	3.31E-19
SE 71	2.55E+01	2.55E+01	2.49E+01	2.02E+01	2.45E+00	1.70E-09	0.0	0.0	0.0	0.0	0.0
SE 72	2.55E+01	2.55E+01	2.55E+01	2.55E+01	2.55E+01	2.53E+01	2.32E+01	9.82E+00	1.82E-03	9.20E-12	0.0
SE 73	1.41E+02	1.41E+02	1.41E+02	1.41E+02	1.40E+02	1.25E+02	7.62E+01	6.58E+01	2.69E+01	3.66E+00	3.36E-03
SE 75	4.61E+01	4.61E+01	4.61E+01	4.61E+01	4.61E+01	4.61E+01	4.58E+01	4.31E+01	2.34E+01	6.05E+00	5.28E-02
BR 74	2.55E+01	2.55E+01	2.54E+01	2.44E+01	1.62E+01	2.65E-01	3.77E-19	0.0	0.0	0.0	0.0
BR 75	4.46E+01	4.46E+01	4.46E+01	4.41E+01	3.96E+01	1.33E+01	2.49E-04	0.0	0.0	0.0	0.0
BR 76	1.21E+02	1.21E+02	1.21E+02	1.21E+02	1.20E+02	1.13E+02	5.42E+01	3.21E-03	0.0	0.0	0.0
BR 77	1.02E+02	1.02E+02	1.02E+02	1.02E+02	1.02E+02	9.96E+01	7.37E+01	3.53E+00	2.26E-13	0.0	0.0
BR 78	3.19E+01	3.18E+01	3.13E+01	2.67E+01	5.34E+00	5.46E-07	0.0	0.0	0.0	0.0	0.0
KR 76	5.10E+01	5.10E+01	5.10E+01	5.10E+01	5.04E+01	4.48E+01	1.39E+01	1.16E-04	0.0	0.0	0.0
KR 77	5.74E+01	5.74E+01	5.73E+01	5.65E+01	4.92E+01	1.22E+01	1.10E-05	0.0	0.0	0.0	0.0
KR 79	1.08E+02	1.08E+02	1.08E+02	1.08E+02	1.08E+02	1.03E+02	6.28E+01	4.47E-01	1.49E-22	0.0	0.0
RB 79	3.19E+01	3.19E+01	3.17E+01	3.03E+01	1.93E+01	2.10E-01	4.91E-21	0.0	0.0	0.0	0.0
RB 80	1.28E+02	1.25E+02	1.04E+02	1.66E+01	1.79E-07	0.0	0.0	0.0	0.0	0.0	0.0
RB 81	1.21E+02	1.21E+02	1.21E+02	1.21E+02	1.17E+02	8.09E+01	1.84E+00	6.81E-17	0.0	0.0	0.0
RB 82	2.16E+02	2.15E+02	2.11E+02	1.81E+02	1.58E+02	1.58E+02	1.53E+02	1.15E+02	6.40E+00	1.06E-02	1.87E-12
RB 83	2.14E+02	2.14E+02	2.14E+02	2.14E+02	2.14E+02	2.14E+02	2.13E+02	1.98E+02	8.57E+01	1.33E+01	1.98E-02
RB 84	3.75E+01	3.75E+01	3.75E+01	3.75E+01	3.74E+01	3.74E+01	3.66E+01	2.93E+01	3.24E+00	2.42E-02	8.75E-10
RB 86	6.37E+00	6.37E+00	6.37E+00	6.37E+00	6.37E+00	6.34E+00	6.10E+00	4.14E+00	8.62E-02	1.58E-05	1.31E-18
SR 81	1.91E+01	1.91E+01	1.90E+01	1.83E+01	1.23E+01	2.25E-01	9.68E-19	0.0	0.0	0.0	0.0

TABLE 4-III (SHEET 2)

	INITIAL	1s	10s	10^2s	10^3s	10^4s	10^5s	10^6s	10^7s	3 x 10^7s	10^8s
SR 82	1.58E+02	1.58E+02	1.58E+02	1.58E+02	1.58E+02	1.58E+02	1.53E+02	1.15E+02	6.40E+00	1.06E-02	1.87E-12
SR 83	2.23E+02	2.23E+02	2.23E+02	2.23E+02	2.22E+02	2.10E+02	1.23E+02	5.90E-01	0.0	0.0	0.0
SR 85	2.63E+02	2.63E+02	2.63E+02	2.63E+02	2.63E+02	2.63E+02	2.60E+02	2.33E+02	7.64E+01	6.44E+00	1.12E-03
SR 89	1.79E+01	1.79E+01	1.79E+01	1.79E+01	1.79E+01	1.79E+01	1.77E+01	1.54E+01	3.84E+00	1.75E-01	3.58E-06
SR 91	6.93E+00	6.93E+00	6.93E+00	6.92E+00	6.79E+00	5.66E+00	9.10E-01	1.05E-08	0.0	0.0	0.0
SR 93	8.89E-02	8.88E-02	8.75E-02	7.62E-02	1.91E-02	1.82E-08	0.0	0.0	0.0	0.0	0.0
Y 83	1.28E+01	1.27E+01	1.25E+01	1.08E+01	2.48E+00	9.99E-07	0.0	0.0	0.0	0.0	0.0
Y 84	1.40E+02	1.40E+02	1.40E+02	1.36E+02	1.04E+02	6.98E+00	1.31E-11	0.0	0.0	0.0	0.0
Y 85	2.23E+02	2.23E+02	2.23E+02	2.22E+02	2.09E+02	1.10E+02	1.71E-01	0.0	0.0	0.0	0.0
Y 86	2.36E+02	2.36E+02	2.36E+02	2.36E+02	2.34E+02	2.09E+02	6.44E+01	5.05E-04	0.0	0.0	0.0
Y 87	4.08E+02	4.08E+02	4.08E+02	4.08E+02	4.08E+02	4.01E+02	3.23E+01	3.74E+01	1.59E-08	2.37E-29	0.0
Y 88	2.77E+02	2.77E+02	2.77E+02	2.77E+02	2.77E+02	2.77E+02	2.77E+02	2.75E+02	2.15E+02	7.52E+01	5.97E-01
Y 90	1.21E+02	1.21E+02	1.21E+02	1.21E+02	1.21E+02	1.18E+02	8.97E+01	6.01E+00	1.08E-11	0.0	0.0
Y 91	8.51E+01	8.51E+01	8.51E+01	8.51E+01	8.51E+01	8.50E+01	8.40E+01	7.43E+01	2.17E+01	1.40E+00	9.65E-05
Y 91M	3.99E+00	3.99E+00	3.99E+00	3.99E+00	3.98E+00	3.53E+00	5.74E-01	6.62E-09	0.0	0.0	0.0
Y 92	5.74E+01	5.74E+01	5.74E+01	5.71E+01	5.44E+01	3.33E+01	2.46E-01	1.19E-22	0.0	0.0	0.0
Y 93	6.39E+01	6.39E+01	6.39E+01	6.37E+01	6.27E+01	5.29E+01	9.67E+00	4.05E-07	0.0	0.0	0.0
Y 94	6.38E+00	6.37E+00	6.34E+00	6.00E+00	3.47E+00	1.46E-02	0.0	0.0	0.0	0.0	0.0
Y 95	6.38E+00	6.37E+00	6.31E+00	5.71E+00	2.12E+00	1.06E-04	0.0	0.0	0.0	0.0	0.0
ZR 85	3.83E+01	3.82E+01	3.77E+01	3.30E+01	8.78E+00	1.56E-05	0.0	0.0	0.0	0.0	0.0
ZR 86	9.57E+01	9.56E+01	9.50E+01	8.92E+01	4.75E+01	8.87E-02	0.0	0.0	0.0	0.0	0.0
ZR 87	1.47E+02	1.47E+02	1.47E+02	1.45E+02	1.30E+02	4.30E+01	6.92E-04	0.0	0.0	0.0	0.0
ZR 88	2.64E+02	2.64E+02	2.64E+02	2.64E+02	2.64E+02	2.64E+02	2.61E+02	2.40E+02	1.01E+02	1.47E+01	1.76E-02
ZR 89	1.43E+03	1.43E+03	1.43E+03	1.43E+03	1.42E+03	1.39E+03	1.12E+03	1.23E+02	3.11E-08	1.48E-29	0.0
ZR 95	1.17E+03	1.17E+03	1.17E+03	1.17E+03	1.17E+03	1.17E+03	1.16E+03	1.04E+03	3.45E+02	2.97E+01	5.62E-03
ZR 97	2.08E+02	2.08E+02	2.08E+02	2.08E+02	2.06E+02	1.86E+02	6.63E+01	2.20E-03	0.0	0.0	0.0
NB 88	2.55E+01	2.55E+01	2.51E+01	2.20E+01	5.80E+00	9.44E-06	0.0	0.0	0.0	0.0	0.0
NB 89	3.19E+01	3.19E+01	3.19E+01	3.16E+01	2.90E+01	1.24E+01	2.42E-03	0.0	0.0	0.0	0.0
NB 90	9.93E+01	9.93E+01	9.92E+01	9.91E+01	9.80E+01	8.77E+01	2.75E+01	1.94E-04	0.0	0.0	0.0
NB 95	9.86E+02	9.86E+02	9.86E+02	9.86E+02	9.86E+02	9.86E+02	9.90E+02	1.01E+03	5.86E+02	6.25E+01	1.21E-02
NB 95M	1.43E+01	1.43E+01	1.43E+01	1.43E+01	1.43E+01	1.43E+01	1.42E+01	1.31E+01	4.38E+00	3.78E-01	7.14E-05
NB 96	2.26E+00	2.26E+00	2.26E+00	2.26E+00	2.24E+00	2.08E+00	9.94E-01	6.04E-04	0.0	0.0	0.0
NB 97	2.08E+02	2.08E+02	2.08E+02	2.08E+02	2.08E+02	1.97E+02	6.70E+01	2.37E-03	0.0	0.0	0.0
NB 97M	1.80E+02	1.80E+02	1.80E+02	1.80E+02	1.78E+02	1.60E+02	5.72E+01	1.89E-03	0.0	0.0	0.0
MO 90	6.38E+00	6.38E+00	6.38E+00	6.36E+00	6.17E+00	4.54E+00	2.14E-01	1.14E-14	0.0	0.0	0.0
MO 93	1.20E-03	1.20E-03	1.20E-03	1.20E-03	1.20E-03	1.20E-03	1.20E-03	1.20E-03	1.20E-03	1.20E-03	1.20E-03
TC 93	6.38E+00	6.38E+00	6.37E+00	6.33E+00	5.95E+00	3.17E+00	5.75E-03	0.0	0.0	0.0	0.0
RH100	1.28E+01	1.28E+01	1.28E+01	1.28E+01	1.28E+01	1.27E+01	1.19E+01	1.84E+00	4.23E-09	2.69E-28	0.0
PD100	1.28E+01	1.28E+01	1.28E+01	1.28E+01	1.27E+01	1.25E+01	1.02E+01	1.40E+00	3.22E-09	2.05E-28	0.0
AG100	6.38E+00	6.35E+00	6.07E+00	3.86E+00	4.20E-02	9.82E-22	0.0	0.0	0.0	0.0	0.0
CD107	6.38E+00	6.38E+00	6.38E+00	6.38E+00	6.35E+00	5.16E+00	3.60E-01	9.50E-13	0.0	0.0	0.0
IN107	6.38E+00	6.38E+00	6.36E+00	6.15E+00	4.47E+00	1.80E-01	2.09E-15	0.0	0.0	0.0	0.0
SN113	8.51E+00	8.51E+00	8.51E+00	8.51E+00	8.51E+00	8.50E+00	8.45E+00	7.93E+00	4.24E+00	1.05E+00	7.98E-03
SB114	6.38E+00	6.36E+00	6.17E+00	4.59E+00	2.40E-01	3.56E-14	0.0	0.0	0.0	0.0	0.0
TOTAL	9.58E+03	9.58E+03	9.55E+03	9.38E+03	9.03+03	8.21E+03	6.45E+03	3.89E+03	1.58E+03	2.39E+02	3.27E+00

TABLE 4-IV

ACTIVITIES FROM TABLE 4-III SUMMED OVER ISOTOPES

	INITIAL	1s	10s	10^2s	10^3s	10^4s	10^5s	10^6s	10^7s	3 x 10^7s	10^8s
MN	1.18E-06	1.18E-06	1.18E-06	1.18E-06	1.18E-06	1.18E-06	1.18E-06	1.18E-06	1.18E-06	1.18E-06	1.18E-06
CO	2.29E+01	2.29E+01	2.29E+01	2.29E+01	2.29E+01	2.29E+01	2.28E+01	2.12E+01	1.07E+01	3.60E+00	3.81E-01
NI	1.28E+01	1.28E+01	1.28E+01	1.27E+01	1.27E+01	1.21E+01	7.47E+00	6.07E-02	1.47E-04	1.47E-04	1.47E-04
CU	4.46E+01	4.46E+01	4.43E+01	4.11E+01	2.48E+01	1.27E+01	1.45E+00	1.66E-06	0.0	0.0	0.0
ZN	2.70E+01	2.70E+01	2.70E+01	2.68E+01	2.54E+01	2.09E+01	2.06E+01	2.00E+01	1.49E+01	7.70E+00	7.71E-01
GA	1.01E+02	1.01E+02	1.00E+02	9.90E+01	8.80E+01	6.66E+01	4.37E+01	1.43E+01	8.58E+00	4.92E+00	7.00E-01
GE	2.22E+02	2.22E+02	2.22E+02	2.22E+02	2.22E+02	2.18E+02	1.86E+02	8.58E+01	8.70E+00	4.92E+00	7.00E-01
AS	3.14E+02	3.14E+02	3.13E+02	3.12E+02	3.02E+02	2.67E+02	2.13E+02	8.98E+01	2.69E+01	3.64E+00	3.36E-03
SE	2.39E+02	2.38E+02	2.38E+02	2.33E+02	2.14E+02	1.96E+02	1.45E+02	1.19E+02	5.03E+01	9.70E+00	5.61E-02
BR	3.25E+02	3.25E+02	3.25E+02	3.18E+02	2.83E+02	2.26E+02	1.28E+02	3.54E+00	2.26E-13	0.0	0.0
KR	2.17E+02	2.17E+02	2.17E+02	2.16E+02	2.08E+02	1.60E+02	7.67E+01	4.47E-01	2.64E-04	2.64E-04	2.64-04
RB	7.54E+02	7.51E+02	7.25E+02	6.07E+02	5.52E+02	4.97E+02	4.11E+02	3.47E+02	9.55E+01	1.34E+01	1.98E-02
SR	6.89E+02	6.89E+02	6.89E+02	6.88E+02	6.80E+02	6.55E+02	5.55E+02	3.64E+02	8.67E+01	6.62E+00	1.12E-03
Y	1.64E+03	1.64E+03	1.64E+03	1.63E+03	1.57E+03	1.30E+03	8.49E+02	3.93E+02	2.36E+02	7.66E+01	5.97E-01
ZR	3.35E+03	3.35E+03	3.35E+03	3.34E+03	3.25E+03	3.06E+03	2.60E+03	1.40E+03	4.45E+02	4.45E+01	2.39E-02
NB	1.55E+03	1.55E+03	1.55E+03	1.54E+03	1.52E+03	1.46E+03	1.16E+03	1.02E+03	5.90E+02	6.28E+01	1.27E-02
MO	6.38E+00	6.38E+00	6.38E+00	6.36E+00	6.17E+00	4.54E+00	2.15E-01	1.20E-03	1.20E-03	1.20E-03	1.20E-03
TC	6.38E+00	6.38E+00	6.37E+00	6.33E+00	5.95E+00	3.17E+00	5.75E-03	0.0	0.0	0.0	0.0
RH	1.28E+01	1.28E+01	1.28E+01	1.28E+01	1.28E+01	1.27E+01	1.19E+01	1.84E+00	4.23E-09	2.69E-28	0.0
PD	1.28E+01	1.28E+01	1.28E+01	1.28E+01	1.27E+01	1.25E+01	1.02E+01	1.40E+00	3.22E-09	2.05E-28	0.0
AG	6.38E+00	6.35E+00	6.07E+00	3.86E+00	4.20E-02	9.82E-22	0.0	0.0	0.0	0.0	0.0
CD	6.38E+00	6.38E+00	6.38E+00	6.38E+00	6.35E+00	5.16E+00	3.60E-01	9.50E-13	0.0	0.0	0.0
IN	6.38E+00	6.38E+00	6.36E+00	6.15E+00	4.47E+00	1.80E-01	6.51E-15	4.42E-15	4.42E-15	4.42E-15	4.42E-15
SN	8.51E+00	8.51E+00	8.51E+00	8.51E+00	8.51E+00	8.50E+00	8.45E+00	7.93E+00	4.24E+00	1.05E+00	7.98E-03
SB	6.38E+00	6.36E+00	6.17E+00	4.59E+00	2.40E-01	3.56E-14	0.0	0.0	0.0	0.0	0.0
TOTALS	9.58E+03	9.58E+03	9.55E+03	9.38E+03	9.03E+03	8.21E+03	6.45E+03	3.89E+03	1.58E+03	2.39E+02	3.27E+00

TABLE 4-V

PRODUCTION RATES FOR SHORT LIVED NUCLIDES IN THE D_2O TARGET COOLANT

NUCLIDE	HALF LIFE	DECAY MODE	PRODUCT	PRODUCTION RATE NUCLEI PER INCIDENT PROTON	SATURATION ACTIVITY Ci/litre
^{19}O	26.76s	β^-	^{19}F (Stable)	2×10^{-8}	$<5 \times 10^{-4}$
^{15}O	122.1s	β^+	^{15}N (Stable)	1×10^{-2}	.69
^{14}O	70.6s	β^+	^{14}N (Stable)	3.2×10^{-4}	.03
^{18}N	0.63s	β^-	^{18}O (Stable)	2.5×10^{-5}	.001
^{17}N	4.174s	$\beta^- n^o$ 95.1%	^{16}O (Stable)		.03
		β^- 4.9%	^{17}O (Stable)		.002
^{16}N	7.13s	β^-	^{16}O (Stable)	1.6×10^{-3}	.59
^{13}N	9.963m	β^+	^{13}C (Stable)	2.6×10^{-3}	.15
^{12}N	0.011s	β^+ 96.5%	^{12}C (Stable)		1.9
		$\beta^+\alpha$ 3.5%	$^{8}Be \rightarrow 2\alpha$		.07
^{16}C	0.75s	$\beta^- n^o$	^{15}N (Stable)	2.4×10^{-6}	.007
^{15}C	2.45s	β^-	^{15}N (Stable)	7.7×10^{-5}	.08
^{11}C	20.4m	β^+	^{11}B (Stable)	1.1×10^{-3}	.064
^{10}C	192s	β^+	^{10}B (Stable)	2.2×10^{-4}	.03
^{16}B	?	?	?	2.2×10^{-7}	-
^{15}B	?	?	?	4.3×10^{-7}	-
^{14}B	.016s	β^-	^{14}C	1.1×10^{-4}	0.66
^{13}B	.0173s	β^- 99.72%	^{13}C (Stable)		1.3
		$\beta^- n$ .28%	^{12}C (Stable)		.004
^{12}B	.0203s	β^- 98.4%	^{12}C (Stable)		0.65
		$\beta^-\alpha$ 1.6%	$^{8}Be \rightarrow 2\alpha$		0.01
^{9}B	8.5×10^{-19}s	P 2α	-	4.3×10^{-4}	-
^{13}Be	?	?	?	2.2×10^{-7}	-
^{12}Be	.0114s	β^- (50%?)	^{12}B		.001
		$\beta^- n$ (50%?)	^{11}B (Stable)		.001
^{11}Be	13.81s	β^- 97%	^{11}B (Stable)		.02
		$\beta^-\alpha$ 3%	^{7}Li (Stable)		.001
^{8}Li	.84s	β^-	$^{8}Be \rightarrow 2\alpha$	5.0×10^{-6}	.01
^{5}Li	?	?	?	2.2×10^{-4}	-
^{7}He	? ?	?	?	4.3×10^{-7}	-
^{6}He	.808s	β^-	^{6}Li (Stable)	3.1×10^{-7}	.001
^{5}He	?	?	?	2.2×10^{-4}	-

Total = 6.3 ci/litre

TABLE 4-V1

ACTIVITIES DUE TO SHORT LIVED NUCLIDES IN D_2O TARGET COOLANT

NUCLIDE	HALF-LIFE	DECAY MODE	PRODUCE	PRODUCTION RATE NUCLEI/INCIDENT PROTON	HEAT EXCHANGER ACTIVITY AVERAGE OVER 70 litres	EXTERIOR VOLUME ACTIVITY AVERAGE OVER 519 litres
^{17}N	4.174s	β^- 4.9%	^{17}O (Stable)	5×10^{-5}	0.02	.009
		β^-n 95.1%	^{16}O (Stable)		0.34	0.17
^{16}N	7.13s	β^-	^{16}O (Stable)	1.6×10^{-3}	14.3	16.2
^{13}N	9.96m	β^+	^{13}C (Stable)	2.6×10^{-3}	10.7	76.7
^{14}O	70.6s	β^+	^{14}N (Stable)	3.2×10^{-4}	1.6	9.1
^{15}O	122.1s	β^+	^{15}N (Stable)	1×10^{-2}	45.2	290
^{15}C	2.45s	β^-	^{15}N (Stable)	7.7×10^{-5}	0.28	0.0
^{11}C	20.4m	β^+	^{11}B (Stable)	1.1×10^{-3}	4.45	32.5
^{10}C	19.2s	β^+	^{10}B (Stable)	2.2×10^{-4}	1.58	5.1
^{11}Be	13.81s	β^-	^{11}B (Stable)	1.1×10^{-4}	0.86	2.1
		$\beta^-\alpha$	^{7}Li (Stable)		0.03	.07
					79	430

TABLE 4-VII

ACTIVITY DUE TO LONG LIVED NUCLIDES IN THE D_2O TARGET COOLANT.

HEAT EXCHANGER (70 litres)						EXTERIOR VOLUME (519 litres)				
Irradiation time	^{7}Be	^{3}H	^{14}C	Sum	(a) Total Activity	^{7}Be	^{3}H	^{14}C	Sum	(a) Total Activity
1 week	.59	.04		.63	80	4.4	.32		4.7	430
1 month	2.2	.19		2.4	81	16.5	1.4		18	450
3 months	4.7	.56		5.3	84	35	4.1		39	470
6 months	6.2	1.1		7.3	86	46	8.2		54	480
1 year	6.7	2.2		8.9	88	49	16		65	500
1.5 years	6.7	3.2		9.9	89	50	24		74	500
2 years	6.7	4.2	.001	11	90	50	32	.009	82	510
5 years	6.7	9.8	.003	17	96	50	73	.02	120	550
∞	6.7	40.0	4.8	52	130	50	296	36	380	810

Note (a) Includes the contribution from short lived nuclides from Table 4-V1

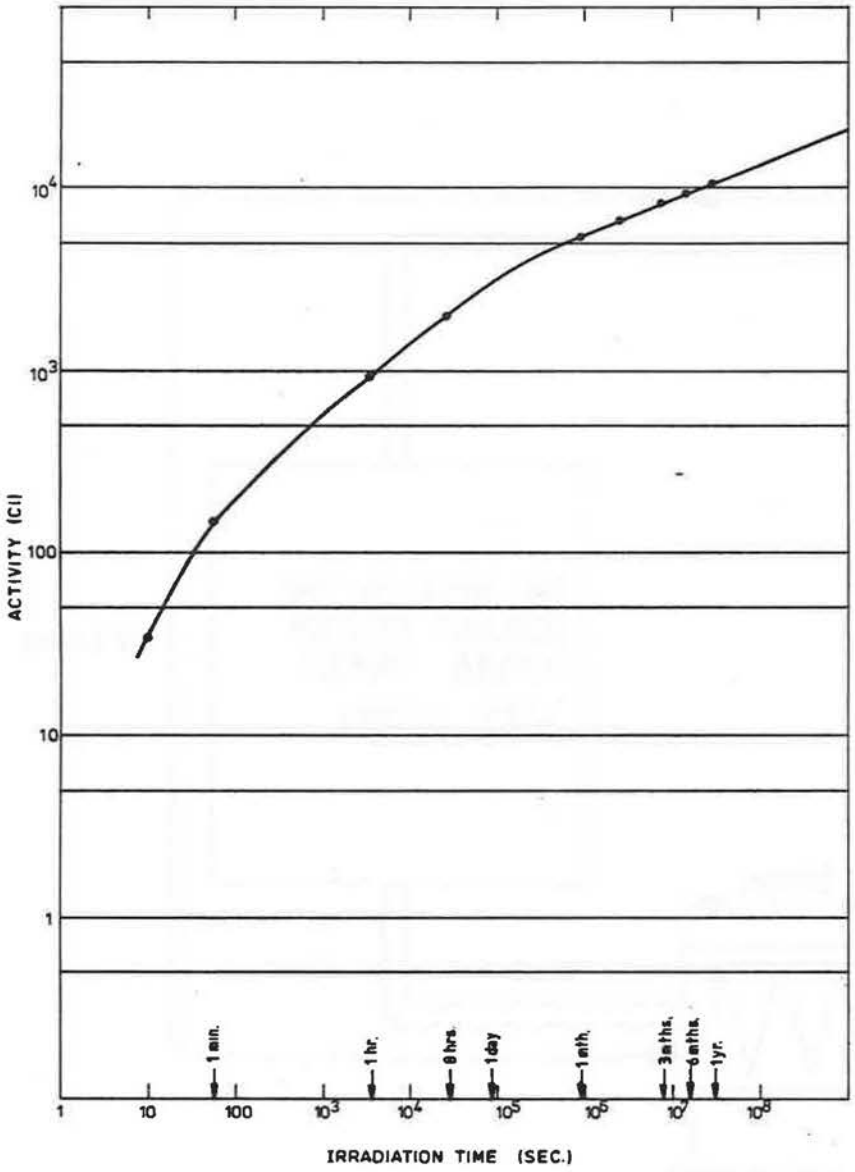

Fig IV 1.1: Buildup of activity in Zircaloy 2.

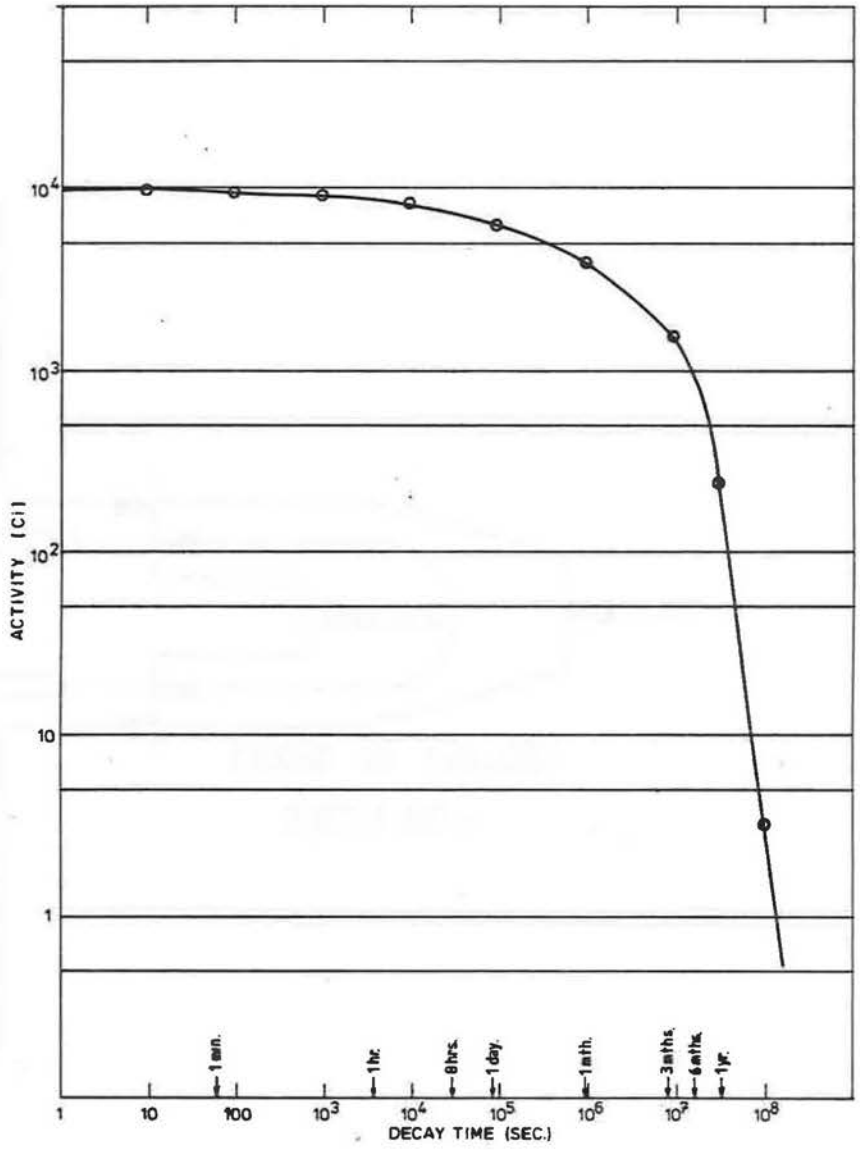

Fig IV 1.2: Decay of activity in Zircaloy 2 following 6 months continuous irradiation.

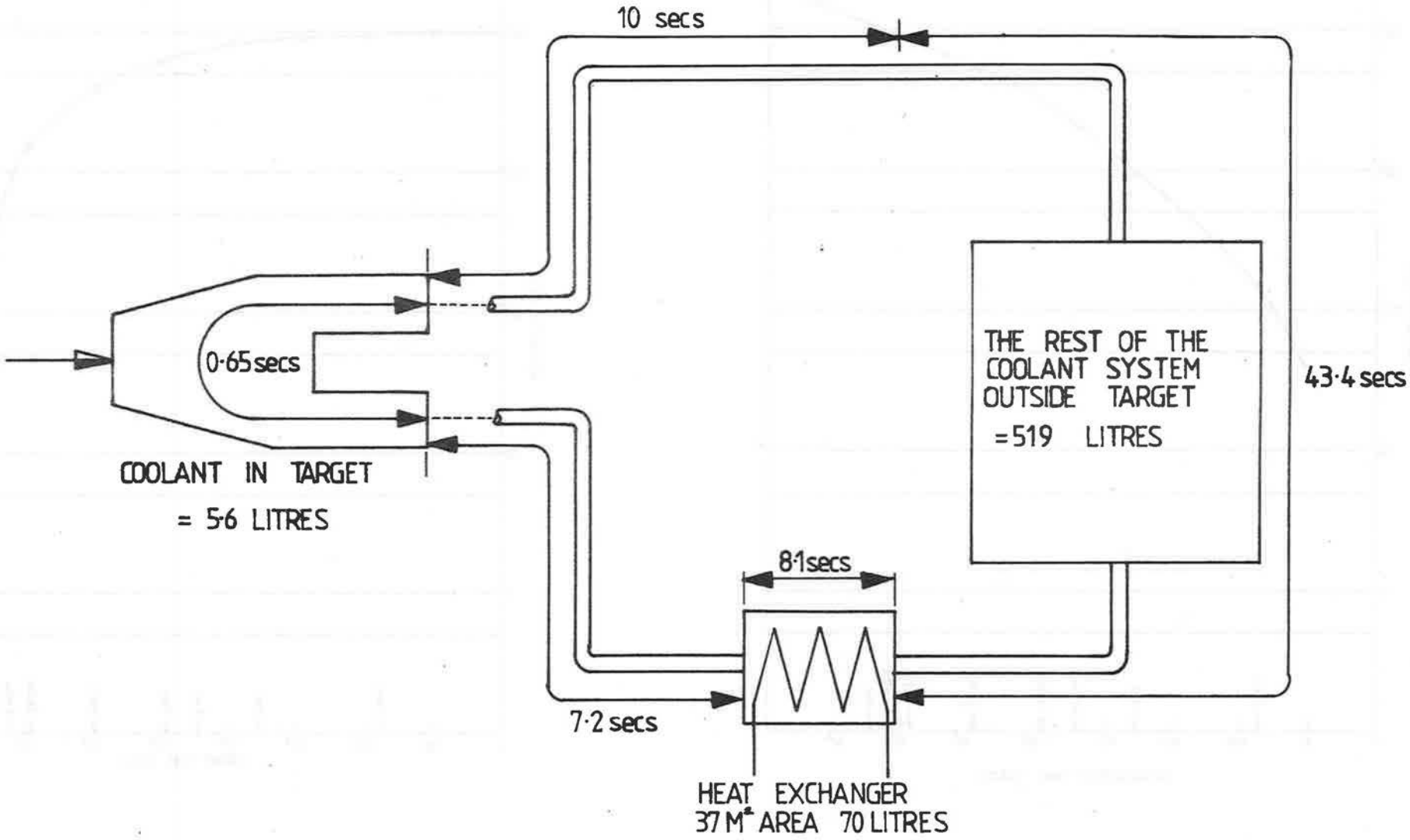

Fig IV 1.3: Representation of cooling system used in activation calculation.

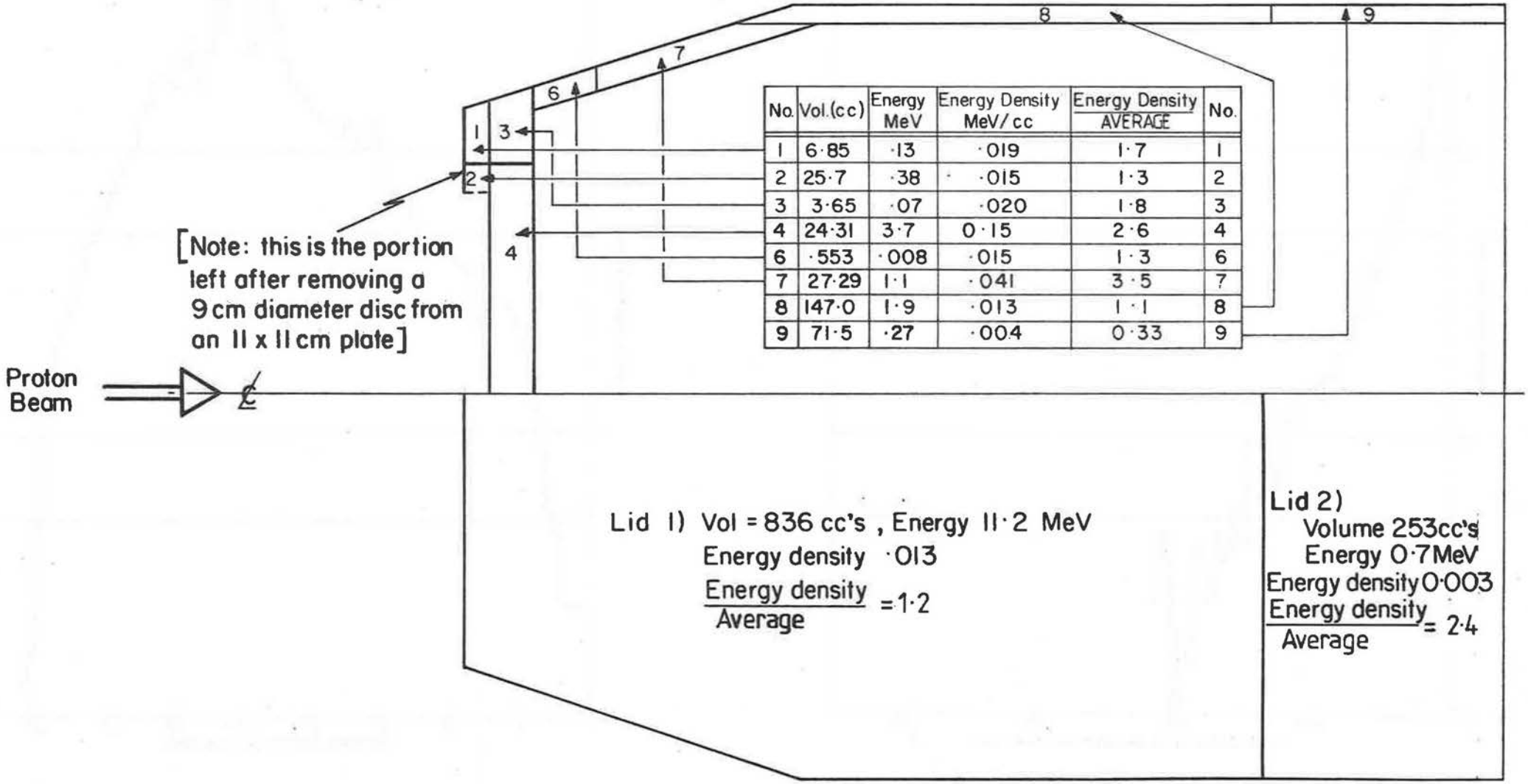

No.	Vol.(cc)	Energy MeV	Energy Density MeV/cc	Energy Density AVERAGE	No.
1	6·85	·13	·019	1·7	1
2	25·7	·38	·015	1·3	2
3	3·65	·07	·020	1·8	3
4	24·31	3·7	0·15	2·6	4
6	·553	·008	·015	1·3	6
7	27·29	1·1	·041	3·5	7
8	147·0	1·9	·013	1·1	8
9	71·5	·27	·004	0·33	9

Fig IV 2.1: Distribution of energy deposited in target pressure vessel.

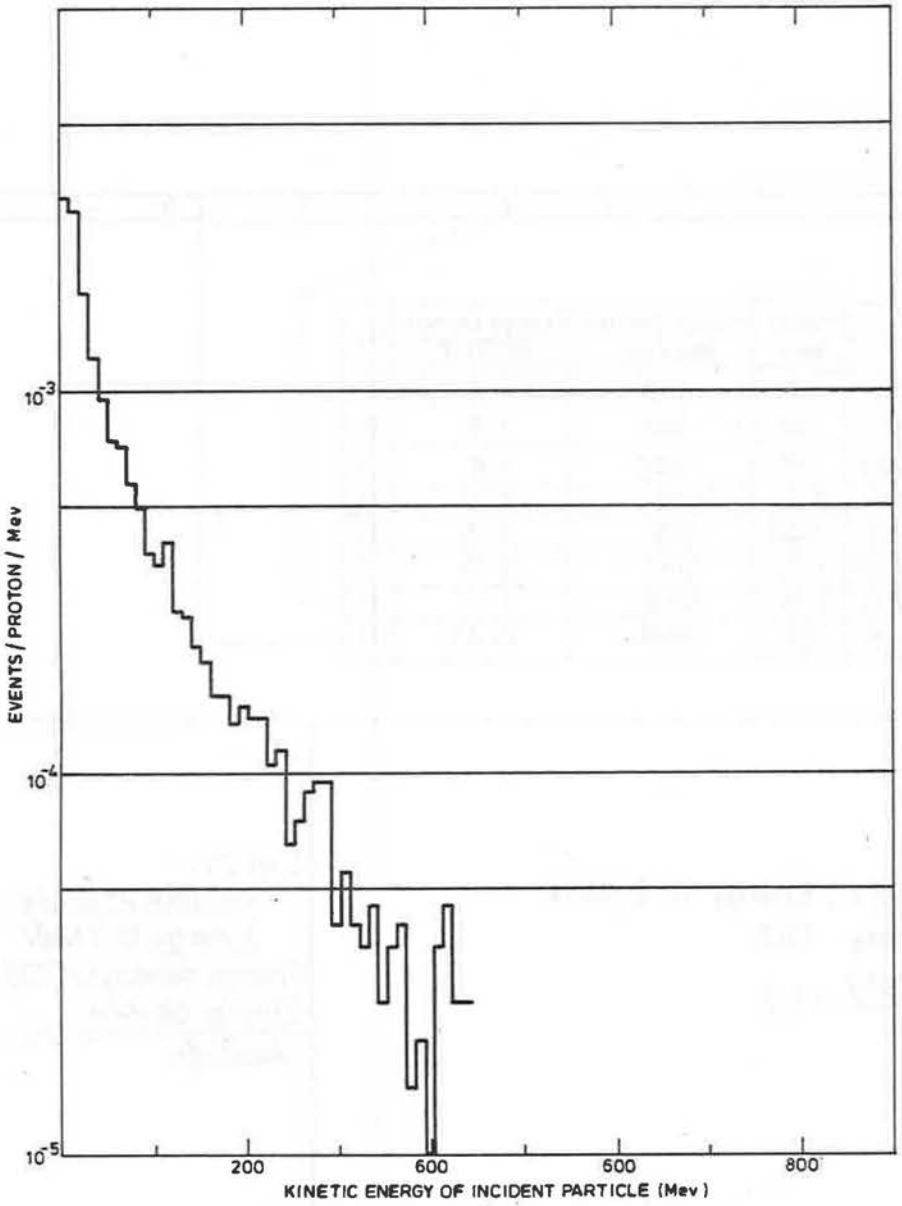

Fig IV 2.2: Distribution of energy of particles inducing HE reactions with Inconel.

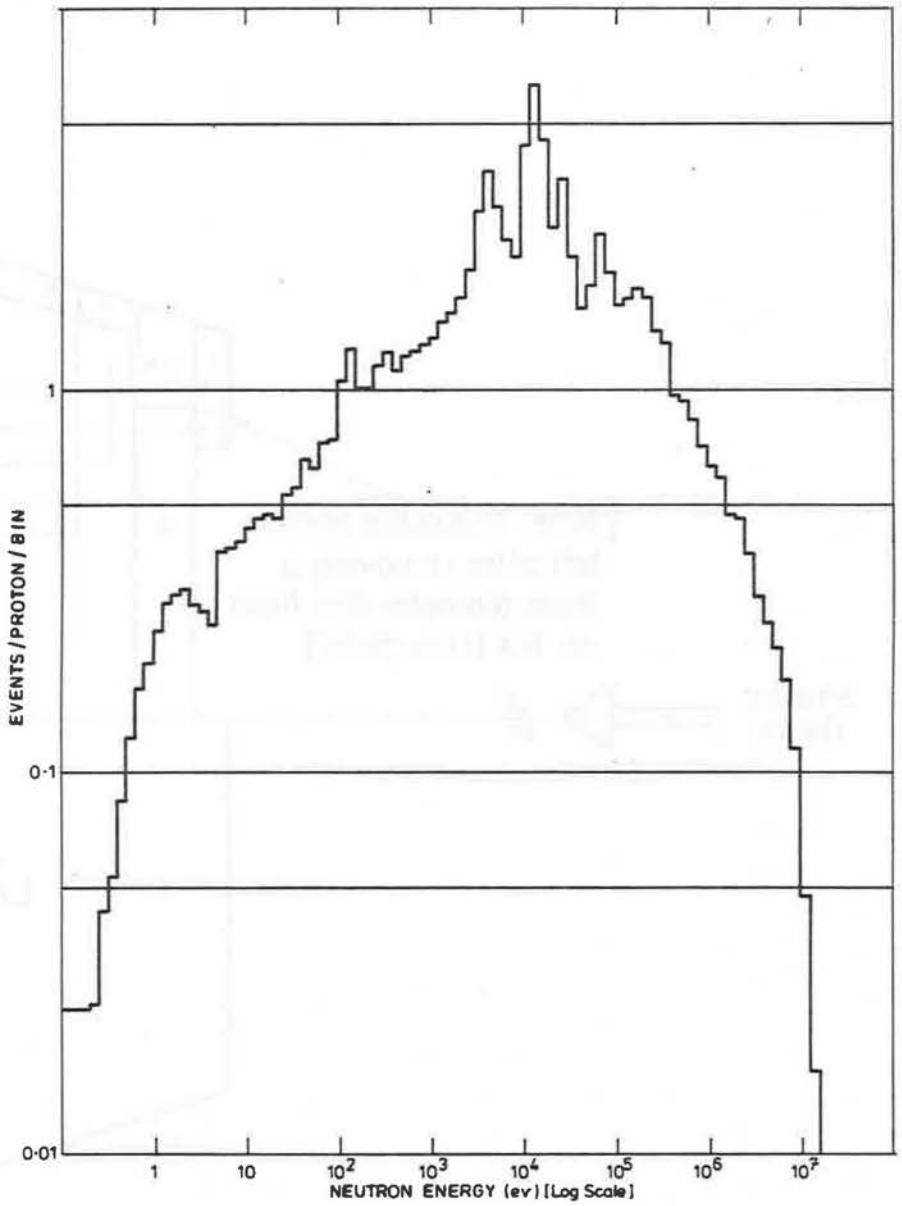

Fig IV 2.3: Distribution of energy of neutrons interacting with Inconel.

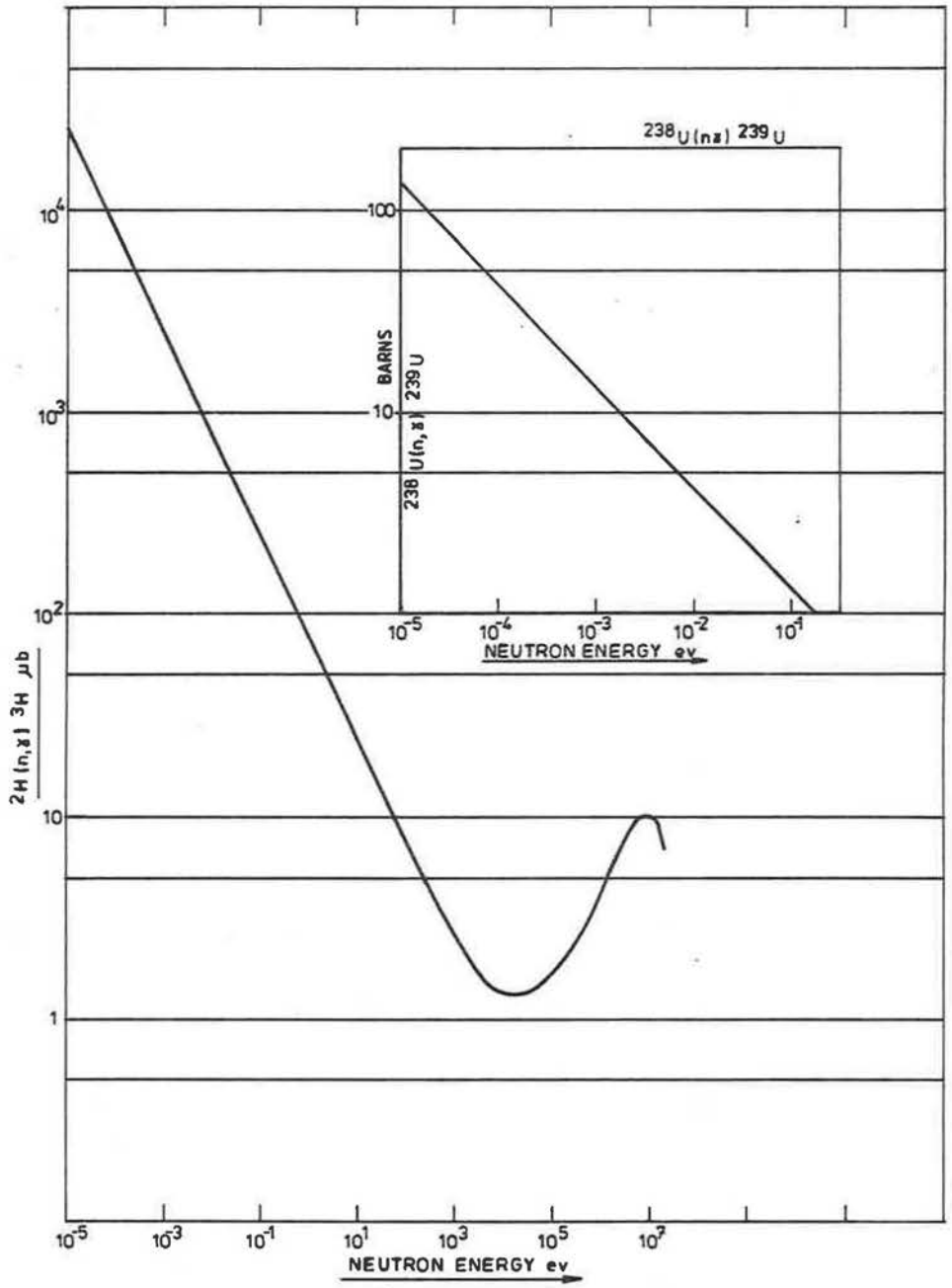

Fig IV 2.4: *Cross-section for $^{2}H\ (n,\gamma)^{3}H$ and $^{238}U\ (n,\gamma)^{239}U$ reactions as a function of neutron energy (from ENDF/BIV [12]).*

CHAPTER 5

REFLECTOR MODERATOR AND DECOUPLER

1 INTRODUCTION

The present calculation does not treat either thermal neutron transport or the time structure for moderator neutron flux. The choice and disposition of materials is the result of the extensive study by Taylor [1] to produce an acceptable neutron pulse; his calculations were made using the time dependent code TIMOC [25], which employs a similar neutron transport scheme to O5R. The time averaged results from TIMOC should provide a check on the present calculation through comparison of neutron transport results.

The geometric layout has been described in Chapter 2 Section 2. Specific points concerning the simplifications and approximations will be given in the appropriate sections following.

This calculation includes a direct estimate for the contribution from the high-energy target escapes.

2. REFLECTOR

The reflector consists of beryllium rods cooled by heavy water. The model used assumes the reflector to contain 80% by volume Be and is represented by a homogenous mixture of Be and D_2O in these proportions. The 'model' reflector contains 134.8 litres of Be and 33.7 litres of D_2O.

2.1 Energy Deposition

The calculated total energy deposited is 36 MeV/proton; this corresponds to 7.2 kW at 200μA proton current. The contributions to this energy from the various stages of the calculation are:-

(a) O5R for 'target escape' neutrons	15.4 MeV
(b) HET for 'target escape' high energy particles	20.11 MeV
(c) O5R for neutrons produced in calculation '(b)'	0.49 MeV

Roughly 56% of the energy deposited comes from the extension of the high energy cascade from the target. The energy has not been apportioned between the Be and D_2O; the 7.2 kW represents the estimated total heat load on the reflector cooling circuit at full intensity.

The distribution of energy is indicated by giving the contribution from various parts in Tables 5-I to 5-IV with Figs V 2.1, V 2.2, V 2.3(a) and V 2.3(b) showing their location. The results for half the reflector only are given because of the {up/down & x→−x} symmetry. This symmetry is explicitly shown in Table 5-III where results for Fig V 2.3(a) & (b) and its mirror reflection about the centre line are both quoted.

The highest power density is 470 mW cm^{-3} (Table 5-II) and is roughly 11 times the overall average of 43mW cm^{-3}. In view of the large volume of this piece, 85cm^3, the 'true' peak to average for energy deposition will probably be higher than this.

If we assume the beryllium to be made up from 2.7cm diameter rods, a surface area of ~20m^2 will be available for cooling. Were all the 7.2kW deposited in the beryllium this would mean an average heat transfer rate of 36mW cm^{-2} would be required, with a peak transfer rate of more than an order of magnitude higher. The temperature difference between the surface and the centre should be no more than a few degrees.

2.2. Activation

2.2.1 Collision Information

The transport calculation gives the following collision information normalised to per proton incident at the uranium target:-

	Be	O	D
High energy collisions	.48	.05	.06
Neutron elastic scattering	528.	25.	43.
Neutron non-elastic scattering	-	.014	.02
(n,2n)	1.6	-	-
(n,γ)	3.6×10^{-2}	3.9×10^{-5}	2.5×10^{-4}

(n,p)	1.3×10^{-5}	4×10^{-4}	-
(n,d)	-	8.9×10^{-5}	
(n,t)	2.2×10^{-3}	-	-
(n,d)	.36	1.3×10^{-2}	-
TOTALS	~ 530	~ 25	~ 43

2.2.2 Activity

(a) Beryllium. The intranuclear cascade model becomes increasingly unreliable as the target nucleus mass becomes very light; in view of this, the nuclide distribution from HET for the 'high-energy' reactions is not quoted and no estimate for the activity of the Be made. The energy distribution for the particles inducing Be spallation is shown in Fig V 2.4 along with those for oxygen collisions.

(b) D_2O. Ultimately a coolant activation calculation on the lines of that for the target coolant {qv Chapter 4 Section 1.3} should be made. As details of the coolant system design are not known at this stage, only estimates of tritiation and neutron activity are presented.

Direct tritiation from neutron capture by deuterium is predicted to be at the rate of 2.5×10^{-4}/proton. On the assumption of 10% of the spallations leading to the production of a triton, the spallation events will contribute a further 5×10^{-3}/proton. The average activity from tritium rises at a rate of 5.3×10^{-9}Ci/litre/sec. This gives an activity of .08, .14 and .32 Ci/litre at 0.5, 1 and 2 years irradiation. Neutron activity will come from ^{17}N, ^{13}B, ^{12}Be and ^{16}C. The estimated production for these is 2.9×10^{-5}/proton. This corresponds to an equilibrium rate of 4×10^{10} neutrons/sec for 200μA proton current throughout the D_2O. The most persistent component is ^{17}N with a half life of 4.2 seconds.

2.2.3 Damage

There are 530 collisions with Be nuclei throughout the 134.8 litres. This corresponds to an average rate of 4.1×10^{-11} primary displacements

per atom. Energy desposition indicates a peak to average of >10 to 1. On this basis rates greater than 4×10^{-10} primary displacements per atom could occur in localised regions.

2.2.4 Removal of Beryllium

2.5 Be nuclei are destroyed per proton incident on the target. This is equivalent to 1.9×10^{-11}%/sec at 200 μA averaged over the full volume.

2.25 Helium Evolution

~ 3.6 helium atoms are emitted for each proton on the target. This corresponds to 1.7×10^{-7} litres/sec (NTP) averaged over the full volume.

2.3 Thermal Group Neutrons

4.1 n^o/proton incident at the target, reach an energy below 0.1eV and have their histories terminated. It is assumed that these will not contribute significantly to tritation of the D_2O coolant.

The possible fates are:-

(a) Capture by Be to form ^{10}Be
(b) To escape the full system
(c) Capture by ^{10}B in the decoupler

3. MODERATORS

The system modelled contains four moderators. Although their geometric disposition is close to that for the day 1 assembly, the details of the moderators themselves have been simplified (Taylor [26]). All four moderators are of the same size and contain H_2O; their dimensions are 5cm deep by 10cm wide and 12.6cm high. The geometry of the moderator layers is shown in Fig V 3.1 and the upper layer is related to the lower by x→-x transform: This means the main portions of void for the neutron beam exits do not coincide vertically.

The moderator containers have not been included in the model.

The numbering system illustrated in Fig II 2.2 of chapter 2 is used to identify moderator faces and neutron beam exit holes.

3.1 Energy Deposition

In this modelling we include a direct estimate for the deposition from the high energy particles escaping the target. The energy depositions from the three components - high energy particles, target escape fast neutrons and neutrons created by the passage of the fast particles are shown in the following table; the main entries are in units of MeV/proton incident on the target, and the figures in brackets the power in watts assuming a 200 μA beam.

	High Energy Particles	Target Neutrons	Supra-target Neutrons	Total
1. Top Front	.17 (34)	.84 (168)	.05 (11)	1.06 (212)
2. Top Back	.22 (44)	.36 (72)	.05 (11)	.63 (126)
3. Bottom Front	.17 (34)	.82 (164)	.05 (11)	1.04 (208)
4. Bottom Back	.22 (44)	.34 (68)	.06 (12)	.62 (124)

From the symmetry in the system we should expect the results from moderators 1&3 and 2&4 to be the same. The overall energy deposited in the four moderators is 3.35 MeV/proton or 670 watts. It should be noted that an additional heat load for a coolant system will come from the containers and has not been included; this will depend on the details of the final design (volume and material).

3.2 Collision Information

The following list contains the inventory of collisions which took place in the water of the moderators and is the sum of collisions over all four moderators. The numbers are normalised to per proton incident in the target.

1)	High energy collisions with oxygen	.015
2)	High energy proton collisions	.019
3)	Neutron elastic scatters with oxygen	4.5
4)	Neutron non-elastic scatters with oxygen	6.1×10^{-3}
5)	(n,γ) reactions with oxygen	5.5×10^{-6}
6)	(n,p) reactions with oxygen	1.6×10^{-4}
7)	(n,d) reactions with oxygen	3.4×10^{-5}
8)	(n,t) reactions with oxygen	5.2×10^{-3}
9)	Neutron elastic scatters with protons	36.3
10)	(n,γ) captures by protons	2×10^{-2}

It is inappropriate at this stage to make activation estimates. The following are relevant to the use of water moderators.

(a) The high energy oxygen collisions will lead to tritiation.

(b) The (n,p) and high energy collisions will lead to the production of neutron emitting nuclides and provide a further (but probably insignificant) contribution to the time independant background.

(c) Activation will make a contribution to the charged particle and proton background.

(d) The .015 oxygen collisions and the .02 hydrogen collisions along with elastic scatters, all by high energy particles will cause a high energy flux from the moderators into the experimental area.

3.3 Fluxes from the Moderators

The moderator fluxes have been estimated in terms of the flux at 1eV normal to a $100cm^2$ face per eV per steradian by fitting the calculated moderated neutron energies to a slowing down spectrum in the energy region 1eV to 1keV.

The analysis has been made using information on all low energy neutron escapes from the full system. Neutron escapes with trajectories which backwards-project onto a moderator face and down a beam exit void, were collected and used to give an unnormalised leV flux by fitting to a slowing down spectrum. The phase space normalisation (in units of 100cm^2 steradian) was calculated using Monte Carlo to work out the fraction of isotropically distributed neutrons from the whole 10 x 12.6 cm^2 face which directly escaped down a given beam hole.

The spectra for the three top-moderator faces and their slowing down spectra fits, are shown in Fig V 3.2. The low probability of moderator escapes is reflected by the fluctuations on these spectra; the results must be subject to considerable uncertainty due to this alone.

The calculated numerical leV fluxes along with other information is given in the following table.

Moderator No.	1	2	3	4	5	6
leV flux unnormalised	1.8×10^{-3}	1.8×10^{-3}	1.1×10^{-3}	1.4×10^{-3}	1.8×10^{-3}	$.86 \times 10^{-3}$
Slowing down spectrum index	.11	.14	.044	.093	.12	.12
Total flux 0.1+15 MeV	.045	.065	.027	.042	.064	.031
Phase space volume 100 cm^2 sr.	.328	.476	.379	.328	.476	.379
leV flux/eV/ 100 cm^2 face/ sr/proton	5.5×10^{-3}	3.7×10^{-3}	3.10×10^{-3}	4.4×10^{-3}	3.8×10^{-3}	2.3×10^{-3}

The total neutron flux [0.1eV to 15 MeV] from neutron beam hole 1 is 0.4 neutrons/proton or 5×10^{14}/sec at 200μA. Of these .072/proton or 9×10^{13}/sec(at 200μA) come from moderator faces 1 and 3. The intensities in these two components as a function of neutron energy are shown in Fig V 3.3 [Note the variable energy-bin widths]. The 'contamination' by escapes from the reflector into the beam exit holes and through the decoupler layer are at an energy considerably higher than the 'thermal' region and have equal intensities at ~ 100eV. It would indicate the decoupler layer in the beam exit holes is doing a good job.

3.4 Comments

(i) The front of the uranium is ~6cm before the centre of the front moderator. In this position the front moderator would seem to produce ~60% more flux per face than the back; the neutron component of energy density is ~2 times, which is in rough agreement. As regards energy density - the forward nature of the high energy escapes from the target is shown rather clearly by the greater components from this source for back moderators.

(ii) In the calculation 1.1 neutrons/proton entered the energy region below 0.leV and had their 'histories' terminated. Some of these will escape the moderators and be the 'thermal neutron' flux, the rest will be absorbed in the decoupler [q.v. Section 4.1].

4. DECOUPLER

The moderators and beam exit holes are lined with a material of high cross section to low energy neutrons so that time spread due to low energy neutrons being reflected back is limited.

The decoupler material used in the calculation is natural B_4C in which 20% of the boron is ^{10}B and has a large (n, α) cross section for low and thermal energy neutrons. The B_4C density assumes the material will be in a powdered form.

4.1 Energy Deposition

The contributions to the total energy are (in units of MeV/proton incident at the target)

1) High energy particles : 1.29 MeV ≡ .26kW @ 200μA

2) Neutrons (≤15MeV) : 43.26 MeV ≡ 8.65kW @ 200μA

the majority of the energy comes from the exoergic $^{10}B(n,\alpha)$ reaction. This gives a total energy deposition of 44.6 MeV or 8.9kW @ 200μA proton current.

The energy deposited in the various regions of the system are shown in Tables 5-V(a), (b) & (c). - Note, because of symmetry only half the values are quoted with the positions of the various volumes shown in Fig V 4.1 and V 4.2.

The average energy deposition is 5.3 keV cm^{-3}. The highest deposition is a factor of 3.7 higher than the average, and occurs in the liner layers on the bottom of the front moderators (nearest to the target). The deposition averaged over this 12 x 5cm^2 piece is .02MeV cm^{-3} or ~4 watts cm^{-3} at 200μA proton current.

The .001 neutrons/proton which are below the 0.1eV lower energy limit will contribute .003MeV, which is negligble. The 1.1 neutrons which reach this energy in the moderators may make an extra contribution. Were they <u>all</u> lost in the decoupler, they might increase the energy by 40% at the peak position. Were they all lost, SNS would produce no thermal neutron flux.

4.2 ACTIVATION

4.2.1 Collision Information

High energy particle interaction with ^{11}B	.027
High energy particle interaction with ^{12}C	.01
High energy particle interaction with ^{10}B	.007
$^{10}B(n,n)^{10}B$	2.3
$^{10}B(n,n')^{10}B$	.01
$^{10}B(n,d)\ ^{9}B$	7.8×10^{-4}
$^{10}B(n,\alpha)^{7}Li$	9.0
$^{10}B(n,t2\alpha)$	8.9×10^{-3}
$^{11}B(n,n)^{11}B$	15.4
$^{11}B(n,n')^{11}B$	.03
$^{11}B(n,2n)^{10}B$	2.7×10^{-5}
$^{11}B(n,\gamma)^{12}B$	1.5×10^{-4}
$^{11}B(n,p)^{11}Be$	3.9×10^{-6}
$^{11}B(n,t)^{9}Be$	3.3×10^{-5}
$^{11}B(n,d)^{8}Li$	4.1×10^{-4}
$^{12}C(n,n)^{12}C$	4.6
$^{12}C(n,n')^{12}C$	.009
$^{12}C(n,\gamma)^{13}C$	8×10^{-6}
$^{12}C(n,\alpha)^{9}Be$	2.2×10^{-3}

Summary Information

Total High energy particle interactions	.044
Total Neutron interactions with ^{10}B	11.3
Total Neutron interactions with ^{11}B	15.4
Total Neutron interactions with ^{12}B	4.6

The nuclides produced by high energy bombardment are shown in Table 5-VI. The comments regarding the ICE model in Section 2.2.2 are relevant in this case also and the results should be viewed with caution.

4.2.2 Estimated Activities

From the information in Section 2.1 and Table 5 VI - the following products will contribute to the activity.

1.	^{11}C	20.38m	β^+	3.0×10^{-5}/proton
2.	^{10}C	19.2s	β^+	3.0×10^{-5}/proton
3.	^{13}B	17.4ms	β^-(99.72%), β^-n°(.28%)	1.3×10^{-4}/proton
4.	^{12}B	20.4ms	β^-(98.42%), 3α(1.58%)	6.7×10^{-3}/proton
5.	^{11}Be	13.8s	β^-(97%), $\beta^-\alpha$(3%)	6.5×10^{-3}/proton
6.	^{10}Be	1.6×10^6y	β^-	3.3×10^{-3}/proton
7.	^{11}Li	8.5ms	β^-(39%), β^-n(61%)	8.0×10^{-5}/proton
8.	^{10}Li	v. short?	n°?	8.0×10^{-5}/proton
9.	^{9}Li	.178s	β^-(65%), $\beta^-2\alpha$(35%)	3.9×10^{-4}/proton
10.	^{8}Li	.844s	$\beta^-2\alpha$	1.9×10^{-3}/proton
11.	^{5}Li	v. short?	p?	1.0×10^{-4}/proton
12.	^{3}H	12.346y	β^-	1.4×10^{-2}/proton

Only two of the products have very long half lives; ^3H (12.346y) and ^{10}Be (1.6×10^6y). The activity buildup rate for these products is 8.2×10^{-7} Ci sec^{-1} for ^3H, and 1.5×10^{-12} Ci sec^{-1} for ^{10}Be, the latter will always be negligible. The contribution from ^3H after 1 year's irradiation in ~25 Ci and at 10 years would reach ~200 Ci.

The short lived products will all be at equilibrium within a few minutes.

The estimated β activity is 530 Ci

Four neutron decay channels are present; ^{13}B (0.28% and negligible), ^{11}Li (61%), ^{10}Li (100%??) & ^{9}Li (35%). These give a neutron production rate of 2.7×10^{-4}/proton incident at the target or 3.3×10^{11} n°/sec at 200μA.

If we assume the nuclide production follows the energy deposition, and note that the production of these nuclides is from High Energy collisons, then the decoupler layer below the front moderator has a peak to average

for this energy component only of 7.4: that is, this piece of liner would be equivalent to neutron source of $\sim 2 \times 10^{10}$ neutrons per second.

4.2.3 Helium Evolution

The $^{10}B(n,\alpha)$ reaction liberates helium at the rate of 9 atoms per incident proton. The few α decay products contribute a further (and negligble) 3×10^{-2} He atoms per proton.

The production rate of helium is 1.1×10^{16} atoms per second at 200μA or 4.2×10^{-7} litres (at NTP) per second. As we might expect this production to follow overall energy deposition, at the worst place - 60cm^3 of liner below the front moderator - the rate will be ~3.9 x higher; that is 1.2×10^{-8} litres (at NTP) per second at this point or ~ 0.4 litres/year.

4.2.4 Damage

From section 4.2.1 there are ~31 primary atomic displacements per proton incident at the target averaged over the whole decoupler. This is an average of 7.4×10^{-11} primary displacements per atom per second. Again taking a peak to average of 3.9 from the energy deposition, this gives a maximum of 2.9×10^{-10}.

TABLE 5-I

ENERGY DEPOSITION FOR REFLECTOR IN TOP/BOTTOM LAYERS.

POSITION (SEE FIG V 2.1)	MeV/PROTON	W @ 200 μA	mW cm^{-3}
Areas 1 + 2 and void between, and above line XX'	.69	140	12
Area between lines XX' and YY' above moderators	2.5	500	28
Area 9 and void below line YY'	1.1	220	19
		TOTAL 860	

TABLE 5 - II

ENERGY DEPOSITION IN THE REFLECTOR

	LINER LAYER ABOVE MODERATORS			MODERATOR LAYER			LINER LAYER BELOW MODERATOR (NEAREST TARGET)			
No. of area on plan Fig. V-2.1	Energy MeV/ Proton	Power W @ 200μA	Power Density mW cm^{-3}	Energy MeV/ Proton	Power W @ 200μA	Power Density mW cm^{-3}	Energy MeV/ Proton	Power W @ 200μA	Power Density mW cm^{-3}	No. of area on plan Fig. Fig. V-2.1
1	.025	5	14	0.53	110	24	.061	12	34	1
2	.016	3.2	28	0.27	54	37	.021	4.2	37	2
3	.024	4.8	19	1.1	220	64.0	.20	40	150	3
4	.009	1.8	87				.041	8.2	380	4
5	.022	4.4	52	.96	190	180	.20	40	470	5
6	.012	2.4	59	.45	90	170	.089	18	420	6
7	.042	8.4	35	1.1	220	72	.16	32	140	7
8	.036	7.2	35	.77	150	59	.08	16	78	8
9	.066	13	19	1.3	260	29	.17	34	49	9
	Total = 50.2			Total = 1294			Total = 204.4			

TABLE 5 - III

ENERGY DEPOSITION IN REFLECTOR IN LAYER ADJACENT TO TARGET PRESSURE VESSEL.

AREA ON PLAN Fig V-2.3 (a) & (b)	VOLUME (cm^3)	ENERGY (MeV/PROTON)		POWER (WATTS)	POWER DENSITY (mW/cm^3)
		LEFT	RIGHT		
1	9921	2.83	2.87	570	57
2	117.7	.045	.045	9	76
3	992.6	.864	.851	170	170
4	3.1	.002	.002	0.4	130
5	19.2	.03	.027	5.7	300
6	1.5	.002	.002	0.4	270
7	9.4	.015	.015	3	320
8	1.3	.001	.001	0.2	150
9	7.8	.012	.012	2.4	310
10	119.7	.167	.186	35	290
11	351.3	.693	.691	140	390
			Total =	940	

TABLE 5 IV

ENERGY DEPOSITIONS IN REFLECTOR IN LAYER ADJACENT TO TARGET PRESSURE VESSEL TOP/BOTTOM

Ref No for position on Fig V 2.2	Volume (cm^3)	Energy deposited (MeV/Proton)	Power @ 200 μA (W)	Power density ($mW\ cm^{-3}$)
1	987.6	0.25	50	51
2	405.3	0.41	82	200
3	51.1	0.062	12	230
4	51.1	0.063	13	250
5	987.6	0.24	48	49
			Total =	205

TABLE 5 V(a)

ENERGY DEPOSITION IN LINEAR/DECOUPLER LAYERS FURTHEREST FROM TARGET

Location No. in Fig V 4.1	High Energy Particles MeV/proton	Neutrons (MeV/proton)	Total Energy (MeV/proton)	Volume (cm^3)	Energy Density (MeV/cm^3/proton)	Power Density at 200μA (W cm^{-3})	Peak to Average Energy Density
40103	.023	1.01	1.033	387.6	2.67×10^{-3}	.534	.507
40104	.002	.044	.046	40.0	1.15×10^{-3}	.230	.218
50103	.013	.726	.739	132.9	5.56×10^{-3}	1.112	1.06
50104	.003	.323	.326	60.0	5.44×10^{-3}	1.09	1.03
50105	.010	.886	.896	220.0	4.07×10^{-3}	.814	.77
50201	.011	.208	.219	44.7	4.89×10^{-3}	.978	.93
50203	.022	.567	.589	140.1	4.21×10^{-3}	.842	.8
60102	.004	.432	.436	196.2	2.22×10^{-3}	.444	.42
TOTALS	.088	4.196	4.284	1221.5	-	-	-

TABLE 5 V(b)

ENERGY DEPOSITION IN LINEAR/DECOUPLER WITHIN MODERATOR LAYER

Location No. in Fig V. 4.2	High Energy particles (MeV/proton)	Neutrons (MeV/proton)	Total Energy (MeV/proton)	Volume (cm^3)	Energy density (MeV cm^{-3})	Power Density @ 200 μA (W cm^{-3})	Peak to Average Energy Density
70102	.0058	.820	.826	244.44	3.38×10^{-3}	.676	.64
70203	.0135	.194	.208	76.86	2.71×10^{-3}	.541	.51
70204	.0076	.128	.136	114.66	1.19×10^{-3}	.237	.23
80102	.009	.737	.746	95.76	7.79×10^{-3}	1.56	1.5
80103	.003	.663	.666	63.0	1.06×10^{-2}	2.11	2.0
80104	.009	.993	1.002	240.66	4.17×10^{-3}	.833	.79
80108	.026	.523	.549	73.08	7.52×10^{-3}	1.50	1.4
80109	.026	.765	.791	63.0	1.26×10^{-2}	2.51	2.4
80110	.015	.863	.878	143.64	6.11×10^{-3}	1.22	1.2
80202	.014	.169	.183	36.54	5×10^{-3}	1.0	.95
80206	.050	.872	.922	97.65	9.44×10^{-3}	1.89	1.8
80207	.034	.941	.975	126.0	7.74×10^{-3}	1.55	1.47
80209	.024	.407	.431	110.25	3.91×10^{-3}	.78	.74
80210	.021	.359	.380	75.6	5.02×10^{-3}	1.00	.95
90102	.008	.694	.702	229.32	3.06×10^{-3}	.61	.58
TOTALS	.2659	9.128	9.395	1790.46	-	-	-

TABLE 5 V(c)

ENERGY DEPOSITION IN LINEAR/DECOUPLER LAYERS NEAREST TO TARGET

Location No. in Fig V. 4.1	High energy particles (MeV/proton)	Neutrons (MeV/proton)	Total Energy (MeV/proton)	Volume (cm^3)	Energy density (MeV/cm^{-3} proton $^{-1}$)	Power Density @ 200 μA (W cm^{-3})	Peak to average Energy density
100103	.045	1.53	1.575	387.6	4.06×10^{-3}	.812	.77
100104	.003	.046	.049	40.0	1.23×10^{-3}	.245	.23
110103	.068	1.50	1.568	132.9	11.8×10^{-3}	2.35	2.24
110104	.034	1.129	1.163	60.0	19.4×10^{-3}	3.88	3.68
110105	.025	1.848	1.873	220.0	8.51×10^{-3}	1.70	1.62
110201	.017	.290	.307	44.7	6.86×10^{-3}	1.37	1.30
110203	.094	1.263	1.357	140.1	9.69×10^{-3}	1.94	1.84
120102	.006	.7	.706	196.2	3.6×10^{-3}	.72	.68
TOTALS	.292	8.306	8.598	1221.5	-	-	-

TABLE 5 VI

PRODUCT NUCLIDES FROM HIGH ENERGY COLLISIONS WITH DECOUPLER

The asterisks identify the parent nuclei. The numbers correspond to the intensity for 10^5 protons incident on the target. A further 923 bombarded nuclei are completely broken-up into evaporation fragments.

Z / A	1	2	3	4	5	6	A TOTALS
1							
2							
4							
5			10				10
6	3	64	5				72
7			510				510
8		26	144				170
9		13	39				52
10			8	326	18*	3	355
11			8	654	728*	3	1393
12					656	100*	756
13					13	149	162
Z TOTALS	3	103	724	980	1415	255	3480

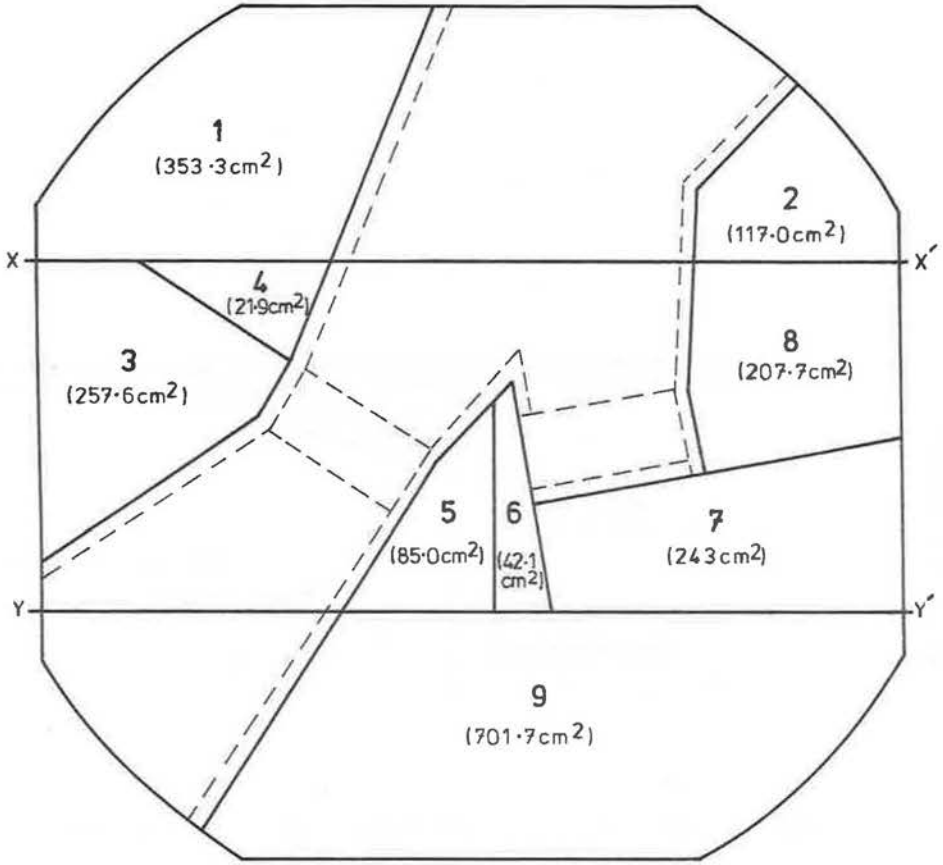

Fig V 2.1: *Plan showing position and areas for pieces used in calculation of energy deposition for reflector. "Liner' layers are 1.0cm thick and 'moderator' layers are 12.6cm thick (see Table 5-I and 5-II).*

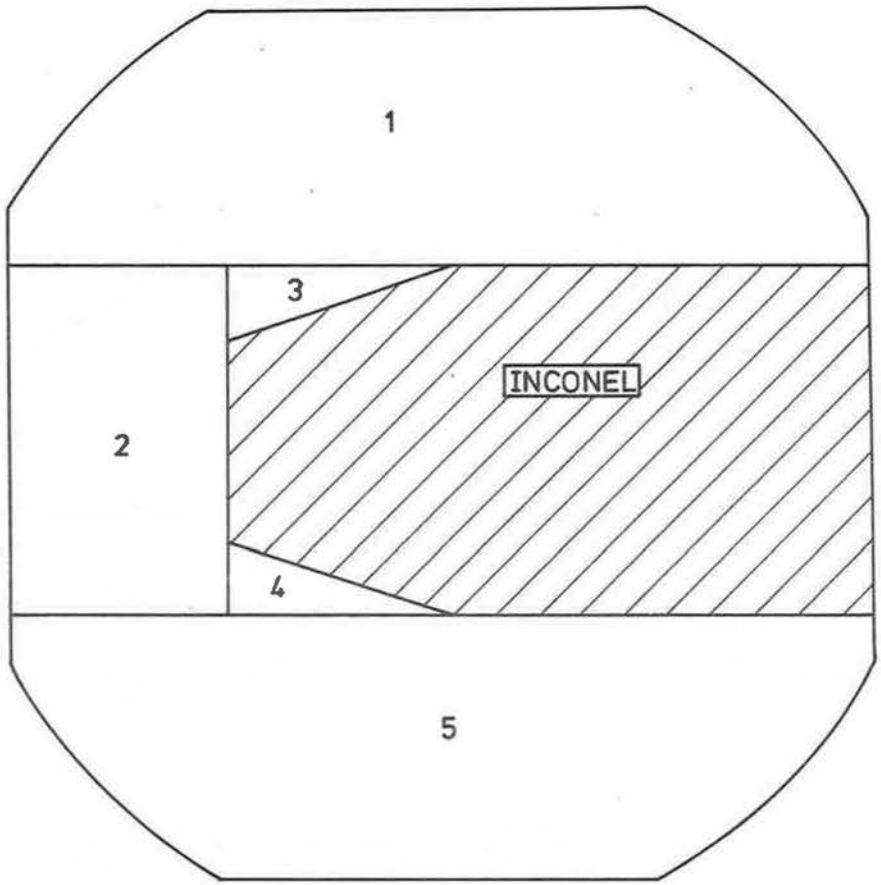

Fig V 2.2: *Plan showing positions for reflector pieces in energy deposition calculation for layer containing the target pressure vessel base and lid. (see Table 5-IV).*

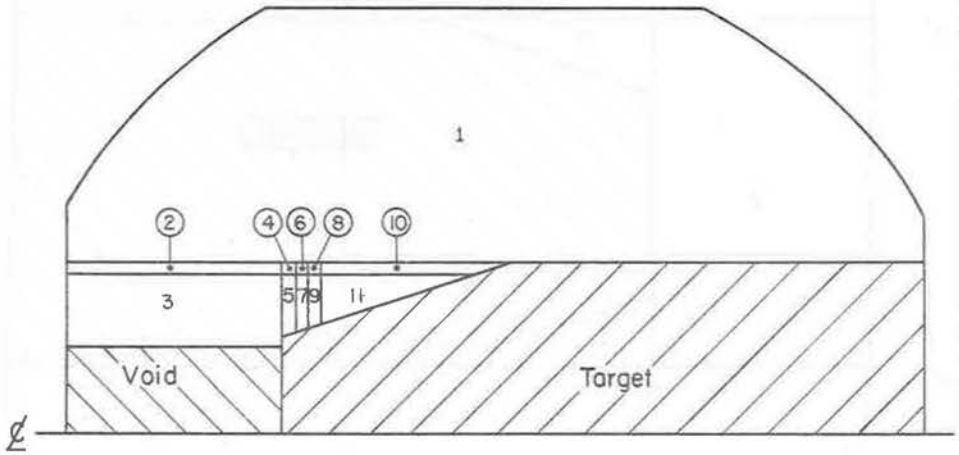

Fig V 2.3 (a): Positions of reflector pieces used in estimation of energy deposition in target layer. (see Table 5-III).

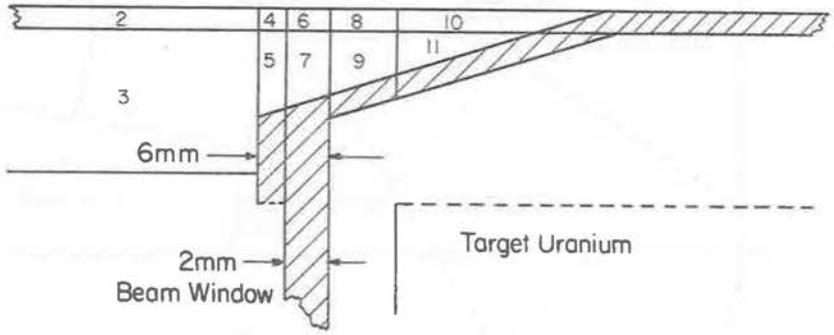

Fig V 2.3 (b): Detail of the front end of the target container in Fig V 2.3 (a).

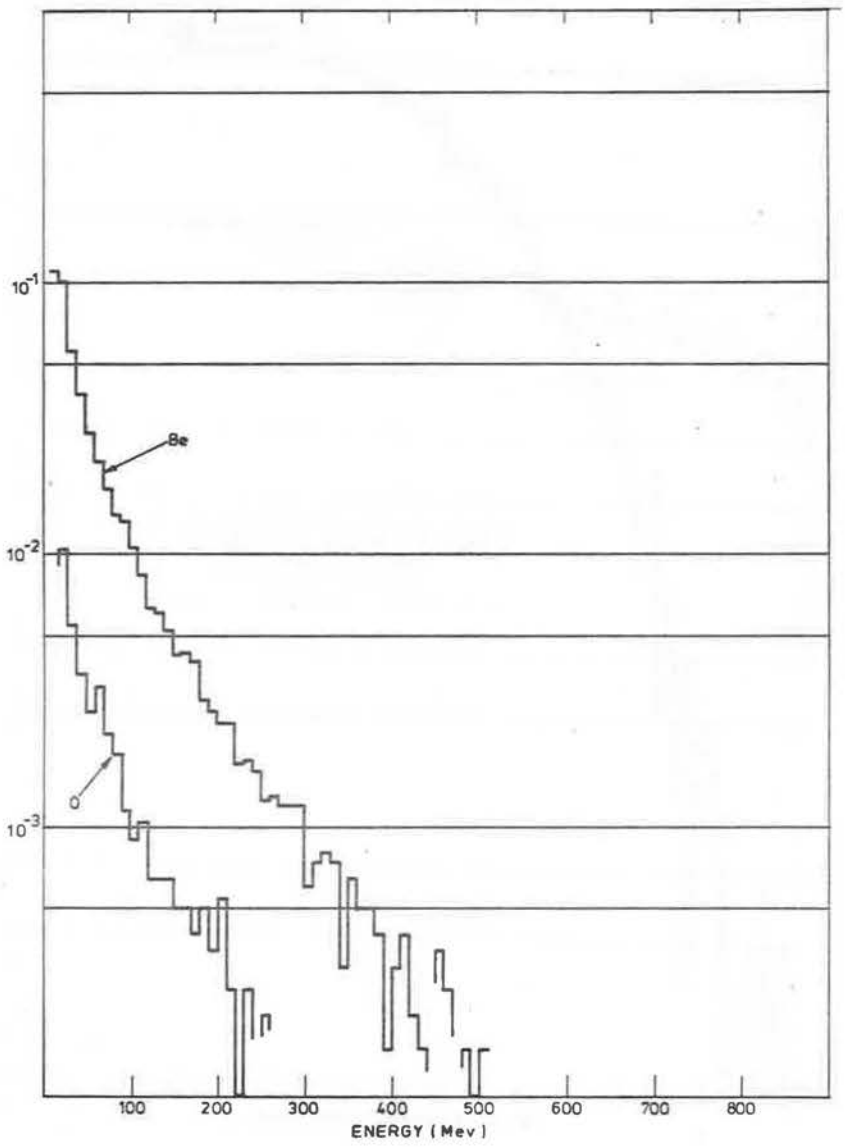

Fig V 2.4: *Spectrum of energies of high energy particles colliding with ^{9}Be and 0 in the relector.*

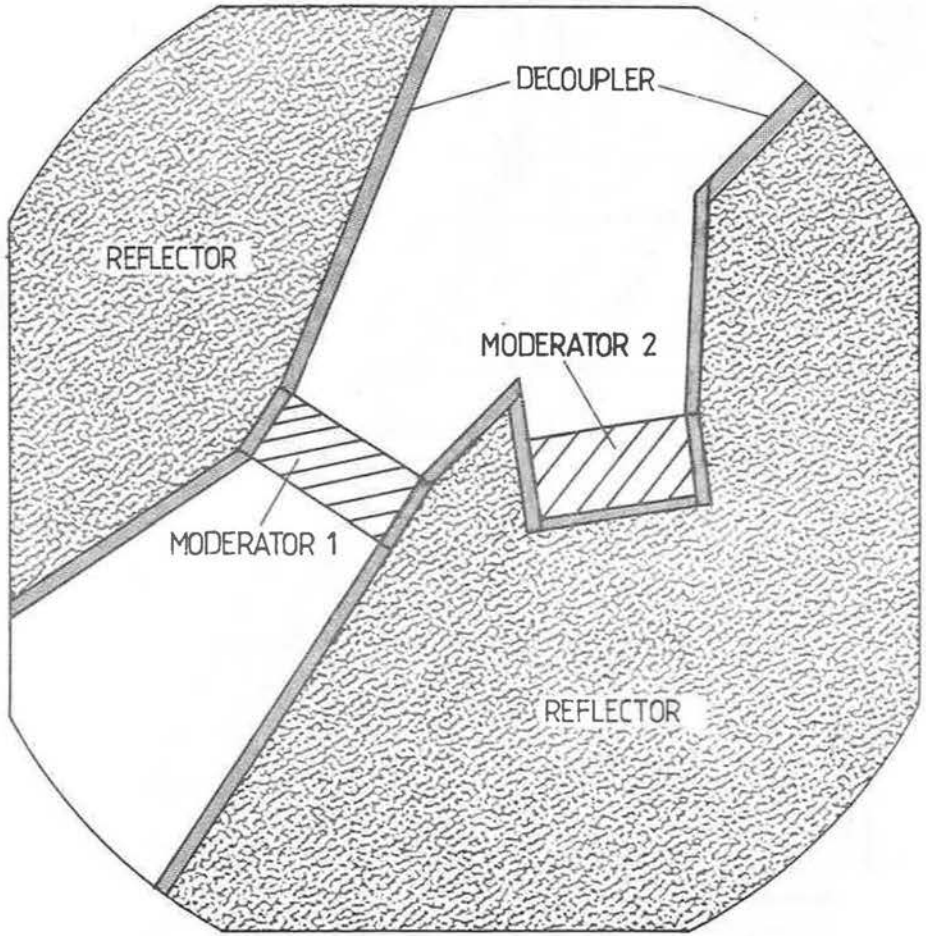

Fig V 3.1: *Layout for upper moderator layer.*

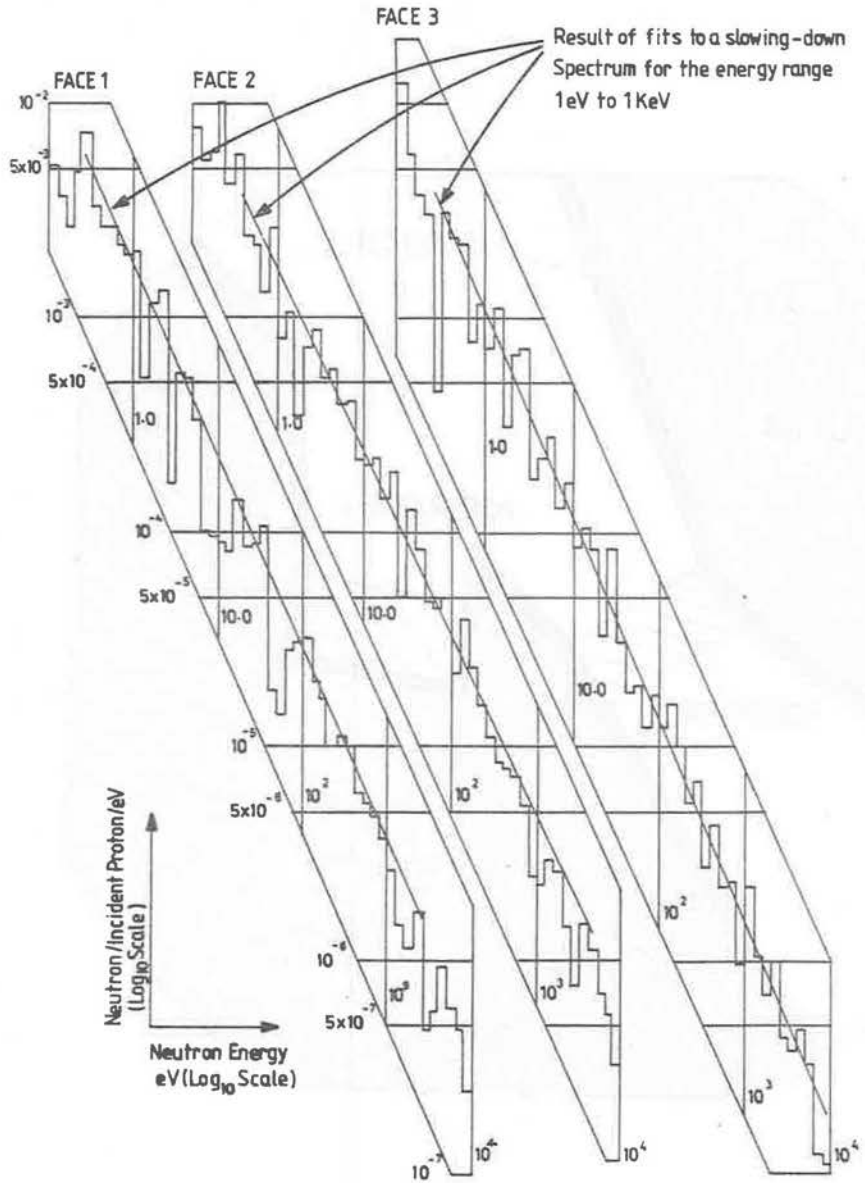

Fig V 3.2: Moderator neutron flux spectra in region 1eV to 1 KeV.

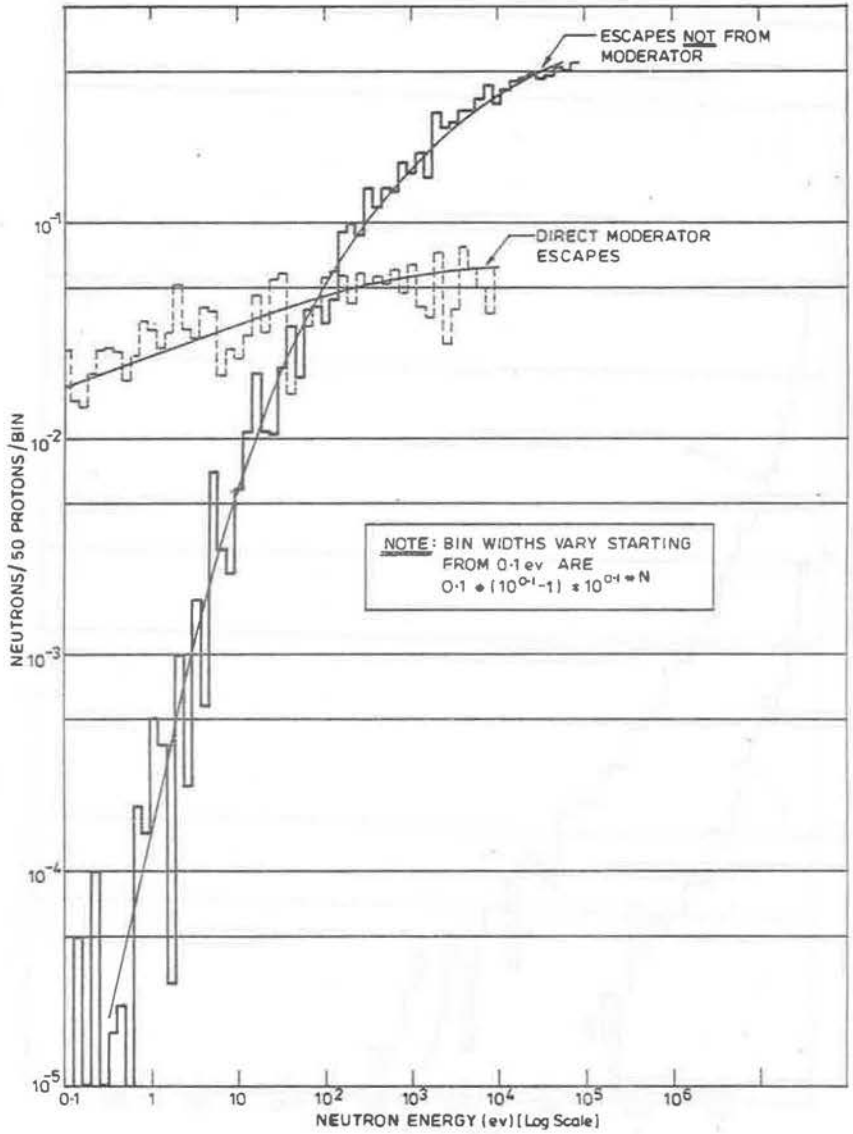

Fig V 3.3: Intensity vs energy for escapes from neutron beam hole No. 1; dashed histogram-moderator escapes; full histogram - escapes NOT from a moderator.

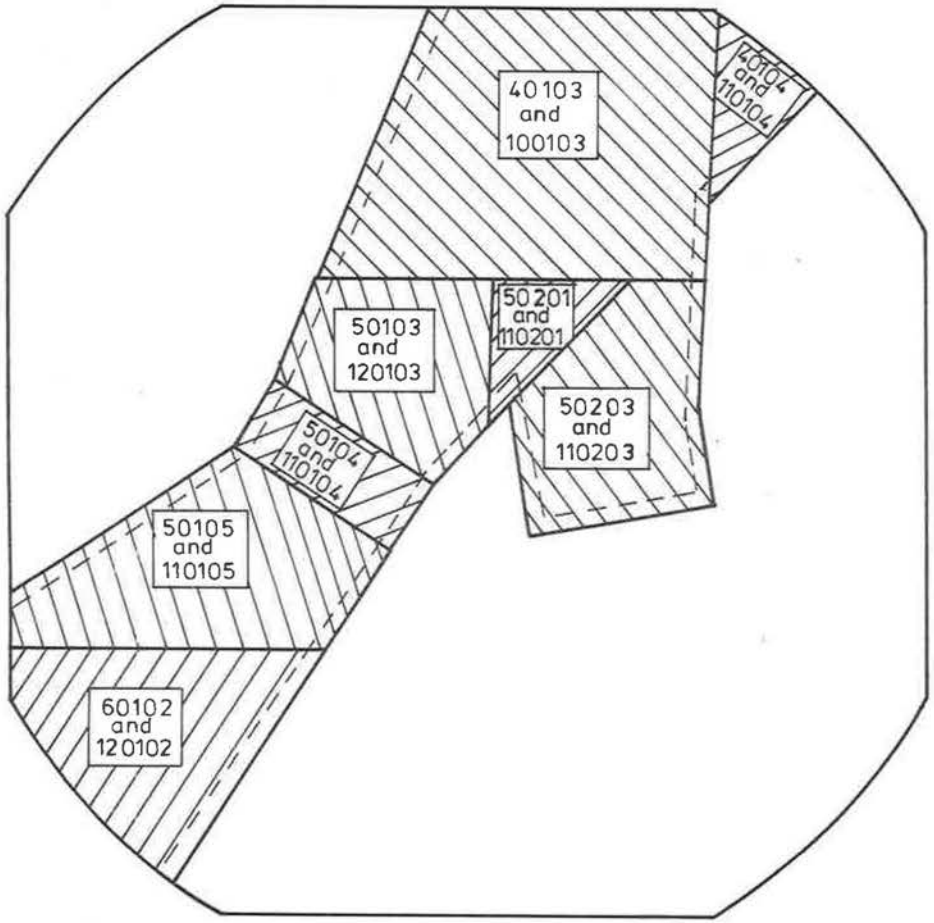

Fig V 4.1: *Position and location reference numbers for liner/decoupler sheets above and below neutron beam holes and moderators. The layers are 1cm thick (see Table V-5).*

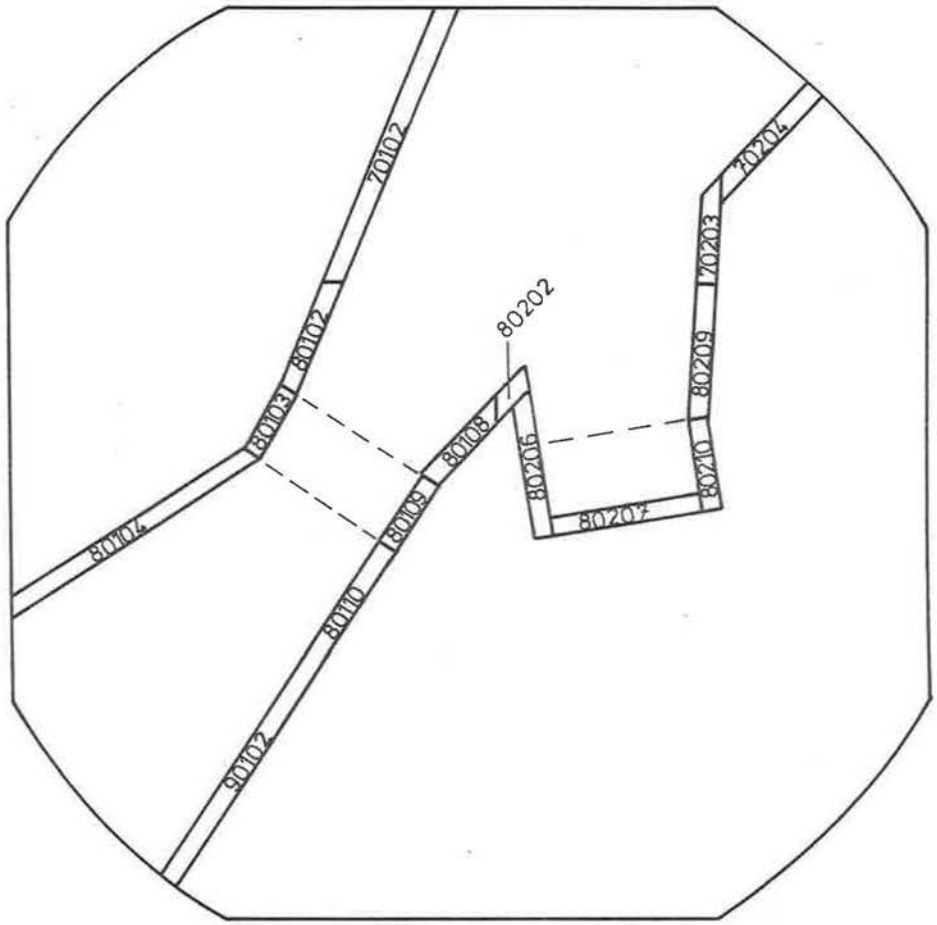

Fig V 4.2: *Position and location reference numbers for liner/decoupler sheets on walls of neutron beam holes. The sheets are 1cm thick and the layer has a depth of 12.6cm. (see Table V.5).*

CHAPTER 6

DISCUSSION AND CONCLUSIONS

1. INTRODUCTION

The calculation which has given the results quoted in this report is on the grandest scale. Extensive use of computational techniques presents technical difficulties in simply obtaining numbers and the quantity of data being handled offers excellent opportunities for making errors. The aim of this report is to present the results of the calculation to a wide and critical audience, who can use specialist knowledge to assess individual answers. The results all come from looking at the same nuclear processes from different angles; wrong answers for a particular aspect will have consequences for all others, although the coupling strength will be very variable.

2. ERRORS

The formal estimation of errors has not been done. This task would involve orders of magnitude more work. The calculation of errors would require assessment of the precision for the components of the nuclear physics models and a study of how they are propogated by the Monte Carlo to each quantity calculated. It is not certain one would be any the better off afterwards.

Hence the numbers quoted should be treated as predictions only.

The calculational method used is considered to be close to the best that is available. Fullwood et al [7] assign a global error of 20% to their calculational method, and Takahashi et al [27] have obtained 10% agreement with experiment in examining a large system of similar complexity to this study; both studies use a similar calculational system to the one for this study, but they are not identical. Whilst not disagreeing with an error of ~20%, it should be noted that orders of magnitude greater errors for particular quantities can occur. If these can be identified some estimate might be made of the consequence on other results.

When the target station is operational, comparison with measurement may provide some check on the validity of the calculational method.

3. THE CONSEQUENCE OF ERRORS FOR THE TARGET

To offset the lack of error estimation an examination of the consequence of errors is now made, along with steps available to mitigate their effect. The major concern is for the target uranium; whilst not attempting to dismiss the consequences of errors in other predictions, they are most serious for the target.

Fig. V1 1 shows a schematic structure for elements of the target assembly design.

There are two interlinked and closed loops; target dimensions, neutron production and neutronic performance, which aims at producing the best possible neutron source; target dimensions, temperature and safe operational lifetime, which aims at producing a target assembly which may be operated in a reasonable fashion.

Safe operational lifetime is a quantity which takes into account those effects during operation which would lead to target failure and sets a period after which the target sub-assembly should be replaced. This is probably most influenced by cost - of replacement of the sub-assembly - of 'down-time' for SNS etc -

Cost plays the role of main constraint on the design, whilst neutronic performance is what one aims to optimise.

The effect of errors may now be viewed in terms of:- how much better a performance would have been obtained were the design optimised using 'correct' values for parameters compared to operating in some non-optimium way.

3.1 Damage Mechanisms

These have been examined by Hudson & Steer [28] and Hudson [29]. The main 'damage' effects which lead to a target lifetime limit are:-

(a) Swelling due to production of 'solid' fission products.
(b) Swelling due to production of 'gaseous' fission products.
(c) Cavitational swelling.
(d) Thermal stress & cyclic thermal stress.

The first three effects are temperature dependant and also (but not considered here) influenced by manufacturing history.

By operating with an uranium temperature below 400^0C, the life limiting process is changed from cavitational swelling to cyclic stress from the gross thermal cycles at beam on and beam off [29].

The maintenance of the 400^0C temperature criterion is taken as the specific parameter for assessment of errors.

3.2 Temperature of the Uranium

The main influences on the temperature of the uranium are:-

(a) The thermal conductivity.
(b) The coolant system parameters.
(c) The total energy deposited.
(d) The distribution of deposited energy.
(e) The plate thickness.

3.2.1 The Thermal Conductivity is a physical attribute of the uranium - the number we use may be incorrect, its actual value we cannot alter. The coolant system parameters are part of a separate study, but again tend to be based on physical attributes of materials and a similar effect in any error to thermal conductivity should apply.

3.2.2. The total energy deposition is inexorably linked to neutron production. The calculated value may be wrong but the heat per proton, or per neutron will be a constant of the system. The energy deposition may be linked to "useful" neutron flux (e.g. The sum leV flux from all six moderator faces is calculated to be $.023 eV^{-1} sr^{-1} proton^{-1}/100cm^2$ face, if we take .023 neutrons/proton as the "useful" neutron flux, then this corresponds to an energy deposition of 45GeV per useful neutron). It is the variation of this type of parameter which is significant to both design optimisation and error examination: the actual choice of normalisation flux will vary depending on the proper figure of merit for judging the neutronic performance.

3.2.3 The energy distribution is the parameter over which we have the greatest control. It is mainly influenced by the density distribution of the proton beam and the reaction cross sections for uranium. The proton beam density distribution function will tend to be a characteristic of the accelerator, but the distribution width may be influenced by the beam transport system from accelerator to target. Both the width and distribution function may be wrong in the calculation.

The reaction cross sections are a physical attribute of uranium fixed in nature, the calculated values may be in error.

3.3. Compensation of Errors

The first four quantities in subsection 3.2 combine to allow a choice of target plate thickness which will maintain the temperature criterion. The effect of the errors will be that the plate thickness will be incorrect.

Limiting the discussion to the case where the observed temperature is too high, the design should have selected thinner plates and/or specified a wider beam distributions.

In both these cases, the "useful" neutron flux will decrease.

3.3.1 Thinner Plates

Thinner plates will cause a reduction of neutron production due to an increase in the non-uranium collisions in the 'target' volume. The thinner plates will also mean the neutron production will be more spread out. Fig VI 2 shows an estimate of how the various portions of a target couple neutronicaly to a moderator. These results were collected during the study reported in Ref 16 (But not quoted therein) and use a highly idealised moderator/reflector system and should therefore be treated as illustrative only. It is outside the scope of the present calculation to make numerical estimates for the loss of "useful" neutron flux.

If the proton current is reduced to compensate, the 'real' loss of performance will be less than pro rata, as a design using 'correct' values would have incorporated thinner plates and consequently have a degraded performance.

3.3.2. Alteration of beam width

If we consider compensating for the excess temperature by increasing the beam width, then for a parabolic distribution of width w, the change ΔT_u and the uranium temperature T_u are linked by:-

$$\frac{\Delta T_u}{(Tu-To)} = \frac{2\Delta w}{w}$$

Where T_o is the (essentially energy independent) temperature of the surface of the plate.

Taking T_o as 140°C, then an 8% increase in w (from 3.5cm to 3.8cm) would reduce the uranium temperature by 50°C; and in this case the optimisation study of Ref.16 should have used a 3.8cm beam. The moderator to proton coupling is the product of neutron production per proton and the fast neutron coupling to the moderator. The change of beam width should affect the neutron production only.

The Ref.16 neutron production results have been scaled to a 3.8cm beam and a new optimisation function generated (Fig.VI 3). This calculation indicates the moderator performance is reduced by 7% (as compared with the alternative reduction of the proton current and hence moderator performance by 16%). The moderator performance by using 9cm diameter uranium instead of the indicated optimum of 10cm is ~2% worse.

In practice the optimum would be a balance of beam width, beam intensity and target diameter.

3.4 Conclusion

If the operating temperature of the uranium is found to be too high it will be less harmful to neutronic performance to use an increased beam width than to reduce the proton beam current.

The actual loss in performance would be less than observed as the target installed should have had a degraded performance if the correct parameters had been used.

4. EFFECT OF ERRORS ON OTHER PARTS OF THE SYSTEM

Most other parameters of the system, other than those discussed above, will be insensitive to beam profile. The compensation for unsatisfactory operating conditions would have to be made by reduction of the proton current and consequently a degradation of the performance. Aspects of the performance which might lead to this situation should be identified and the subjects of detailed scrutiny.

5. SUMMARY OF RESULTS

To conclude this report a summary of the leading predictions is now given.

Summary for 200μA proton current

(i) Target Assembly

(a) Power

Prompt in Uranium	200kW
Nuclide Decay	8.7kW
Zircaloy	6.4kW
Coolant	5.2kW
Inconel Vessel	7.0kW

Total heatload on target assembly cooling system (Rounded) 230kW

(b) Activity

1 days irradiation	.65MCi
1 months "	.82MCi
6 months "	.86MCi

(c) Post irradiation (6 months)

Cooling time	decay power	α-activity	total activity
1 min	4kW	1000Ci	.65MCi
30 min	1.7kW	660Ci	.44MCi
1 hour	1.4kW	600Ci	.4 MCi
8 hours	.7kW	500Ci	.26MCi
1 day	.5kW	470Ci	.2 MCi
6 months	30W	70Ci	7000 Ci
1 year	14W	54Ci	3200 Ci

(d) Coolant Activity

Short lived products ~ 500Ci (in plumbing outside target void)

Tritium ~ 35Ci (after 2 years operation)

^{7}Be ~ 60Ci

(ii) Reflector heat load 7.2kW

(iii) Moderator heat load (No allowance for containers) .7kW

(iv) Decoupler/Liner 8.9kW

(v) Escape particles

Low energy neutrons (15MeV)	$1.3 \times 10^{16} sec^{-1}$ - 1.4kW
High energy neutrons (15-800MeV)	$1.0 \times 10^{15} sec^{-1}$ - 14kW
Protons	$2.8 \times 10^{13} sec^{-1}$ - 0.6kW
Mesons	$2.5 \times 10^{12} sec^{-1}$ - 18W
Total Energy carried away	16kW

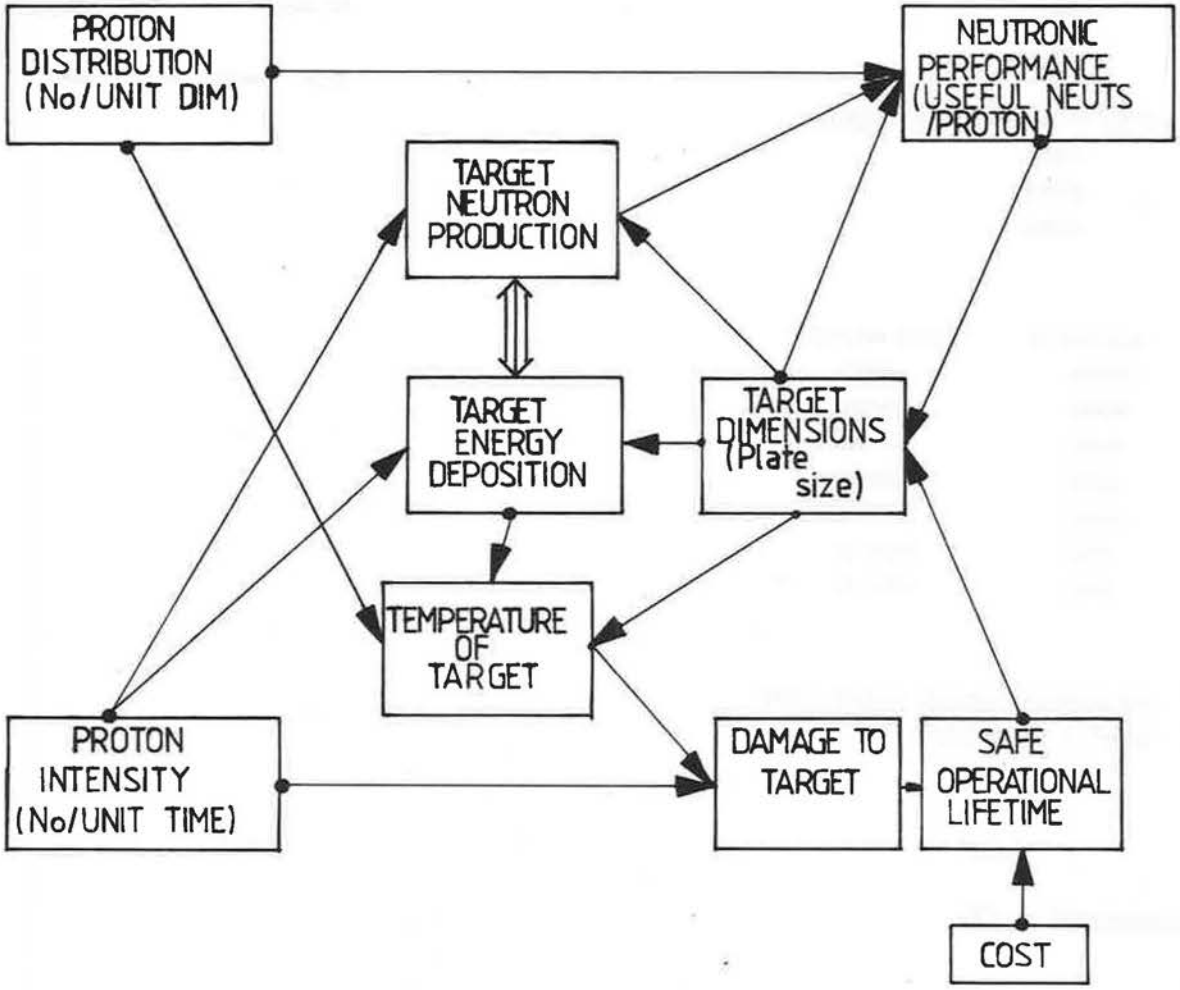

Fig VI.1: *Schematic structure for elements of TRAM assembly design and optimisation.*

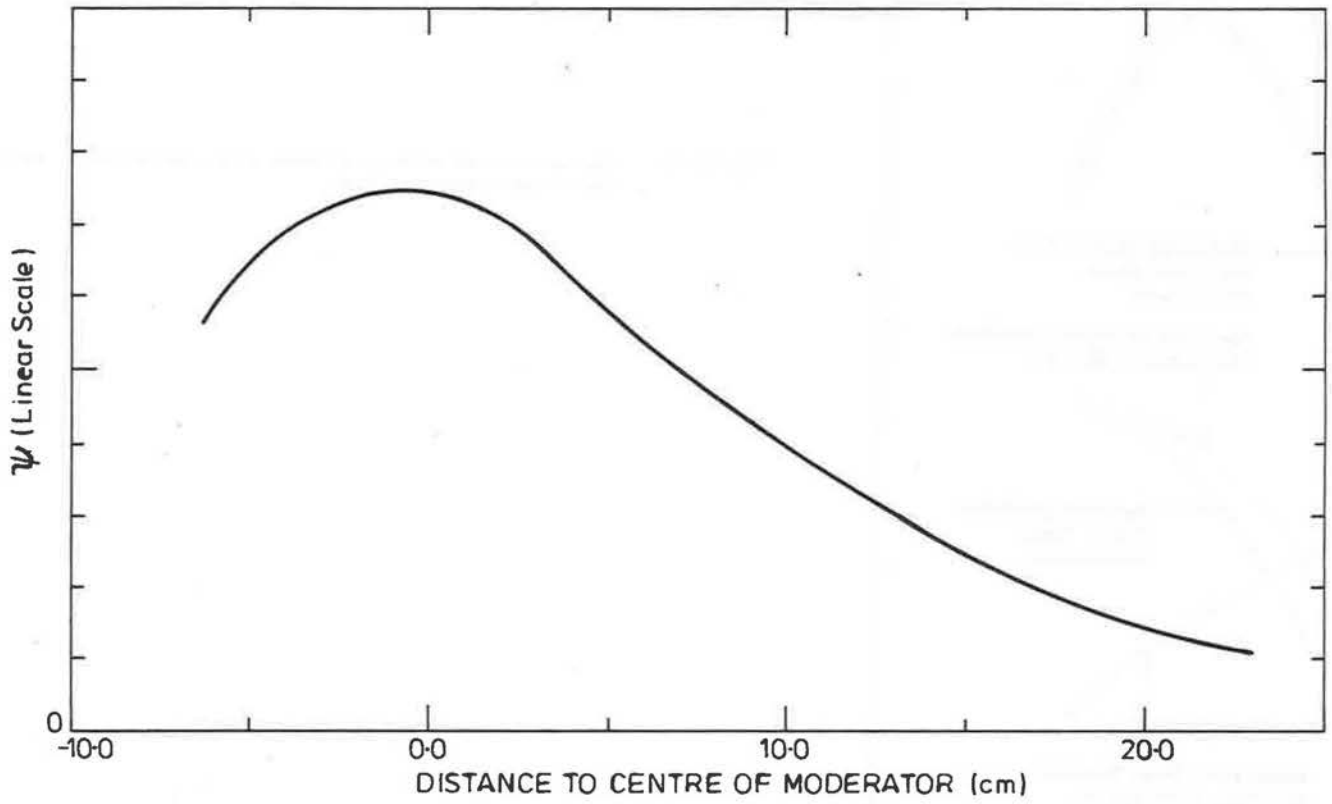

Fig VI.2: Fast neutron coupling, ψ (arbitary scale), as a function of axial distance to production site in target.

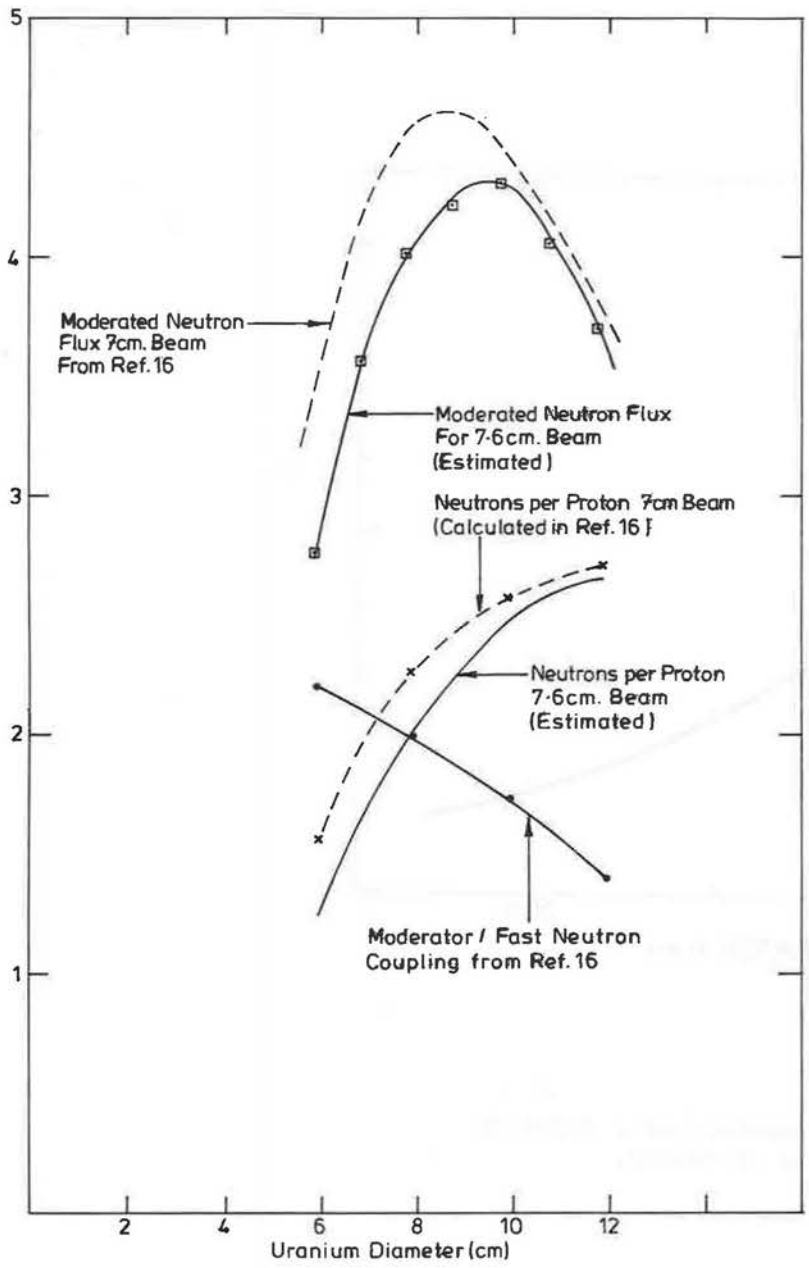

Fig VI.3: Estimation of effect of beam size variation on overall epithermal neutron flux.